EXPERIMENTAL STUDY AND SIMULATION OF THROUGH TRANSMISSION LASER WELDING OF DISSIMILAR TRANSPARENT POLYMERS

A thesis submitted towards partial fulfillment of the requirements for the degree of

Master of Technology in Laser Technology

Course affiliated to

FACULTY OF ENGINEERING & TECHNOLOGY

Under

FACULTY COUNCIL OF INTERDISCIPLINARY STUDIES LAW & MANAGEMENT

JADAVPUR UNIVERSITY

submitted by

SOUMYABRATA CHAKRAVARTY

Examination Roll No. M4LST19004
Registration No. 141051 of 2017-18

School of Laser Science and Engineering

Faculty of Interdisciplinary Studies, Law and Management

Jadavpur University

Kolkata -700032

India

2019

M.TECH. IN LASER SCIENCE AND TECHNOLGY

Course affiliated to

FACULTY OF ENGINEERING & TECHNOLOGY

Under

FACULTY COUNCIL OF INTERDISCIPLINARY STUDIES LAW & MANAGEMENT

JADAVPUR UNIVERSITY

CERTIFICATE OF RECOMMENDATION

I HERE BY CERTIFY THAT THE THESIS PREPARED UNDER MY SUPERVISION BY **SOUMYABRATA CHAKRAVARTY** ENTITLED **EXPERIMENTAL STUDY AND SIMULATION OF THROUGH TRANSMISSION LASER WELDING OF DISSIMILAR TRANSPARENT POLYMERS** BE ACCEPTED IN THE PARTIAL FULFILLMENT OF THE REQUIREMENTS FOR THE DEGREE OF MASTER OF TECHNOLOGY IN LASER TECHNOLOGY DURING THE ACADEMIC SESSION 2017-2019.

THESIS SUPERVISOR
Dr. Asish Bandyopadhyay
Mechanical Engineering Department
Jadavpur University, Kolkata-7000032

Countersigned

DIRECTOR
Sri. Dipten Misra
School of Laser Science and Engineering
Jadavpur University, Kolkata-700 032

DEAN
Faculty of Interdisciplinary Studies, Law and Management
Jadavpur University, Kolkata-700 032

M.TECH. IN LASER SCIENCE AND TECHNOLGY

Course affiliated to

FACULTY OF ENGINEERING & TECHNOLOGY

Under

FACULTY COUNCIL OF INTERDISCIPLINARY STUDIES LAW & MANAGEMENT

JADAVPUR UNIVERSITY

CERTIFICATE OF APPROVAL **

This foregoing thesis is hereby approved as a creditable study of an engineering subject carried out and presented in a manner satisfactory to warrant its acceptance as a pre-requisite to the degree for which it has been submitted. It is understood that by this approval the undersigned do not necessarily endorse or approve any statement made, opinion expressed or conclusion drawn therein but approve the thesis only for the purpose for which it has been submitted.

COMMITTEE OF FINAL EXAMINATION FOR EVALUATION OF THESIS

** Only in case the recommendation is concurred

DECLARATION OF ORIGINALITY AND COMPLIANCE OF ACADEMIC ETHICS

The author hereby declares that this thesis contains original research work by the undersigned candidate, as part of his **Master of Technology in Laser Technology** studies during academic session 2017-2019.

All information in this document has been obtained and presented in accordance with academic rules and ethical conduct.

The author also declares that as required by this rules and conduct, the author has fully cited and referred all material and results that are not original to this work.

NAME: SOUMYABRATA CHAKRAVRTY

EXAMINATION ROLL NUMBER: M4LST19004

THESIS TITLE: EXPERIMENTAL STUDY AND SIMULATION OF THROUGH TRANSMISSION LASER WELDING OF DISSIMILAR TRANSPARENT POLYMERS

SIGNATURE: DATE:

ACKNOWLEDGEMENT

The author has taken immense pleasure to express his sincere gratitude to everyone who has helped him to complete this thesis. First and foremost, the author is deeply grateful to his thesis supervisor Dr. Asish Bandyopadhyay, Professor, Mechanical Engineering Department, Jadavpur University for his valuable suggestions, guidance and constant inspiration throughout the period of the thesis work.

The author is grateful to Sri. Dipten Misra, Director, School of Laser Science and Engineering, Jadavpur University for his valuable suggestion during the period of thesis work. The author would like to thank Sri Kingsuk Pal, Staff Member of School of Laser Science and Engineering, Jadavpur University for his assistance towards the completion of this thesis work.

The author has been grateful to Dr. Nikhil Kumar, Post Doctorial Fellow, ITSligo, Ierland and Sri Nitesh Kumar, PhD. Research Scholar of Mechanical Engineering Department, Jadavpur University for their constant support and guidance throughout the period of the thesis work. The author would like to thank Dr. Somnath Paul, Dr. K. Paramsivam, Research Associate of School of Laser Science and Engineering, Jadavpur University, for their support and cooperation in completing the thesis work. The author would also like to thank Dr. Debabrata Das, Instrumentation Science Department, Jadavpur University and Sri Swagatam Paul, PhD. Research Scholar of Mechanical Engineering Department, Jadavpur University for their cordial cooperation.

The author also would like to thank Sri. Debojyoti Bandyopadhyay, Sri Souradip Paul, Sri Subha Nath, Sri Indranuj Lahiri, Sri Akashdip Nath, Sri Debmalya Haldar and Sri Nandakishor Maity for their valuable moral support.

Lastly but obviously not the least I would like to pay my special admiration thanks to my parents for their constant support, love and faith.

My eternal gratitude goes to God.

SOUMYABRATA CHAKRAVARTY
Examination Roll No. M4LST9004
Registration No. 141051 of 2017-2018

Contents

Chapter 1

1. Introduction

Plastics have been the fastest growing material in the present world. It is due to its light weight, flexibility, weather resistance, durability, strength and relative inexpensiveness. Plastics do not decay, but instead can be recycled. Plastics can be used extensively in a variety of applications including packaging industries, aerospace, coating, adhesives, construction, electrical, electronics, medical, household products and automotive industries. The increasing demands of plastic products have forced to use plastics in a new technical way so that the process by which plastics can be used should be much more environment friendly, faster and safer. Laser processing of material can be used as an emerging alternative to fulfil these high precision demands of plastic processing.

Common joining processes for different material are threads, rivet, staple, welding, etc. Among these, welding is a very popular joining technique in which two or more materials are joined together with or without application of heat, pressure and filler materials. Welding can be applied for joining of plastics. The conventional welding techniques such as TIG, MIG, Plasma Arc welding, etc. are not suitable for joining of plastics because large heat generated in the process damages the parent materials. On the other hand, in laser welding, heating is localized and desired power can be controlled for precision heating. Hence, for joining of plastics, probably the best solution is laser welding. In the present work, an attempt has been made to join two transparent thin plastic sheets using Through Transmission Laser Welding (TTLW).

1.1. Plastics

Plastics are generally defined as materials which contain essentially one or more polymers of high molecular weight. The properties of plastics are defined chiefly by the organic chemistry of polymers such as hardness, density and resistance to heat, organic solvents, oxidation and ionizing radiation. Plastics also differ greatly in their ability to transmit light. Materials that allow light to pass through them are called transparent. Many materials do not allow light to pass through them, they are called opaque materials. Some plastic materials have light transmission properties between transparent and opaque and these are called translucent. The reflectivity of light from the surface of a plastic material depends on the amount of gloss on the surface. The index of refraction is a measure of the change in

the direction of an incident ray of light as it passes through a surface boundary. If the index of refraction of the plastic is near about the same as that of the index of air, the light will pass through the boundary without significant change in direction. If the relative refractive index between the air and the plastic is large, the ray of light will significantly change direction.

1.2. Types of Plastic

Plastics are broadly classified into two groups: thermoplastics and thermosets. Typically, thermoplastics are plastics which can be repeatedly softened by heating and hardened by cooling, and can be shaped by flow into various articles in the softened state. They are usually filament molecules which are either amorphous or partially crystalline as shown in Figure 1.1(a). Acrylic, polypropylene, polystyrene, polythene and PVC are some of the good examples of thermoplastics.

Thermosets are plastics which after being cured with heat or some other modes, from a three-dimensional amorphous cross-linked molecular network as shown in Figure 1.1(b), which no longer melt or soften upon application of heat. If excessive heat is given thermoset material will degrade. Some examples of these types of plastics are polyester, epoxy resins and melamine.

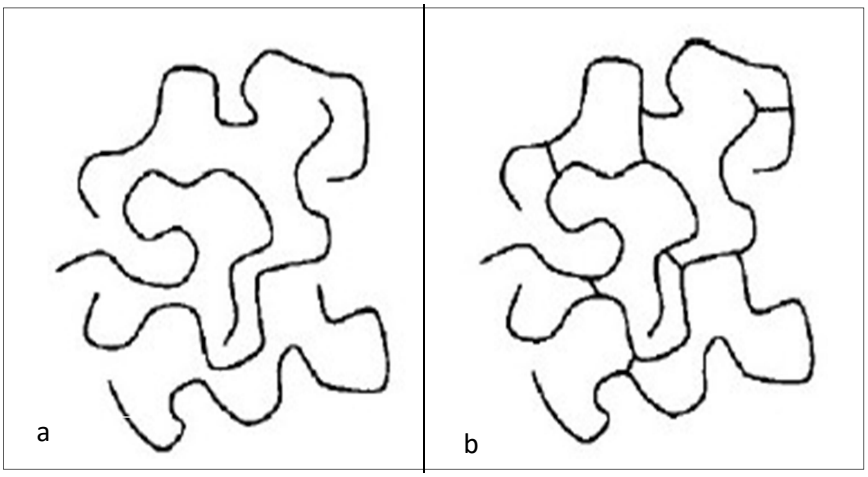

Figure 1.1(a) Thermoplastic and (b) Thermoset polymers

1.2.1. Some commonly known plastic materials

a) Nylon:

Nylon is a generic designation for a family of synthetic polymers, more specifically aliphatic or semi-aromatic polyamides. They can be melt-processed into fibers, films or shapes. The first example of nylon (nylon 6, 6) was produced on February 28, 1935, by

Wallace Carothers at DuPont's research facility at the DuPont Experimental Station. Nylon polymers have found significant commercial applications in fibers (apparel, flooring and rubber reinforcement), in shapes (molded parts for cars, electrical equipment, etc.), and in films (mostly for food packaging).

b) Acrylic:

Poly-methyl acrylic, also known as acrylic or acrylic glass as well as by the trade names Plexiglas, Lucite, and Perspex among several others, is a transparent thermoplastic often used in sheet form as a lightweight or shatter-resistant alternative to glass. The same material can be utilized as a casting resin, in inks and coatings, and has many other uses.

c) PVC:

Polyvinyl chloride (PVC) is the world's third-most widely produced synthetic plastic polymer, after polyethylene and polypropylene. PVC comes in two basic forms: rigid (sometimes abbreviated as RPVC) and flexible. The rigid form of PVC is used in construction for pipe and in profile applications such as doors and windows. It is also used for bottles, other non-food packaging, and cards (such as bank or membership cards). It can be made softer and more flexible by the addition of plasticizers, such as phthalates. In this form, it is also used in plumbing, electrical cable insulation, imitation leather, signage, inflatable products, and many applications where it replaces rubber. Pure PVC is white in colour and brittle solid. It is insoluble in alcohol but slightly soluble in tetra-hydro-furan.

d) Polythene:

Polyethylene (PE) is the most common plastic. The annual global production is around 80 million tons. Its primary use is in packaging (plastic bags, plastic films, geo-membranes, containers including bottles, etc.).

e) Polypropylene:

Polypropylene (PP), also known as polypropene, is a thermoplastic polymer used in a wide variety of applications including packaging and labeling, textiles (e.g., ropes, thermal underwear and carpets), stationery, plastic parts and reusable containers of various types, laboratory equipment, loudspeakers, automotive components, and polymer banknotes. An addition polymer made from the monomer propylene, is rugged and unusually resistant to many chemical solvents, bases and acids. Polypropylene has a relatively slippery "low energy surface", that means that many common glues will not form adequate joints. Joining of

polypropylene is often done using welding processes. In 2013, the global market for polypropylene was about 55 million tons.

f) Polycarbonate:

Polycarbonates (PC) are a group of thermoplastic polymer containing carbonate groups in their chemical structures. Polycarbonates used in engineering are strong, tough materials, and some grades are optically transparent. They are easily worked, moulded and thermo formed.

g) Bakelite:

It is a thermosetting plastic. Its colour is dark brown. It is used as a composite reinforced with paper or cloth. It is used to make circuit boards and heatproof insulated parts in the electronics industry.

h) Epoxy resin:

It is a two part mix which can be used as glue or be reinforced with carbon fibre to produce a very strong and light composite materials which is used in aerospace and Formula 1 cars.

i) Melamine:

It is a thermoset, very tough and heat resistant. It is white but can be produced in a full range of colours.

1.3. Joining Process of Plastic

Joining is one of the most critical steps in manufacturing components from plastic and polymeric composites. Plastic components are used in widespread, so joining techniques has become to play an important role in their processing industries. Making the complex plastic components in one piece is not always feasible and cost-effective. Various joining techniques have been developed over the years. Joining of plastic materials and their composites can be broadly classified as chemical, mechanical and welding or fusion as seen in Figure 1.2. Mechanical and chemical bonding can be used for joining all materials. On the other hand, welding which requires the materials at the joining interface to melt is only applicable to thermoplastics, since thermosets cannot be melted. The general advantages of welding technology over other joining techniques are fast and easy processing, tightness of joint and high strength.

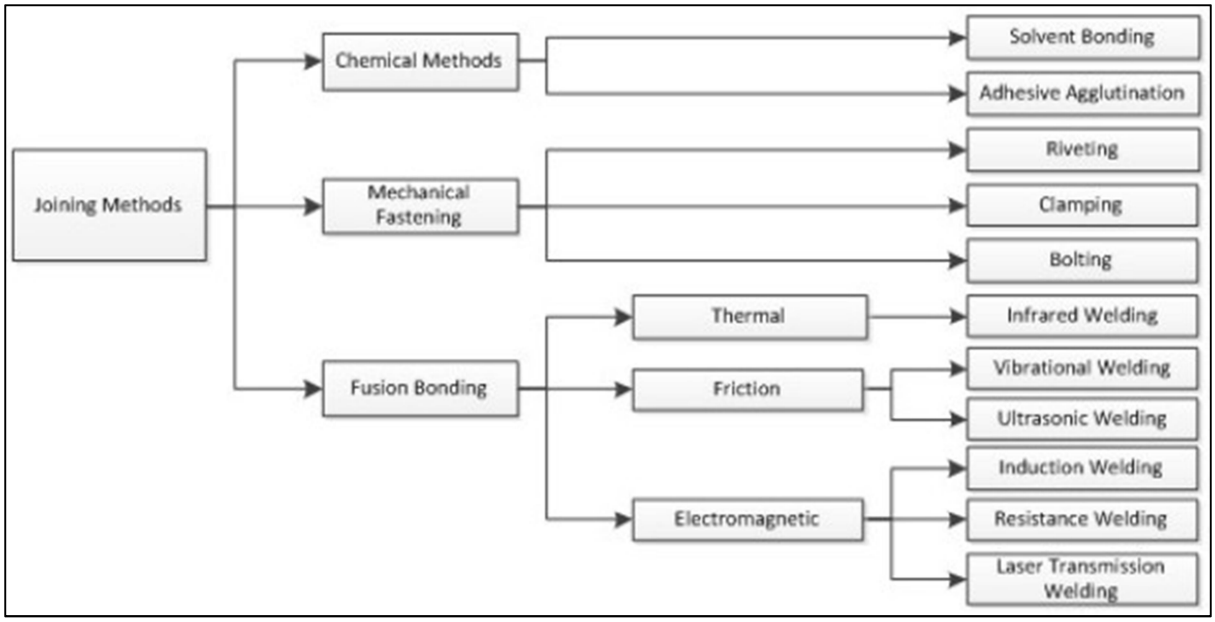

Figure 1.2 Joining methods for plastics

1.4. Welding of Plastics

Generally, plastic welding is done by joining the two workpieces together either by doing lap joint, butt joint or by applying any other configurations as joint design suggestions. The most special requirement for plastic welding is that the melting should occur in between the interface. So depending on how the heat for melting is supplied, the thermoplastic welding can broadly be classified as

i. Thermal bonding
ii. Friction bonding
iii. Electromagnetic boding

Thermal bonding generally includes hot gas welding, extrusion welding and hot tool (hot plate) welding and infra-red welding. Friction welding generally includes spin welding, angular welding, orbital welding and ultrasonic welding. Electromagnetic bonding includes resistance welding, induction welding, dielectric welding and microwave welding.

A brief overview of some conventional welding process that is used for plastics:

a) Ultrasonic welding: In ultrasonic welding, a metal tool delivers energy to one part to weld. The part of the other side of the joint area rests on the rigid anvil, ensuring that the energy applied must be dissipated in the weld zone. The oscillatory force of the horn is at the rate of 10-70 kHz flexes. Viscous-elastic loses occurring in this projection cause the polymer to melt and flow across the bond line creating a weld. Ultrasonic welding joins amorphous

thermoplastics more efficiently than crystalline ones. Figure 1.3 shows the arrangement of ultrasonic welding.

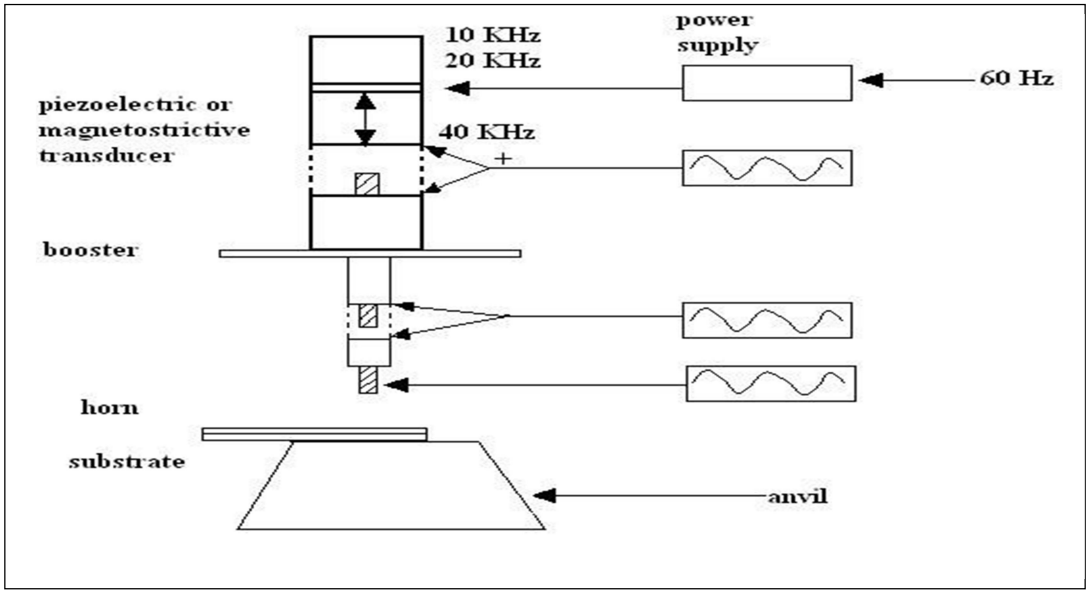

Figure 1.3 Arrangement of an ultrasonic welding device

b) Rotary welding: Rotary welding involves rotating one thermoplastic component relative to a stationary mating component while under pressure at a specific velocity. The friction between the parts created heating resulting in strong weld. The advantages of spin welding are fast cycle times, low capital cost and ability to weld most type of thermoplastics. This process is suitable for round weld joints and is especially requires the joint design. The steps spin welding is shown in Figure 1.4.

c) Hot gas welding: This is usually a manual process where the hot gas or air is usually directed simultaneously at weld joints and a filler rod is used to create a weld in a similar fashion as that of oxy-fuel welding. To ensure good welding, adequate temperature and pressure must be applied to the rod, along with the use of correct welding speed and positions. This process is very economical and very suitable for large kind of structures and repair works. This kind of welding is slow and is a function of operator dependent. Figure 1.5 shows the hot gas welding.

d) Hot plate welding: This type of welding is also known as hot tool welding. This welding process is one of the simplest and is most commonly used in plastic welding. To make the sample weld, the heated tool is brought into contact with the parts to create a zone of melted polymers. Fusing the melted zones under pressure creates the weld. The process is simple enough to be used for applications in the field such as joining gas distribution pipe and adaptable enough to be used for complex geometries like front seat consoles in the automotive industry.

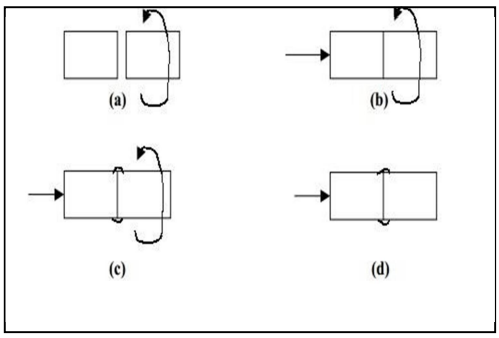

Figure 1.4 Steps in rotary friction welding (a) Rotary member brought up to speed (b) Rotary member advanced into contact under axial load (c) Rotary contact pressure maintained for the specified period. (d) Rotation stopped and pressure maintained or increased for a specified period to produce the weld

Figure 1.5 Hot gas welding

e) Vibration welding: This type of welding comes under the category of friction welding. The process involves rubbing of two thermoplastic parts together in a linear or orbital fashion, while under pressure at a specific frequency and amplitude to generate sufficient heat for melting and welding. The parts at the completion of the vibration motion

are held together until the weld joint cools and the re-solidification occurs in the melted parts. This process offers advantages of relatively fast cycle times; suitable for the medium of large assemblies and ability to weld most type of thermoplastics.

1.5. Joint Designs for Plastic Welding

As laser welding is a non-contact process, there are a broad number of joint geometries that can be welded. In addition the laser is able to weld into areas with limited access. The main joint designs are shown in Figure 1.6. Ideally, in any weld joint, the thinner material is the top sheet.

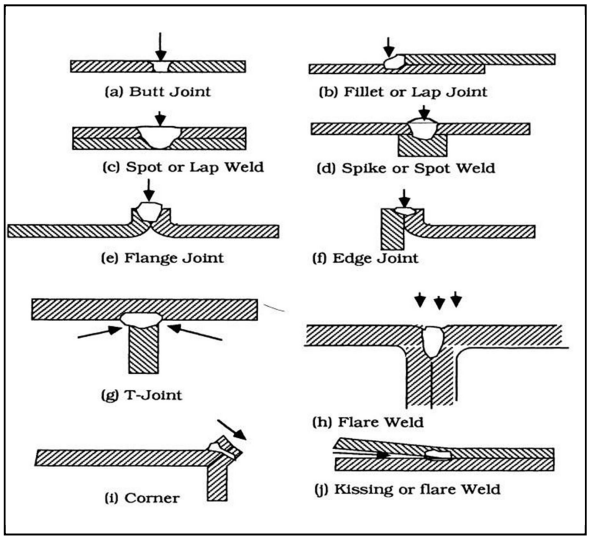

Figure 1.6 Potential families of joint designs

1.6. Through Transmission Laser Welding (TTLW) Process

Through transmission laser welding process is an innovative joining technology for plastics, which is used for its well-known advantages such as non-contact, non-contaminant process, easy to control and automate. Moreover, this joining process is flexible, has shorter processing times, can provide consistent quality and repeatability. The laser systems that are used are generally Nd:YAG laser, fiber laser and sometime diode laser are also used. In case of polymer welding, the upper part must be transparent to the wavelength of the specified laser and the lower part is absorbent to the wavelength of the specified laser. One thing that should keep in mind is that at the joining interface, additives components should be used or both the parts should be clamped together. The parts to be weld is placed under the laser head. The upper part is transparent to the laser beam transmits the beam and the lower part being absorbent to the laser beam absorbs it. Since both parts are pressed together with

predetermined clamping pressure, the heat is transfer from the upper part to the lower part due to thermal conduction and starts melting. Melting takes place due to localized heating of the interface, which leads to fuse by creating weld seams.

1.6.1. Types of TTLW

There are four types of TTLW

a) **Contour welding:** To generate long and 3D weld seams, contour welding is generally used. Here the laser spot is guided sequentially along with a predetermined welding pattern, melting it locally. Depending upon the type of laser used and its corresponding wavelength, the width of the weld can be varied from 0.01 mm to 7-8 mm. Here the melting of the weld takes place sequentially, so a small joint gap is permissible. Fig. 1.7(a) shows the contour welding.

b) **Simultaneous welding:** In this technique, one or more lasers heat the entire weld path simultaneously. High power diode lasers are generally used as a result of their compact design. It is very easy to achieve linear welding seams. Almost any beam geometry can be generated by means of special, state-of-the-art beam shaping elements. Figure 1.7(b) shows the simultaneous welding.

c) **Quasi-simultaneous welding:** Figure 1.7 (c) shows the quasi-simultaneous welding. In the quasi-simultaneous welding method, the whole joint line is plasticized at the same time. The laser supplies energy continues until the specified welding depth has been reached. A galvanometer- scanner guides the laser beam along the joint line. The beam can be controlled in the X and Y directions. Because of the fast scanning speed, the material melts along the whole joint line so that the welding partners join quasi-simultaneously along this seam. Measuring the melt collapse (melt travel monitoring) allows the qualitative evaluation of the welding process results. Pyrometer control reliably identifies any anomalies in the joint line.

d) **Mask welding:** This method is to provide the possibility to generate quasi-static temperature fields. Mask welding is a combination of contour and quasi-simultaneous welding. This process is very much flexible and suitable for small series and mass production. The pictorial view of mask welding is shown in Figure 1.7 (d).

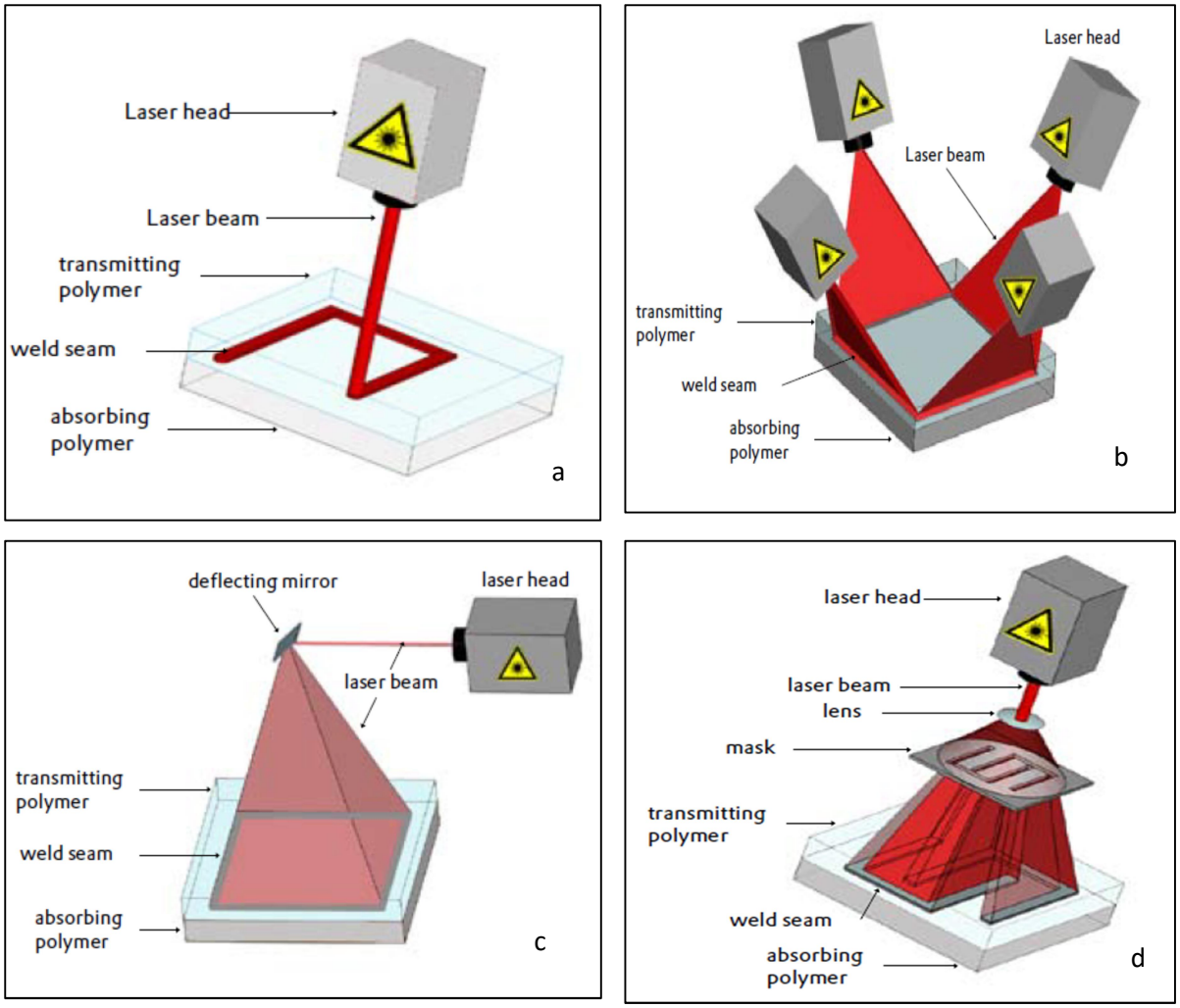

Figure 1.7 Pictorial views of (a) Contour welding, (b) Simultaneous welding, (c) Quasi simultaneous welding and (d) Mask welding

1.7. Light Amplification by Stimulated Emission of Radiation (LASER)

The term laser originated as an acronym for "light amplification by stimulated emission of radiation". Theodore H. Maiman at Hughes Laboratories, based on theoretical work by Charles Hard Townes and Arthur Leonard Schawlow, built the first laser in 1960. The main properties of a laser beam are MMC, i.e. Monochromatic, Coherent, Collinear. A laser differs from other sources of light as it emits light coherently. Spatial coherence allows a laser to be focused to a tight spot, enabling applications which require precise localized heating such as laser cutting and lithography. Spatial coherence also allows a laser beam to stay narrow over great distances (collimation), enabling applications such as laser pointers. Lasers can also have high temporal coherence, which allows them to emit light with a very narrow spectrum, i.e., they can emit a single colour of light. Temporal coherence can be used to produce pulses

of light as short as a femtosecond.

Lasers are used in optical disk drives, printers, and barcode scanners, fiber and free space optical communication, laser surgery and skin treatments, cutting and welding of materials, military and law enforcement devices for marking targets and measuring range and speed; and laser lighting displays for entertainment.

Spatial coherence is typically expressed through the output being a narrow beam, which is diffraction-limited. Laser beams can be focused to very tiny spots, achieving a very high irradiance, or they can have very low divergence in order to concentrate their power at a great distance.

Temporal (or longitudinal) coherence implies a polarized wave at a single frequency whose phase is correlated over a relatively great distance (the coherence length) along the beam. A beam produced by a thermal or other incoherent light source has an instantaneous amplitude and phase that vary randomly with respect to time and position, thus having a short coherence length. Components of the laser are shown in Figure 1.8.

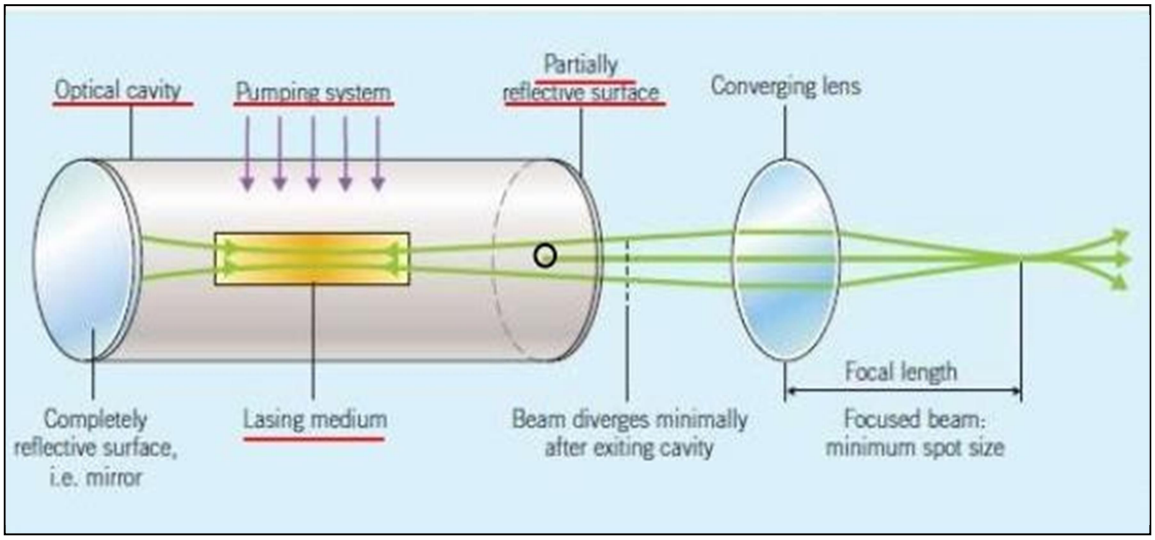

Figure 1.8 Components of Laser

A laser consists of a gain medium, a mechanism to energize it, and something to provide optical feedback. The gain medium is a material with properties that allow it to amplify light by way of stimulated emission. Light of a specific wavelength that passes through the gain medium is amplified (increases in power).

For the gain medium to amplify light, it needs to be supplied with energy in a process called pumping. The energy is typically supplied as an electric current or as light at a different wavelength. Pump light may be provided by a flash lamp or by another laser.

The most common type of laser uses feedback from an optical cavity, a pair of mirrors

on either end of the gain medium. Light bounces back and forth between the mirrors, passing through the gain medium and being amplified each time. Typically one of the two mirrors, the output coupler, is partially transparent. Depending on the design of the cavity, the light coming out of the laser may spread out or form a narrow beam. In analogy to electronic oscillators, this device is sometimes called a laser oscillator. Most practical lasers contain additional elements that affect the properties of the emitted light, such as the polarization, wavelength, and shape of the beam.

There is numerous method of plastic welding out of which laser welding is one of the new methods of welding. In this work, an attempt has been made for laser welding of plastics in lap joint configuration.

Laser welding belongs to fusion-welding category. The necessary heat generated when a focused high energy density laser beam irradiates the surface to be joined. As a result of heating materials melts, part of the material may vaporize. The melted material subsequently solidifies, constituting the weld seam. During welding, the process gas is provided onto the surface.

Laser welding of thermoplastics is used to be done by CO_2 lasers or by Nd:YAG laser which is quite expensive. These types of technology are generally used in the early 1990's. Laser transmission welding is a well-known technology which is used to weld two overlapping thermoplastics of the same or different optical properties by using a laser beam. This technique requires two parts of materials, one being transparent to the laser beam and other being absorbent to the laser beam. Two parts are overlapped and pressure is created between the parts. Laser beam moves through the joining line under pressure. The transparent upper part transmits most of the radiation and it is being absorbed by the lower part creating localized heating to a certain depth at the joining surface depending on the thickness and the absorption coefficient of the lower part.

1.8 Types of Lasers

Depending upon the use of active medium the lasers are categorized into four types. These are the following.

(a) Solid State Laser:

(1) Ruby laser (- alumina: most stable form of Al_2O_3)

(2) Neodymium laser (Nd)

(3) Neodymium Yttrium Aluminium Garnet (Nd:YAG)

(b) Gas Laser:

(1) Carbon dioxide (CO_2) laser

(2) Carbon monoxide laser

(c) Liquid Laser:

Based on fluids such as Nitrobenzene

(d) Semiconductor Laser:

Based on Gallium Arsenide

1.9. Advantages and Disadvantages of Laser Welding

Advantages:

Weld strength: The laser weld is narrow with an excellent depth-to-width ratio and higher strength.

Heat affected zone: The heat-affected zone is limited, and due to rapid cooling, the surrounding material is not annealed.

Precision work: The small, tightly controlled laser beam permits accurate micro welding of miniature components.

Deformation: Parts have a minimal deformity or shrink.

No contact: No physical contact between workpeice and tool.

Scrap: Laser welding is controllable and generates low volumes of scrap.

One-sided welding*:* Laser welding can replace spot welding requiring access from one side only.

Disadvantages:

The welding plants are expensive, depending upon the equipment. It requires more safety in the process.

It is applicable up to a certain thickness of the material.

If the surfaces are not properly flat for lap joints, the improper weld will be obtained.

1.10. Applications of Laser Welding

The unique properties of laser welding give it a significant advantage over other forms of welding that can be exploited in several ways:

Precision parts: Lasers are excellent for welding fine and delicate metal components and

generating minimal internal stresses due to the minimal heat input.

Medical devices: Non-contact welding and no welding splatter ensure hygiene when welding medical devices.

Solenoids and machined items: Lasers are ideal for joining machined components such as solenoids, and create minimal distortion due to the low heat input.

Aesthetics: Laser welding finishes are excellent.

Limited access: The non-contact laser beam permits welding in otherwise inaccessible areas. The precise controllability and negligible heating effects make it a good choice for high welding value, high precision parts, including precious metals.

1.11.RSM Method for Experimental Design and Analysis

Response Surface Methodology (RSM), the method was introduced by G. E. P. Box and K. B. Wilson in 1951. It explores the relationships between several input variables and one or more response (Output) variables. The most extensive applications of RSM are in particular situations where several input variables potentially influence some performance measure or quality characteristic of the process. Thus performance measure or quality characteristic is called the response. The input variables are sometimes called independent variables, and they are subject to the control of the user. The field of response surface methodology consists of the experimental strategy for exploring the space of the process or independent variables, empirical statistical modelling to develop an appropriate approximating relationship between the yield and the process variables, and optimization methods for finding the values of the process variables that produce desirable values of the response. Once it is suspected that only significant independent variables are left, then a more complicated design, such as a central composite design can be implemented to estimate a second-degree polynomial model, which is still only an approximation at best.

1.11.1. Design of Experiment

Design of experiments is an organized way of conducting and analyzing controlled tests to evaluate the factors affecting response variables. It is one of the phases of experimental work where participating factors along with their levels are decided. The design specifies the particular setting levels of the combination of factors at which the individual runs in the experiments have to be conducted. It is a multivariable testing method where the simultaneous variation of factors are performed and as the factors are varied independently of

each other, a causal predictive model can be determined. Modern computer-based DOE tools can quickly build a design for any predictive model and they do it virtually for any real-world combination of factor types, additional constraints, and special models. It controls the inputs (factors) purposefully in such a way as to deduce their relationships (if any) with the output (responses).

- If the proposed model is simple, e.g. just main or first-order effects (x_1, x_2, x_3, etc.), the design is called a screening DOE.

- If the proposed model is more complex, e.g. the model is second order so that it includes two-way interaction terms (x_1x_2, x_1x_3, x_2x_3, etc.) and in the case of continuous factors, squared terms (x_1^2, x_2^2, x_3^2, etc.), the design is called a response-surface DOE.

1.11.2. RSM Approach to the Design of Experiment

Response surface methodology is a collection of mathematical and statistical techniques that are useful for analysis of problems in which several variables influence response of interest and the objective is to optimize the response.

If all variables are assumed to be measurable, the response surface can be expressed as follows:

$$\boldsymbol{y = (x_1, x_2, \ldots\ldots x_k) + \epsilon} \tag{1.1}$$

where y is the response of the system, $\boldsymbol{x_i}$ are the variables of action called factors and ϵ represents the noise. Error observed in the response y. If we denote the expected response by $(y) = (\boldsymbol{x_1, x_2}) = \sigma$, then the surface represented by $\sigma = (x_1, x_2)$ and is called a response surface.

In the practical application of RSM it is necessary to develop an approximating model for the true response surface. The approximating model is based on observed data from the process or system and is an empirical model. Multiple regression analysis is a collection of statistical techniques useful for building the types of empirical models required in RSM. If the response is well modeled by a linear function of the independent variables, then the approximating function is the first order model.

$$\boldsymbol{y = \beta_0 + \beta_1 x_1 + \beta_2 x_2 + \cdots + \beta_4 x_4 + \epsilon} \tag{1.2}$$

If there is curvature in the response system, then usually following second order polynomial equation is used in RSM:

$$\boldsymbol{y = \beta_0 + \sum_{i=1}^{k} \beta_i x_i + \sum_{i=1}^{k} \beta_i x_i^2 + \sum_{i=1}^{k-1} \sum_{j=2}^{k} \beta_{ij} x_i x_j + \epsilon} \quad (1.3)$$

where parameters $\boldsymbol{\beta_{ij} = 0, 1, \ldots, k}$ are called regression coefficients.

RSM is a sequential procedure. At a point on the response surface which is remote from the optimum. There is a little curvature in the system and the first-order model will be appropriate. Our objective here is to lead towards the general vicinity of the optimum along a path of improvement rapidly and efficiently. Once the region of the optimum has been found, a more elaborate model, such as the second order model may be employed and analysis may be performed to locate the optimum. From the below Figure 1.9, it can be seen that the analysis of a response surface can be thought of as "climbing a hill", where the top of the hill represents the point of maximum response. If the true optimum is a point of maximum response, then we may think of "descending into a valley".

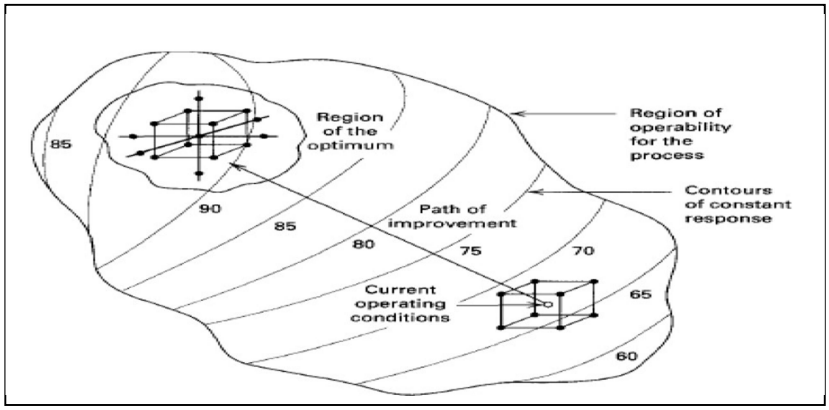

Figure 1.9 Optimization Process

Before exploring the path of steepest ascent, the adequacy of the first-order model should be investigated. The $2n$ design with the center points allow us to

1. Obtain an estimate of the error
2. Check for interactions (cross-product terms) in the model
3. Check for quadratic effects (curvature)

It may obtain a general mathematical solution for the location of the stationary point.

Writing the second order model in matrix notation, we have

$$\boldsymbol{\hat{y} = \widehat{\beta_0} + \dot{x}b + \dot{x}Bx} \quad (1.4)$$

where,

$$\boldsymbol{x} = \begin{bmatrix} \boldsymbol{x_1} \\ \vdots \\ \boldsymbol{x_k} \end{bmatrix} \boldsymbol{b} = \begin{bmatrix} \boldsymbol{\beta_1} \\ \vdots \\ \boldsymbol{\beta_k} \end{bmatrix} \boldsymbol{and\ B} = \begin{bmatrix} \widehat{\boldsymbol{\beta}}_{\boldsymbol{11}} & \cdots & \widehat{\boldsymbol{\beta}}_{\boldsymbol{1k/2}} \\ \vdots & \ddots & \vdots \\ \boldsymbol{sym} & \cdots & \widehat{\boldsymbol{\beta}}_{\boldsymbol{kk}} \end{bmatrix}$$

That is, b is a (k×1) vector of the first-order regression coefficients and B is a (k×k) symmetric matrix whose main diagonal elements are the pure quadratic coefficients (β_{ii}) and whose off-diagonal elements are one half the mixed quadratic coefficients ($\hat{\beta}_{ij}$, $i \neq j$),). The derivatives of$\hat{y}$ with respect to the elements of the vector x equated to 0 is

$$\frac{\partial \hat{y}}{\partial \boldsymbol{x}} = \boldsymbol{b} + \boldsymbol{2Bx} = \boldsymbol{0} \tag{1.5}$$

$$\boldsymbol{x_i} = -\frac{\boldsymbol{1}}{\boldsymbol{2}}\boldsymbol{B^{-1}b} \tag{1.6}$$

$$\hat{\boldsymbol{y}} = \widehat{\boldsymbol{\beta}}_{\boldsymbol{0}} + \frac{\boldsymbol{1}}{\boldsymbol{2}}\boldsymbol{x_0 b} \tag{1.7}$$

Suppose it has been needed to find the levels of $x_1,x_2,\ldots x_k$ that optimize the predicted response. This point if exists, will be a set of $x_1,x_2,\ldots x_k$for which the partial derivative $\frac{\partial \hat{y}}{\partial x_1} = \frac{\partial \hat{y}}{\partial x_2} = \cdots = \frac{\partial \hat{y}}{\partial x_k} = \boldsymbol{0}$. This point, say $x_{1,s},x_{2,s},\ldots x_{k,s}$, called the stationary point. Figure 1.10 shows three possibilities of being stationary point could be represented as (a) a point of maximum response, (b) a point of minimum response, (c) a saddle point.

Depending upon the nature of B, the stationary point either will be a minimum or a maximum, or a saddle point of the fitted response. Moving away from a saddle point in some directions produces an increase in the response, while moving away in other directions produces a decrease in the response.

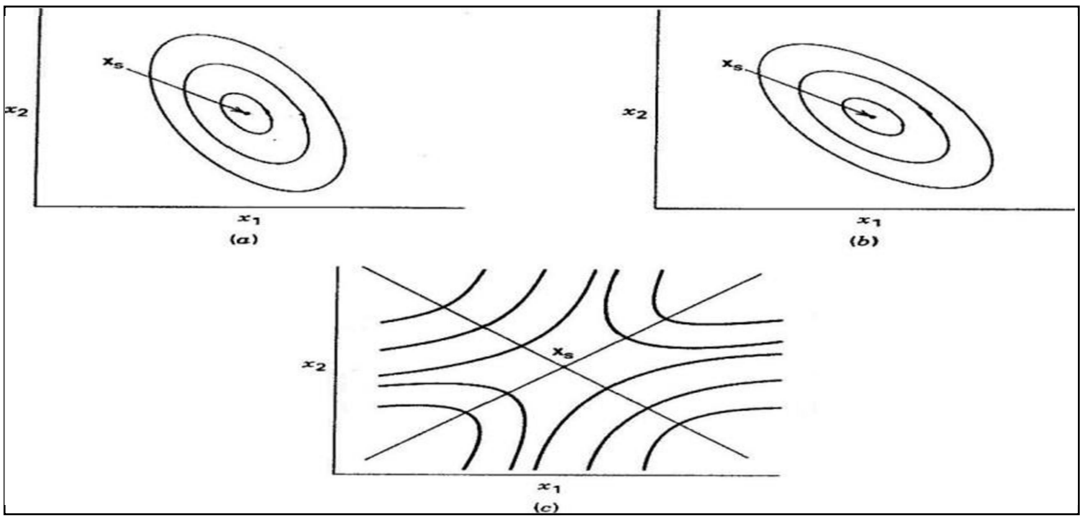

Figure 1.10 Stationary points represented as (a) a point of maximum response, (b) a point of minimum response, and (c) a saddle point.

Characteristics of stationary points:

- If B is positive definite: all Eigenvalues are positive, which indicates the minimum point.
- If B is negative definite: all Eigenvalues are negative, which indicates the maximum point.
- If B is indefinite: Eigenvalues are positive and negative, that indicates the saddle point.

Designs for fitting second order models

Two very useful and popular experimental designs that are followed in this method allow a second order model to be fit are

a. Central composite design (CCD)

b. Bark- Behnken design (BBD)

Both designs are build up from full factorial and fractional factorial designs.

a. Central Composite Design (CCD)

- Each factor varies over five levels
- Typically smaller than Box-Behnken designs
- Built upon two-level factorials or fractional factorials of Resolution V or greater
- Can be done in stages: factorial + centre points + axial points
- Rotatable

General structure of CCD

- $2k$ factorials + 2k star or axial points + nc points
- The factorial part can be a fractional factorial as long as it is of resolution V or greater so that the 2-factor interaction terms are not aliased with each other 2-factor interaction terms.

- The "star" or "axial" points in conjunction with the factorial and centre points allows the quadratic terms (bii) to be estimated.

b. Box-Behnken Designs (BBD)

- The Box-Behnken design is an independent quadratic design in that it does not contain an embedded factorial or fractional factorial design.
- In this design the treatment combinations are at the midpoints of edges of the process space and at the center.
- These designs are rotatable (or near rotatable) and require 3-levels of each factor.
- The designs have limited capability for orthogonal blocking compared to the central composite designs.

General structure of BBD

- Each factor is varied over three levels (within low and high value)
- Alternative to central composite designs which require 5 levels
- BBD not always rotatable
- Combinations of 2-level factorial designs from the BBD

Generally, CCD is preferred over BBD. In this work, a 3 factorial 3 level CCD-RSM approach has been selected for performing the experiments.

1.11.3. Desirability Function Analysis

Derringer and Suich first propose the desirability function analysis method in 1980. This method makes use of a technique for combining multiple responses into a dimensionless measure of performance called the composite desirability function. The general approach of desirability function is to transfer each response y_i into unitless desirability functions (d_i), bounded by $0 \leq d_i \leq 1$. The desirable ranges are from zero to one, at least to most desirable, respectively.

For the goal of maximum, the desirability function is given by,

$$\boldsymbol{d_i} = \begin{cases} \mathbf{0} & \boldsymbol{if\ response\ (y_i) \leq low\ rate\ (L_i)} \\ \left(\frac{\boldsymbol{y_i - L_i}}{\boldsymbol{H_i - L_i}}\right)^{\boldsymbol{wt_i}} & \boldsymbol{as\ response\ (y_i)\ varies\ from\ low\ rate\ (L_i)} \\ \mathbf{1} & \boldsymbol{if\ response\ (y_i) \geq low\ rat\ \ (L_i)} \end{cases} \quad (1.8)$$

For the goal of minimum, the desirability function is given by,

$$d_i = \begin{cases} 1 & if\ response\ (y_i) \le low\ rate\ (L_i) \\ \left(\frac{y_i - L_i}{H_i - L_i}\right)^{wt_i} & as\ response\ (y_i)\ varies\ from\ low\ rate\ (L_i) \\ 0 & if\ response\ (y_i) \ge low\ rate\ (L_i) \end{cases} \quad (1.9)$$

A weight can be assigned to a goal to emphasize the particular desirability function. Weights can be ranged between 0.1 and 10. A weight greater than 1 gives more emphasis to the goal, while weights less than 1 give less emphasis. The simultaneous objective function D is a geometric mean of all transformed responses:

$$D = (d_1^{r_1} \times d_1^{r_2} \times \dots\dots\dots \times d_1^{r_n})^{1/\sum r_i} = (\prod_{i=1}^{n} d_i^{r_i}) \quad (1.10)$$

where, n is the number of responses in the measure. Each response can be assigned importance, relative to the other responses. Importance (r_i) values vary from 1, the least important, to 5, the most important.

1.11.4. Application Procedures

The Response Surface Methodology is used to improve the quality of the experimental procedures. A higher level of performance provides improved quality products consistently.

The highest possible performance is obtained by determining the optimum combination of design factors.

i) Brainstorming:

- To identify all influencing factors and those to be included in the study
- To determine the factor levels

ii) Designing Experiments:

- To select the appropriate model design
- To assign factor and interaction to columns
- To describe each trial condition
- To decide order and repeat trials

iii) Running Experiment:

- To run experiments in random order when possibl

iv) Analyzing Results:

- To achieve the optimum design
- To influence the individual factors
- To achieve performance at the optimum conditions

v) Running confirmation experiments:

- Running the experiments at the optimum condition is the necessary final step.

Once the confirmatory experiment is over it is necessary to do two other things: An accurate costing of the effects of the optimal level of the product is carried out and also a detailed report is presented on the findings to make use of in other similar products.

1.11.5. Analysis of Results

Experimental results are analyzed to achieve the following objectives:

- To achieve the optimal condition for the product or process
- To establish the contribution of individual factors
- To estimate the response under optimal conditions

To analyze the results of the experiments obtained from the Central Composite design model and to determine how much each of quality-influencing factors has contributed to a statistical method- Analysis of Variance (ANOVA) is used.

1.11.6. Analysis of Variance (ANOVA)

Analysis of variance (ANOVA) is a collection of the statistical model used for analysing the differences among the group means and their associated procedures (such as "variation" among and between groups). Statistician and evolutionary biologist Ronald Fisher developed it. The purpose of the analysis of variance is to investigate which welding parameters significantly affect the responses. This process is carried out by comparing the F-test value of the parameter with the standard F table value (F=0.05) at the 5% significance level. The associated P values of less than 0.05 for the models (i.e., α=0.05, or 95% confidence level) indicate that the model terms are statistically significant. Percentage contribution of process parameters on response is determined from Seq SS values of ANOVA table. Percentage contribution is calculated using the following expression.

$$\textbf{\textit{Percentage contribution of a term}} = \frac{\textbf{\textit{Seq SS for the term}}}{\textbf{\textit{Total Seq SS}}} \times 100\% \qquad (1.11)$$

where,

SS=Sum of squared deviation

Seq SS=Sequential sum of square deviation

F=Fisher's ratio,

P=Probability of significance

1.11.7. Applications and Limitations of RSM

Response surface methodology uses statistical models, and therefore, practitioners need to be aware that even the best statistical model is an approximation to reality. Response surface methodology has an effective track-record of helping researchers improve products and services. For example, Box's original response-surface modeling enabled chemical engineers to improve a process that had been stuck at a saddle-point for years. The engineers had not been able to afford to fit a cubic three-level design to estimate a quadratic model, and their biased linear-models estimated the gradient to be zero. Box's design reduced the costs of experimentation so that a quadratic model could be fit, which led to a (long-sought) ascent direction. It also has applications in automotive suspension designs.

In practice, both the models and the parameter values are unknown, and subject to uncertainty on top of ignorance. Of course, an estimated optimum point need not be optimum in reality, because of the errors of the estimates and of the inadequacies of the model [53].

1.12. FEA Analysis of the Physical Model

The finite element method (FEM), is a numerical method for solving problems of engineering. Typical problem areas include structural analysis, heat transfer, fluid flow, mass transport, and electromagnetic potential. The analytical solution of these problems generally requires the solution to boundary value problems for partial differential equations. The finite element formulation of the problem results in a system of linear equations. The method approximates the unknown function over the domain. It subdivides a large system into smaller, simpler parts that are called finite elements to solve the problem. The simple equations of these finite elements are then assembled into a larger system of equations that models the entire problem. FEM then uses variational methods from the calculus of variations to approximate a solution by minimizing an associated error function. Welding is a problem of heat transfer, so for numerical simulation FEA method is used [55].

1.12.1 Variational Formulation for Heat Transfer Problem

The problem of steady-state heat transfer with only the conduction and convection modes have been analyzed (as the radiation mode makes the problem nonlinear). The strong forms of the governing equations have been presented then it is shown how the variational formulations can be derived from it. The independent solution field (the temperature) is a scalar so that its variation is also a scalar field.

1.12.1.1 Strong Form of the Governing Equation

Let Ω be an open domain whose boundary Γ is composed of two open, disjoint regions, $\boldsymbol{\Gamma = \overline{\Gamma_T \cup \Gamma_q}}$. The governing equations are

$$\boldsymbol{\nabla \cdot q = Q \; on \; \Omega},$$

$$\boldsymbol{q = -K\Delta T \; on \; \Omega},$$

$$\boldsymbol{T = \bar{T} on \; \Gamma_T},$$

$$\boldsymbol{h(T - T_\infty) + (k\Delta T) \cdot n = \bar{q} on \; \Gamma_q},$$

where T is the absolute temperature, q is the heat flux, Q is the heat generated per unit volume, k is a symmetric second-order tensor known as the thermal conductivity tensor, n is the outward normal to Γ, T_∞ is the absolute temperature of the surrounding medium (also known as the ambient temperature), $\bar{T}$ is the prescribed temperature on Γ_T , and $\bar{q}$ is the externally applied heat flux on Γq Note that $\bar{q}$ is taken as positive when the heat is supplied to the body. Typical units of the field variables and material constants in the SI system are

$$\boldsymbol{T:} \; ℃, \boldsymbol{k_{ij}:} \; \boldsymbol{W/(m -} \; ℃), \boldsymbol{Q:} \; \boldsymbol{W/m^3}, \boldsymbol{q:} \; \boldsymbol{W/m^2}, \boldsymbol{h:} \; \boldsymbol{W/(}m^2 - ℃).$$

For presenting the variational formulation, we define the function spaces

$$\boldsymbol{V_T = \{v \in H_1(\Omega); \; v = 0 \; on \; \Gamma_T\}},$$

$$\boldsymbol{L_T = \tilde{T} + V_T \; where \; \tilde{T} \in H_1(\Omega) \; satisfies \; \tilde{T} = \bar{T} on \; \Gamma_T}$$

1.12.1.2. Variational formulation

The variation of the governing equation is

$$\int_{\Omega} \boldsymbol{v}\,[\boldsymbol{\nabla \cdot (k\Delta T) + Q}]\boldsymbol{d\Omega} + \int_{\Gamma_q} \boldsymbol{v}[\bar{\boldsymbol{q}} - \boldsymbol{h(T - T_\infty)} - \boldsymbol{(k\Delta T) \cdot n}]\boldsymbol{d\Gamma} = \boldsymbol{0} \; \forall \; \boldsymbol{v} \in \boldsymbol{V_T}$$

using the identity,

$$\boldsymbol{v}\left(\boldsymbol{\nabla}\cdot\left(\boldsymbol{k}\Delta\boldsymbol{T}\right)\right)=\boldsymbol{\nabla}\cdot(\boldsymbol{v}\boldsymbol{k}\Delta\boldsymbol{T})-\boldsymbol{\nabla}\boldsymbol{v}\cdot(\boldsymbol{k}\Delta\boldsymbol{T}),$$

Now the above equation can be written as

$$\int_{\boldsymbol{\Omega}}\boldsymbol{\nabla}\cdot(\boldsymbol{v}\boldsymbol{k}\Delta\boldsymbol{T})\,\boldsymbol{d\Omega}-\int_{\boldsymbol{\Omega}}[\boldsymbol{\nabla}\boldsymbol{v}\cdot(\boldsymbol{k}\Delta\boldsymbol{T})-\boldsymbol{v}\boldsymbol{Q}]\,\boldsymbol{d\Omega}\int_{\boldsymbol{\Gamma_q}}\boldsymbol{v}[\,\overline{\boldsymbol{q}}-\boldsymbol{h}(\boldsymbol{T}-\boldsymbol{T}_\infty)-(\boldsymbol{k}\Delta\boldsymbol{T})\cdot\boldsymbol{n}]\boldsymbol{d\Gamma}=\boldsymbol{0}$$

$$\forall\,\boldsymbol{v}\in\boldsymbol{V_T}$$

Applying the divergence theorem to the first term on the left-hand side, and putting $\boldsymbol{v}=\boldsymbol{0}$ on $\boldsymbol{\Gamma_T}$ from boundary condition, it is found,

$$\int_{\boldsymbol{\Omega}}[\boldsymbol{\nabla}\boldsymbol{v}\cdot(\boldsymbol{k}\Delta\boldsymbol{T})-\boldsymbol{v}\boldsymbol{Q}]\,\boldsymbol{d\Omega}\int_{\boldsymbol{\Gamma_q}}\boldsymbol{v}[-\overline{\boldsymbol{q}}+\boldsymbol{h}(\boldsymbol{T}-\boldsymbol{T}_\infty)]\boldsymbol{d\Gamma}=\boldsymbol{0}\;\forall\,\boldsymbol{v}\in\boldsymbol{V_T}$$

by taking the known term to right-hand side the variational statement can be written as,

Find $\boldsymbol{T}\in\boldsymbol{L_T}$ such that

$$\int_{\boldsymbol{\Omega}}[\boldsymbol{\nabla}\boldsymbol{v}\cdot(\boldsymbol{k}\Delta\boldsymbol{T})]\,\boldsymbol{d\Omega}+\int_{\boldsymbol{\Gamma_q}}\boldsymbol{v}\boldsymbol{h}\boldsymbol{T}\boldsymbol{d\Gamma}\;=\int_{\boldsymbol{\Omega}}\boldsymbol{v}\boldsymbol{Q}\boldsymbol{d\Omega}+\int_{\boldsymbol{\Gamma_q}}\boldsymbol{v}[\;\overline{\boldsymbol{q}}+\boldsymbol{h}\boldsymbol{T}_\infty]\boldsymbol{d\Gamma}\quad\forall\,\boldsymbol{v}\in\boldsymbol{V_T}$$

1.12.2 Methodology of FEM

The steps involved in a finite element formulation are as follows:

1. Discretizing the domain into a collection of elements, Number the nodes of the elements and generating the geometric properties such as coordinates needed for the problem.
2. Assembling the element level matrices to form the global equation, For example, for heat transfer problem a matrix equation of form $Kw = f$ can found.
3. Imposing the boundary conditions,
4. Solving the assembled equations,
5. Carrying out the post-processing of the results.

1.12.3 Finite Element Formulation for Heat Transfer Problem

The purpose of the finite element method is the variational statement can be used directly. The thermal conductivity is a second order tensor so the temperature T can be written in terms of the interpolation functions as

$$\boldsymbol{T}=\boldsymbol{N}\widehat{\boldsymbol{\omega}}+\overline{\boldsymbol{N}}\overline{\widehat{\boldsymbol{\omega}}}$$

where $\widehat{\boldsymbol{\omega}}$ is the vector of the unknown temperatures at the nodes, N is the shape function associated with the nodes where the temperature is unknown, $\overline{\widehat{\boldsymbol{\omega}}}$ is the vector of the prescribed

temperatures at the nodes lying on Γ_T , and $\overline{\boldsymbol{N}}$ are the corresponding shape functions. Noting that the variation, v, of the temperature vanishes on Γ_T, so

$$\boldsymbol{v} = \boldsymbol{N}\widehat{\boldsymbol{v}}$$

The gradient of T is given by,

$$\Delta \boldsymbol{T} = \boldsymbol{B}\widehat{\boldsymbol{\omega}} + \overline{\boldsymbol{B}}\overline{\widehat{\boldsymbol{\omega}}}$$

where

$$\boldsymbol{B_{ij}} = \frac{\boldsymbol{\partial N_j}}{\boldsymbol{\partial x_i}}$$

$$\overline{\boldsymbol{B_{ij}}} = \frac{\boldsymbol{\partial \overline{N_j}}}{\boldsymbol{\partial \overline{x}_i}}$$

Substituting these values in variational statement and considering the arbitrary nature of v FE formulation found as,

$$\boldsymbol{K}\widehat{\boldsymbol{\omega}} = \boldsymbol{f}$$

where

$$\boldsymbol{K} = \int_{\boldsymbol{\Omega}} \boldsymbol{B^t k B d} \quad + \int_{\boldsymbol{\Gamma_T}} \boldsymbol{h N^t N d \Gamma_T}$$

$$\boldsymbol{f} = \int_{\boldsymbol{\Omega}} \boldsymbol{N^t Q d\Omega} + \int_{\boldsymbol{\Gamma_T}} \boldsymbol{N^t}(\overline{\boldsymbol{q}} + \boldsymbol{h T_\infty}) \boldsymbol{d\Gamma_T} - \left(\int_{\boldsymbol{\Omega}} \boldsymbol{B^t k B d\Omega} \right) \overline{\widehat{\boldsymbol{\omega}}}$$

K is symmetric and positive definite by virtue of the symmetry and positive-definiteness of k. The second term in the 'stiffness' matrix, K, involves an integral over part of the surface of the domain. If n is the number of free degrees of freedom and m the number of prescribed degrees of freedom, then the order of the various matrices in a three-dimensional problem is as follows:

$\boldsymbol{K}: \boldsymbol{n} \times \boldsymbol{n}, \widehat{\boldsymbol{\omega}}: \boldsymbol{n} \times \boldsymbol{1}, \boldsymbol{f}: \boldsymbol{n} \times \boldsymbol{1}, \boldsymbol{N}: \boldsymbol{1} \times \boldsymbol{n}, \boldsymbol{B}: \boldsymbol{3} \times \boldsymbol{n}, \overline{\boldsymbol{B}}: \boldsymbol{3} \times \boldsymbol{m}, \overline{\widehat{\boldsymbol{\omega}}}: \boldsymbol{m} \times \boldsymbol{1}, \overline{\boldsymbol{N}} = \boldsymbol{1} \times \boldsymbol{m}$ [54].

1.13. Literature Review

Polymers are found in a broad variety of products from the very simple ones to the extremely complex ones; from domestic products to food and medical product packages, electrical devices, electronics and automobiles because of their good strength to weight ratio, ease of fabrication of complex shapes, low cost and ease of recycling. Plastics joining technology has now been focused on the industries of automobile, telecommunication, construction as well as in medical manufacturing. Conventional plastics joining methods are so far as adhesives, fasteners, hot plate welding, ultrasonic or vibration welding have been established but may no longer be persistent in the recent plastic industry [1].

Welding of plastics using lasers becomes prominent in the industry as well as in the field of research. Laser welding is a trending high-energy-density joining process. Laser welding has several advantages when compared to conventional welding techniques. The method is non-contact type and localized narrow heat zone can result in high-quality welds. Laser welding has been widely applied in various industries including automotive, microelectronics, aerospace, medical, optoelectronics, microsystems, packaging, etc [2]. This welding technique can have a wide application to weld different thicknesses, similar and dissimilar materials or different surface materials together. Generally, for the thick plate, the continuous laser is used and for the thin plate, a pulsed laser is used [3]. In the polymer industry, there are various applications for TTLW and different types of lasers are used. Since the majority of polymers strongly absorb at 10.6 μm, CO_2 lasers are restricted to thin polymer films welding. Whereas, the Nd: YAG laser and diode laser are suitable for thick part welding due to the high transmission of polymers in the near infrared field [4]. The compact design, modular set-up and high efficiency of diode lasers make them more appropriate for industrial applications. Hence, the diode laser transmission welding is an innovative technique for joining thermoplastics [5, 6].

One of the basic configurations for laser transmission welding of polymers is an overlap joint assembled by a transparent polymer work material placed on the top of an absorbing polymer. The laser beam transmits the upper "transparent" part and is converted into heat by the absorbing lower part. Since both parts need to be pressed together, heat is conducted from the absorbing lower part allowing both parts to melt and create a joint only where the laser beam is directed. Special additives/pigments also allow laser transmission welding of dark to dark materials as well as transparent to transparent workpiece [7]. Polycarbonate and acrylics are widely used in several industries and is considered as difficult to join, the diode laser welding technique can overcome this problem [8, 9]. There are various welding parameters (laser power, scanning speed, spot size, clamping pressure etc.) that influence the quality (joint strength, weld width, HAZ, depth of penetration etc.) of the weld. Optimization is an important tool to find the combination of welding parameters to achieve a quality weld.

Several research publications and information are available in the field of transmission laser welding of polymers. Researchers had done experiments, modelling and analyses emphasizing parametric effects on weld quality, process optimization, performance evaluation and other related aspects. Few worked on process optimization of dissimilar

material welding of polycarbonate and acrylic. In the following paragraphs, a comprehensive literature survey is put forward.

The parametric experimentation and observation of laser transmission welding of black acrylic using Taguchi orthogonal array for the design of the experiment and optimisation of process parameters have been conducted by **Acharjee** et al. [10]. **Kumar** et al. [11] have performed multi-objective optimisation of TTLW of dissimilar plastics using response surface methodology (RSM). They have chosen power, scanning speed and frequency as input parameters and for measured responses breaking load and weld width have been selected. **Shin** and **Choi** [12] have studied the design of energy optimisation for laser joining process of polymer (ABS and PC). The heat affected zone (HAZ) and melt zone measurement are performed to find the joining energy threshold and the mechanical properties of welds. **Acherjee** et al. [13] investigated the effects of process parameters, namely, laser power, welding speed, size of the laser beam and clamp pressure, on the lap-shear strength and weld width for laser transmission welding of acrylic using a diode laser system. They have used RSM to develop the mathematical equations between the process parameters and the output variables of the weld joint to determine the welding input parameters that lead to the desired weld quality.

Wang et al. [14] have used an intelligent method for simulation and optimisation of continuous laser transmission welding (LTW) and validate it with experiments. They have developed a thermal model using finite element method (FEM) which has been combined with response surface methodology (RSM) and genetic algorithm (GA) techniques to improve the veracity of the model prediction with less time spending on the experiments. A central composite rotatable experimental design (CCRD) for plan of experiment of laser transmission joining of polycarbonate thermoplastic has been generated by **Wang** et al. [15] They have also established the mathematical relationships between the process parameters (laser power, joining velocity, clamp pressure, scanning number) and the three responses as the joint strength, joint width and joint cost and then the optimisation has been conducted using design-expert software to carry out the multi-objective optimisation of the joining process to get better welding. In the work of **Jiao** et al. [16], experiments with different joining parameters have been carried out on fiber laser welding system to explore the mechanism of CFRTP/stainless steel joining and to find the influence of the parameters on the joining quality. Also, the optimum condition for the best joint quality has been obtained as the laser power at 280 W, the joining speed at 4 mm/s and the clamper pressure at 0.15

MPa. **Katsiropoulos** et al. [17] have applied a generic optimisation concept using LTSM-OPT software tool for the optimization of thermal process cycle and laser welding unit parameters for both the quality and cost of the produced (thermoplastic composite materials) part. **Ai** et al. [18] have studied a defect-reducing optimization method that considers the geometric features of weld bead as evaluation indexes of welding defects and process parameters effect on the responses. The particle swarm optimization and back propagation neural network (PSO-BPNN), which has proved to be good modeling for no-linear problems, are utilized to establish the mathematical model. They have selected genetic algorithm (GA) to solve the model. The effect of significant factors on the responses has been identified based on the calculation of signal to noise (S/N) ratio and analysis of variance (ANOVA). A fuzzy logic technique applied with Taguchi method to optimize the submerged arc welding process for multiple performance characteristics with arc current, arc voltage, welding speed, electrode protrusion and preheat temperature acting as a process parameters have been found in the research of **Tarng** et al. [19]. **Kumar** et al. [20] have applied Taguchi's L9 orthogonal array to find best parameter settings of welding current, welding voltage, welding travel speed and a number of welding passes in MIG welding process. Also, the study of the welding parameters effect on residual stresses and hardness of weld specimen has been carried out by a statistical technique, i.e. analysis of variance (ANOVA) and signal to noise (S/N) ratio.

In the research of **Chen** et al. [21], a model has been developed to describe the laser energy distribution in light scattering polymers. After that, the models have been validated using PA6, PA6GF and PP parts. A three-dimensional, finite element model have been constructed by **Chen** et al. [22], to simulate heat transfer in contour laser transmission welding of an amorphous polymer (polycarbonate). The modeling results have been supported by the experimental observations of weld width and weld initiation power. Also, the simulation results indicate that, in contour welding of polycarbonate, welding initiates when the temperature at the weld interface reaches the maximum of 200 °C. **Aden** [23] have studied the temperature profile for Gaussian- and M-shape beams for laser-transmission welding of PC (non-scattering polymer) and polybutylene terephthalate (strong scattering polymer). They have found that for polycarbonate the seam generated by a Gaussian beam has a non-homogeneous thickness and a width that is smaller than the beam diameter. Whereas, for an M-shape beam it has a homogeneous thickness and its width scales with the width of the integrated intensity. While the distributions of the integrated intensities and the

dimensions of the seam are similar for both types of beams for polybutylene terephthalate. The effect of the optical parameters of polycarbonate on temperature field and molten pool geometry during the welding process has been analysed with the aid of the FE model by **Geiger** et al. [24]. **Hadriche** et al. [25] have proved the reliability of a numerical model based on the finite difference method by calculating the soundness variables for diode laser welding of polycarbonate thermoplastic polymer. Microscopy observation of experimental polycarbonate welds has validated the numerical model. An integrated experimental-simulation study has been carried out to optimise the laser-assisted joining of metals and plastics by **Lambiase** et al. [26]. **Casalino** and et al. [27] have analysed the keyhole and conduction welding for butt and overlap configurations. The thermo-morphologic and mechanical behaviour of moulded thermoplastic polymers during laser welding have been simulated using the finite element method (FEM). A numerical model has been made by **Zoubeir** et al. [28], to study the temperature field and residual stresses distribution for laser diode transmission welding of a polypropylene mini-tank. An investigation on the relationships of process parameters, molten pool geometry and shear strength in laser transmission welding of polyethene terephthalate and polypropylene has been conducted by **Wang** et al. [29]. They suggested in their result that the molten pool depth to width (D/W) ratio has a significant influence on the shear strength. **Mollicone** et al. [30] have developed thermo-elastic–plastic simulation models to study the welding distortion. They have studied the butt welding of thin rectangular plates, the results of main interest are the out-of-plane distortion and longitudinal residual stresses. The welding deformation in the fillet-welded joint using numerical simulation and comparison with experimental results has been studied by **Murakawa** et al. [31]. A two-dimensional thermal model has been developed by **Becker** et al. [32], to simulate the heating phase of the laser transmission welding process along the moving beam direction using FEM. They have validated the results with collected data from experiments. Modelling has been developed by **Liu** et al. [33], for laser heat source by considering light scattering during laser transmission welding. They have proposed the energy transformation algorithm to transform the line energy intensity into the point energy intensity. The weldability of a polymeric material through simulation has been studied by **Ilie** et al. [34]. Infrared thermography has validated the results of the simulation. The Numerical and experimental investigation of laser transmission welding of fibreglass-doped PP and ABS has been done by **Chen** et al. [35]. Modelling has been developed by **Coelho** et al. [36], to find the influence of spot shape on high-speed transmission lap welding of thermoplastics films. **Flock** et al. [37] have developed a numerical model for the thermal characterisation of

laser transmission welding to predict the temperature distribution and the heat affected zone. An efficient tool has been developed by **Ilie** et al. [38], for determining the weldability of polymeric materials for the reduction of time and costs with the experimental exploration. **Purtonen** et al. [39], have given a summary of the overview of non-contact monitoring methods are used for in-process monitoring of laser-based processes like welding, cladding and additive manufacturing of metallic materials. **Shao** et al. [40] have presented a brief introduction of process signal sensing techniques such as acoustic, optical, visual, thermal and ultrasonic during laser welding. **Speka** et al. [41] have used a contact-free method such as IR thermography for surface temperature measurement on a typical configuration for the through-transmission laser welding of polymers. The process for building up a new class of polymer fluidic micro-sensors and actuators with foreign matter free, physicochemical inert flow paths for applications in the field of pharmaceutics, biotechnology and life sciences as well as for high-temperature automotive applications has been investigated by **Truckenmiller** et al. [42].

The influence of process parameters, both the laser power (20–40 W) and the welding speed (3–6 mm/s) on the geometry and the microstructure of the polypropylene weld zone have been investigated by **Ghorbel**et al. [43]. They have determined the effects of selected welding parameters on the seam geometry, defects and material crystallinity. They have found that the increase of the laser power and the decrease of the scanning speed lead to a larger volume of the weld zone with a more important depth penetration and Fourier transform infrared (FTIR) spectroscopy method shows that diode laser welding induces thermal degradation. **Wang** et al. [44] have presented a technique for quantifying the carbon black (CB) morphology in polyamide 6 (PA6) and polycarbonate (PC) used in laser welding applications. The microstructure of the CB has been observed by transmission electron microscopy (TEM). The TEM photomicrographs of CB have been quantitatively analysed using an image processing technique. The microstructural parameters such as size, shape and distribution of CB particles and aggregates are obtained. **Abed** et al. [45] have studied the laser transmission welding of polymers using a diode laser. They have found that the crystalline morphology observed in different zones in the welded part has related to a specific thermal cycle. In the work of **Ma** et al. [46], the Synthesis and characterisation of polycarbonate glycol-based waterborne polyurethane with a high solid content have been investigated. **Hansch** et al. [47] have examined that the pigment has a limited and intensive range of absorption in the visible range. It has been concluded that the different absorption

characteristics of laser energy in the near-infrared region. **Xu** et al. [48] have studied the effect of glass fibre and crystallinity on the light transmission during laser transmission welding of thermoplastics. A study on the relationship between the optical characterisation of coloured and non-coloured polyamides and laser welding process parameters has been studied by **Grewell** et al. [49]. They have concluded that the addition of pigments can enhance the scattering of laser radiation, which can increase the effective weld time or minimal energy requirement to make a weld. **Wehner** et al. [50] have investigated the diode laser in the manufacture of microfluidic devices. A transparent polycarbonate plate cover has been welded with the polycarbonate baseplate containing a different proportion of carbon black content. They have recommended the higher carbon black content due to the shallower weld seam. **Haberstroh** et al. [51] have examined the influence of carbon black content on the formation of the weld seam when joining thermoplastics in micro-technology applications. The carbon black content has varied from 0.5% to 1.5%. It has been noticed that, with an increase in the carbon black content, the penetration depth decreased from 29 μm to 9 μm. The effect of specific nylon composition factors, such as fiberglass, mineral, impact modifier content and the colour version on the near infra-red transmission has been investigated by **Bray** et al. [52].

1.14. Scope and Objective of the Present Work

The literature survey indicates that many researchers have taken into consideration several areas of laser welding. If only "through transmission laser welding" of polymer is concerned, publications are not found to be rare, but at the same time literature in this context is not rich either. Indeed, different aspects (process optimisation, characterisation, finite element modelling, etc.) of laser welding of plastics have been addressed by the researchers. But the process is not a very conventional one; the overall aim of this work is to achieve a deep and broad understanding of the laser welding process with a view to enabling the eventual realization to make laser welding a fully controlled manufacturing process. The requirement is to produce the desired quality of weld including reduce scrap rate (perforation, minimum HAZ), and increase product throughput which is still a challenge to the researchers, technologists and the practising engineers. Quality, in turn, depends on many factors and it is obvious that welding parameters (laser power, scanning speed, frequency, beam diameter, clamping pressure, etc) influence the quality of weld (joint strength, weld width, HAZ, etc). In the domain of "through transmission laser welding" of polymer, a strong and rich knowledge base requires to be developed. This knowledge base may be created only through

continued and extensive research covering various aspect of “through transmission laser welding” of polymers. The results of the research will thus help the researcher and industries in practice to control the process more efficiently. It will thus also be possible to predict, more reliably, the quality of weld under given conditions, i.e., under selected levels of the process variants.

Keeping the above observation in mind, in the present work, TTLW of transparent polycarbonate to transparent acrylic has been investigated. No additional absorbent is used in the process. Emphasis has been given to identify the effect of the most significant input parameters on the quality of the weld. The input parameters are selected from the literature are laser power (P), scanning speed (SS) and repetition frequency (f). The clamping pressure and spot diameter have been kept constant throughout the process. Output responses that describe the quality of the weld are described as weld width (WW), heat affected zone (HAZ), and ultimate load (UL). Lap joints are made and weld profile is square in shape. Planning of the experiment done by, 3 factor 5 level full-factorial CCD using response surface methodologies. The limiting values for RSM are selected using literature and trial and error method. The RSM has been used to define the relationship between inputs and responses. Analysis of variance (ANOVA) is used for testing the adequacy of the developed model. The mathematical relationships are further used to optimize the welding parameters to achieve the desired weld quality. Desired weld quality can also be predicted by thermal modelling. Thermal modelling using FEA has been done to understand the process inputs and there effects more significantly. The results from both the experiment and thermal modelling being observed and compared in the later sections. One dimensional heat transfer model has been used as heat is the main working load for thermal modelling of the welding process. The quality of the weld is tested by measuring the ultimate load, weld width and HAZ of the welded samples. Multi-objective optimization has been conducted to maximize ultimate load and weld width whereas minimizing the HAZ simultaneously. Depth of penetration is also measured for some selected samples the criterion for selection has been chosen as the minimum and maximum ultimate load, i.e. best and worst weld strength. The observed results are discussed later.

Chapter 2

2. Experimental Planning, Set Up, Procedure and Thermal Modeling

Laser transmission welding is one of the best techniques of plastic joining as per the literature survey. Though this process is in trend nowadays, but the joining of transparent to transparent dissimilar material is still a challenge. This work has been aimed to counter the challenge of joining transparent to transparent acrylic and polycarbonate welding. This has been planned by a definite orientation as described below:

- Selecting the most effective process parameters from the literature survey.
- Selecting the upper and lower limit of the process parameters using a trial and error method.
- Identifying suitable experiment design and planning the experiments
- Performing the experiments.
- Characterizing the important experiment responses such as weld width, heat affected zone, ultimate load.
- Identifying the effects of process parameters on responses.
- Simulate the thermal model of the problem.
- Optimizing the responses and comparing them with the thermal model results.
- Analyzing the final results.

2.1. Experimental Planning

2.1.1. Process Parameter and their Limits

In the present work, three key process parameters are Power (W), Frequency (kHz), Scanning Speed has been selected. As for the design of the experiment, a 3 factor 5 level CCD design has been chosen so by trial and error method, these levels are selected. The key process parameters and their levels are shown in Table 2.1.

Table 2.1 Process parameters and their limits

Parameters	Units	Level 1 (-2)	Level 2 (-1)	Level 3 (0)	Level 4 (+1)	Level 5 (+2)
Power (P)	W	7.12	7.42	7.88	8.35	8.67
Frequency (f)	kHz	265.15	300	350	400	434.09
Scanning Speed (SS)	mm/s	0.65	1	1.5	2	2.34

2.1.2. Design Matrix

The experiment is designed, based on a three-factor three-level central composite rotatable design. The design matrix is given in Table 2.2. The CCD comprises of 2^3(=8) factorial design plus 6 center points in cube and 6 axial or star points with alpha value 0.0667. All welding variables at the intermediate (0) level constitute the center points while the combination of each of the welding variables at either its lowest value (-1) or its highest value (+1) constitute the star points. Thus the 20 experimental runs allowed the estimation of the linear, quadratic and two way interactive effects of the process parameters on the response parameters.

Table 2.2 Design matrix obtained from MINITAB 18

Run Order	Power (W)	Frequency (kHz)	Scanning Speed (mm/s)
1	8.35	300.00	2.00
2	8.35	400.00	1.00
3	7.89	350.00	2.34
4	7.42	300.00	2.00
5	8.35	400.00	2.00
6	7.89	350.00	1.50
7	7.12	350.00	1.50
8	7.89	350.00	1.50
9	7.89	350.00	1.50
10	7.89	265.91	1.50
11	7.42	400.00	1.00
12	7.42	400.00	2.00
13	7.89	350.00	1.50
14	7.42	300.00	1.00
15	8.35	300.00	1.00
16	7.89	350.00	1.50
17	7.89	350.00	1.50
18	7.89	350.00	0.65
19	8.67	350.00	1.50
20	7.89	434.09	1.50

2.2. Experimental Setup

2.2.1. Sample Configuration and Work Materials

The work material has been chosen as 0.5mm thick sheet of transparent acrylic plastic and polycarbonate. The dimensions of the samples are set as 100 X 35 X 0.5 and lap welding configuration has been chosen with the overlap zone of 70 mm. The upper plate has been selected as polycarbonate due to its high transparency, whereas the bottom one has been transparent acrylic as it has more absorption. The welding has been done on a profile of 20 mm square. Temperature-dependent properties such as thermal conductivity (K), density (ρ), Specific heat (Cp) of acrylic and polycarbonate are necessary for thermal modeling of the physical welding process. The diagram of the samples is shown in Figure 2.1.

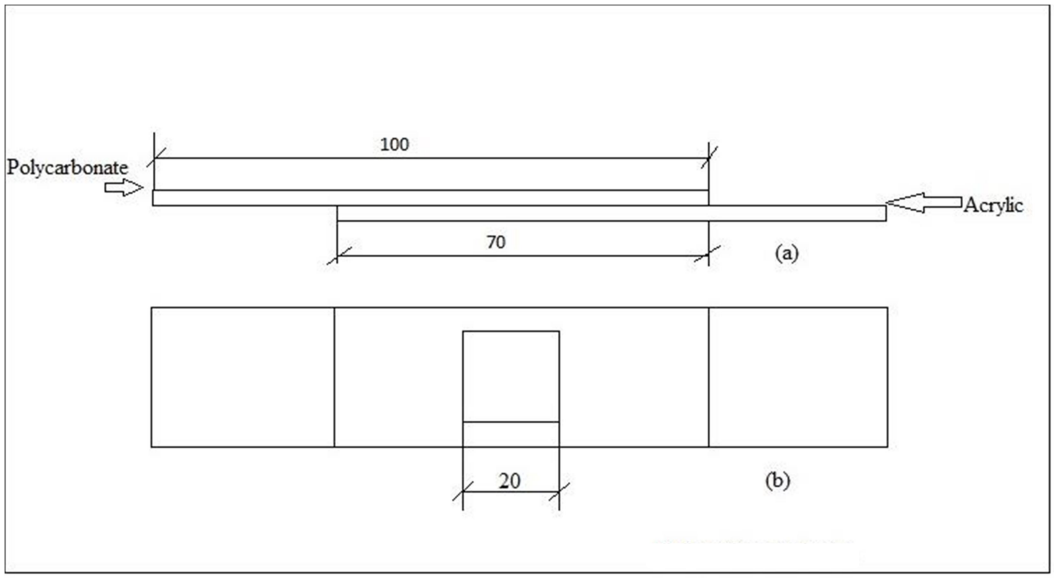

Figure 2.1 Diagram of samples (a) Side view (b) Top view

The properties of acrylic and polycarbonate are as from the literature [11, 53]

Acrylic:

Colour: Transparent

Physical properties:

Abbe No(V)	40.5
Refractive index (n)	1.54
Flammability	94 HB
Limiting Oxygen Index	(17-20)%
Water absorption-Equilibrium(ASTM)	2%
Radiation resistance	Low
UV resistance	Poor

Mechanical Properties:

Young's Modulus (E)	3.2 GPa
Tensile Strength (σ_t)	70 MPa
Elongation At break (ε)	4%
Compressive Strength (σ_c)	97.22-124.10 MPa
Poisson's raio(ν)	0.35-.04
Rockwell hardness	D-785 M-94
Notch test	2.16 J/m

Thermal Properties:

Glass transition temperature	114 ºC
Upper working temperature	124 ºC
Lower working temperature	-40 ºC
Linear thermal expansion coefficient	$65x10^{-6}\,K^{-1}$

Electrical properties:

Surface resistivity	15 Ω/m^2
Volume resistivity	$>10^{14}\,\Omega.m$

Chemical structure:

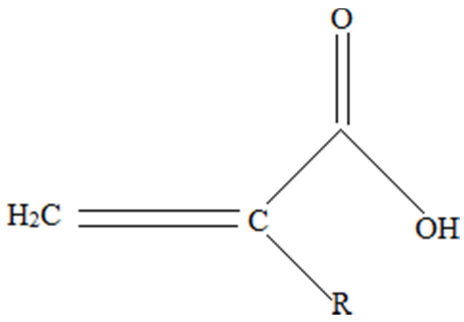

Temperature-dependent property:
The temperature dependent properties of acrylic are shown in Figure 2.2.

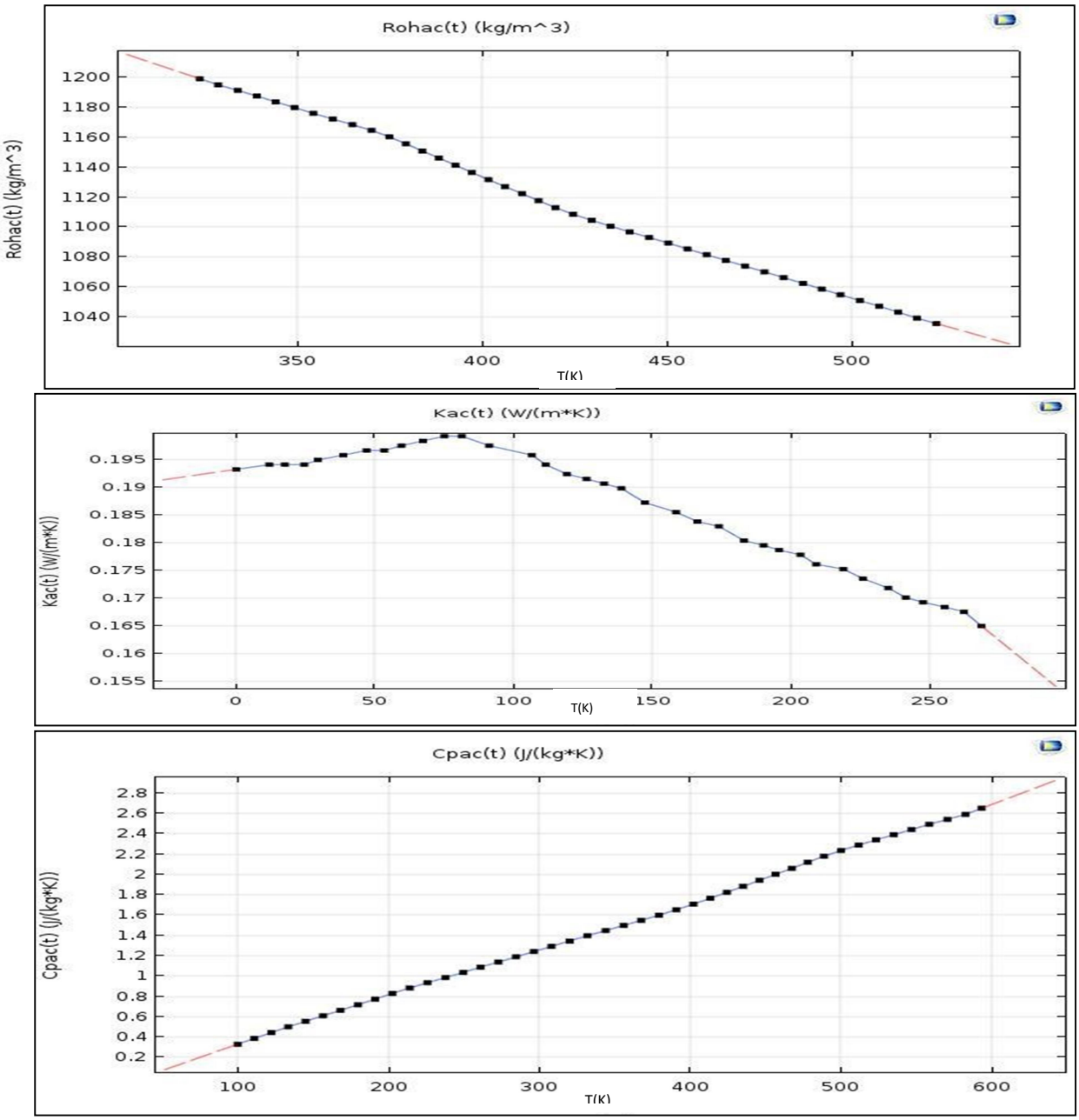

Figure 2.2 Temperature-dependent properties of acrylic

a) **Polycarbonate:**

Colour: Transparent

Physical properties:

Abbe No(V)	34.0
Refractive index (n)	1.584-1.586
Flammability	98 HB
Limiting Oxygen Index	(25-27)%
Water absorption-Equilibrium(ASTM)	0.16 %
Radiation resistance	Fair
UV resistance	Fair

Mechanical properties:

Young's Modulus (E)	2.4 GPa
Tensile Strength ($Б_t$)	75 MPa
Elongation At break (ε)	80 %
Compressive Strength ($Б_c$)	>80 MPa
Poisson's raio(ν)	0.37
Rockwell hardness	M-70
Notch test	20-35 J/m

Thermal properties:

Glass transition temperature	147 ^oC
Upper working temperature	150 ^oC
Lower working temperature	-40 ^oC
Linear thermal expansion coefficient	$65x10^{-6}\ K^{-1}$

Electrical properties:

Surface resistivity	$10^{15}\ \Omega/m^2$
Volume resistivity	$>10^{14}\ \Omega.m$

Chemical structure:

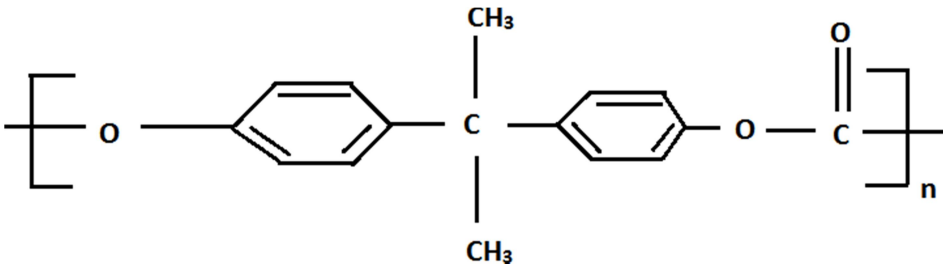

Temperature dependent property:
The temperature dependent properties of acrylic are shown in Figure 2.3.

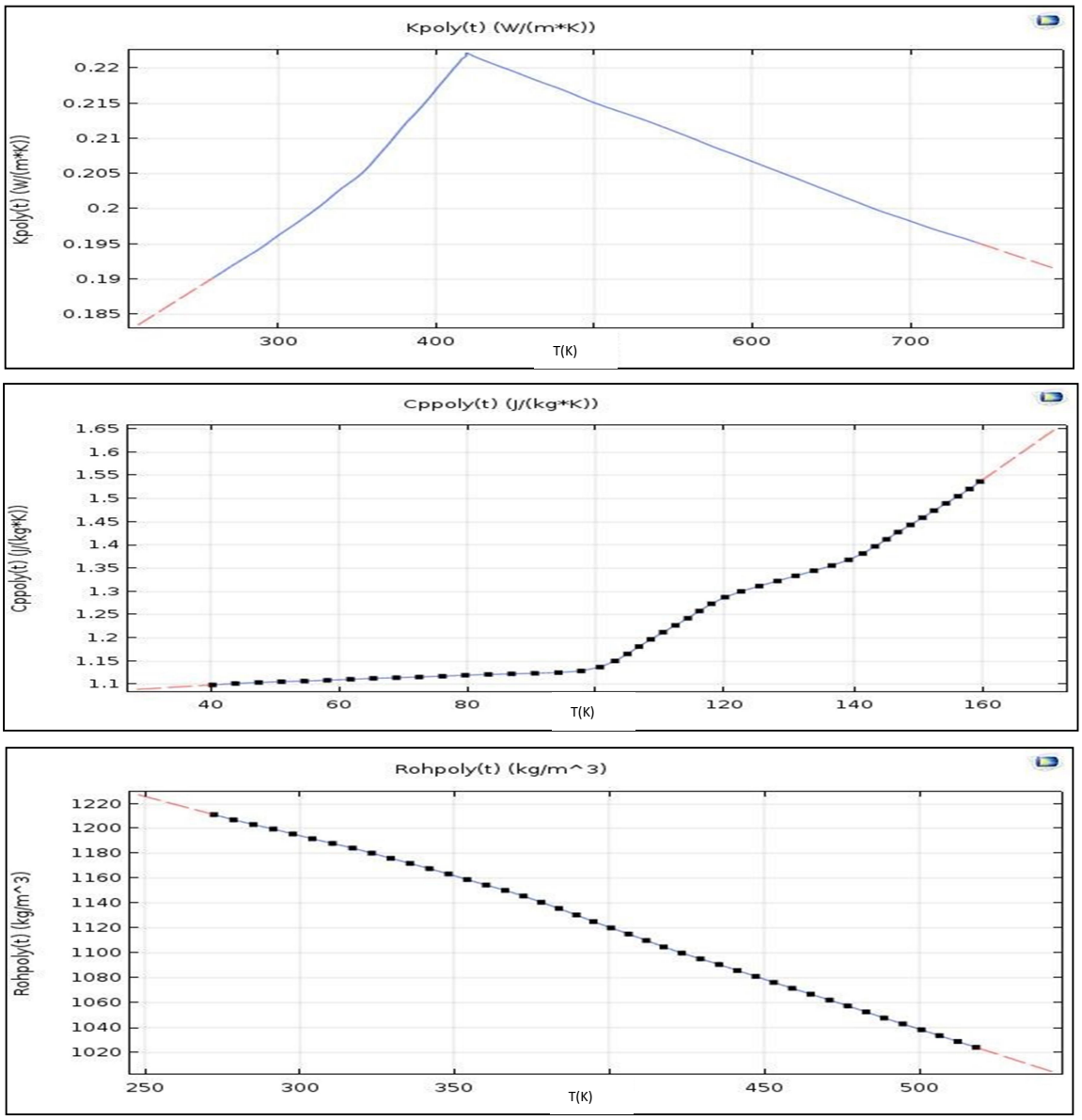

Figure 2.3 Temperature dependent properties for polycarbonate

2.2.1. Instruments Specifications

a) **Main laser unit:** The main welding experiments have been taken places in Electrox EMS 100 laser welding machine. Pictorial view of laser machine is shown in Figure 2.4.

Specifications for main laser unit:
Maker: Electrox
Dimension of work station: 26" wide × 37" deep × 31" tall
Pilot Laser
Laser used: Diode Laser Class: II

Wavelength: 635-680 nm Maximum power: 1 mW Output: CW (continuous type)

Working laser

Nd: YVO_4 (Neodymium-doped yttrium orthovanadate)
Power: 12 W
Frequency: Up to 500 kHz
Marking speed: 0.15 to 10160 mm/s
Wavelength: 1064 nm
Lens type: Galvo lens (S163) Operating temperature: 0°C to 25°C Spot diameter: 40 - 50 µm
Pulse on time: 4 nm Fibre cable: 800 nm
Beam size of laser source: 0.8 mm; Working distance: 184 mm
Field diameter: 144 mm

System specification

An HP PC with 1GHz CPU (Intel), 128 MB of RAM, 16 MB video RAM, CD ROM drive SVGA monitor set to 1024 X 786 resolutions free serial port, free USB port, free Etharnet port minimum 12 MB free disk space. Windows™ 7 professional OS.

Software specification

Program: Electrox scriba 3 laser marking program
Written in C++
Communication port with the laser marking machine RS232 serial port

Figure 2.4 Pictorial view of laser system

b) **Optical Transmissive Microscope:** Microscopic imaging of the weld zones have been done using optical microscope shown in Figure 2.5.
Maker: Diwinter
Facilities: Digital image processing and analysis using Capture pro 5.0 software

Figure 2.5 Optical microscope

c) **Universal testing machine:** Weld strength has been characterized by the ultimate load which has been tested by UTM shown in Figure 2.6.
Maker: Instron
Maximum capacity: 1000N
Accuracy: ± 0.4 %
Control: microprocessor

Figure 2.6 Universal testing machine

2.2.2. Software Specification

a) **Minitab 18:** Statistical software Minitab version 18 has been used for experimental design and response optimization.

b) **COMSOL 5.3a:** Thermal modeling has been done using finite element package COMSOL 5.3 a.

2.3. Experimental procedure

After drafting the panning the two polymer sheet has been cut according to aforesaid specifications which followed by cleaning and preparing the samples for the welding operation. Electrox EMS 100 laser marking machine has been prepared for the welding operation. The suitable clamping pressure is required for the experiment that has been given by a clamping device shown in Figure 2.7. The acrylic plate has been kept on the bottom and the polycarbonate plate have been kept on the up, the overlapped zone then clamped in the clamping device. The schematic diagram of the experimental set up is shown in Figure 2.8. The laser follows the square shape profile for welding. Twenty runs of the experiment have been conducted following the design matrix made with variable input parameters like power, frequency, scanning speed. This welding is followed by characterizations of the weld quality such that weld width, heat affected zone (HAZ) and ultimate load. Weld width and HAZ is measured by using an optical microscope followed by suitable image processing technique. Ultimate loads have been measured by pull test in UTM. The results have been tabulated and analyzed after that.

Figure 2.7 Clamping device used for welding

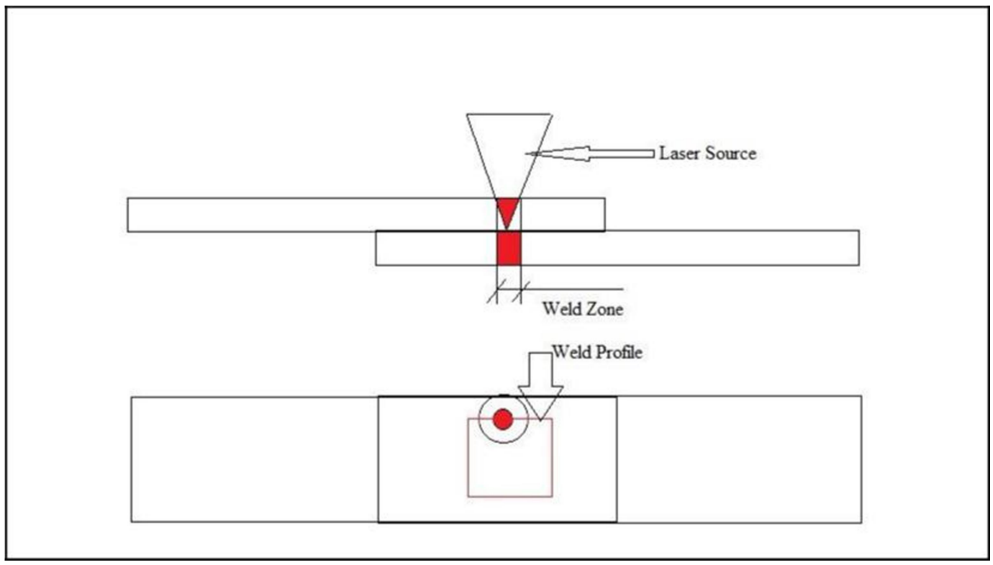

Figure 2.8 Schematic diagram of laser transmission welding

2.4. Thermal Modelling

Thermal modelling has been done after the experiment to have a deep insight into the heat transfer effect on the physical welding process. The process parameters are set as per the physical experiment. Some assumptions have been taken reasonably to reach time saving and easy computation. The process of computing the FE model using COMSOL 5.3a has been discussed in the following paragraphs.

2.4.1. Assumptions

Some assumption has been taken with valid reasons for decreasing the number of nodal points and reduces computation errors. Those are as follows:

a) Materials, i.e. acrylic and polycarbonate are homogeneous and isotropic in nature throughout the domain of study.
b) The half portion of the physical welding is studied as there is symmetry in the model.
c) A small part of square welding profile has been selected to reduce the number of nodal points.
d) A perfect contact is there between melting parts of plates.
e) Repetition frequency of the process is 300 kHz to 400 kHz, which is too high and the pulse on time is 4 ns which is too small, so pulse on time coupled with frequency has been lead to computational error. This can be avoided from the understanding of

physical process that repetition is too fast i.e. 3 x 10^5 to 4 x 10^5 cycles per second which can be considered as continuous. The physical experiment does show continuous behaviour while experimentation.

f) Ambient temperature for the study has been taken as 300 K and convective heat transfer coefficient has been taken as 10 W/ m^2 –K and the emissivity for radiation are taken as 0.92 for the materials from the literature.

g) The phase change phenomenon due to heating is neglected.

h) The Gaussian mode of laser intensity is followed.

2.4.2. Governing Equations

The following 3-D heat transfer equations are used to model heat transfer in the LTW of acrylic and polycarbonate that defines the temperature distribution within the body based on energy conservation law:

$$\boldsymbol{\rho c \frac{\partial T}{\partial t} = \nabla(k \Delta T) + q} \quad (2.1)$$

where ρ is material density, c is specific heat. T is the temperature and t is time. Thermal conductivity is denoted by k while q represents internal heat generation.

Heat transfer between the workpiece and surrounding medium by convection q_{conv} is given by,

$$\boldsymbol{q_{conv} = h(T_s - T_0)} \quad (2.2)$$

Radiation heat transfer is given by,

$$\boldsymbol{q_{rad} = \sigma \varepsilon (T_s^4 - T_0^4)} \quad (2.3)$$

where h is the convective heat transfer coefficient, T_s system temperature, T_0 ambient temperature, ε is emissivity of material and σ is Stefan- Boltzman's constant (5.64 x 10^{-8} W/m^2K^4).

The materials used are transparent but in acrylic, there is some absorptivity of light so acrylic has been selected as absorbent part and polycarbonate is the transparent part. The heat flux equation is modified from Beer-Lambert law. It is given by

$$q(x,y,z) = \begin{cases} 0 & \textit{tranparent part} \\ (1-R_a)\alpha I_a \exp(-KZ_a) & \textit{absorbent part} \end{cases} \quad (2.4)$$

where R_a is reflectivity of the absorbent part for acrylic it is 0.97. α is the absorbent coefficient it value for transparent acrylic is 15454 m^{-1}. Z_a is the depth of the beam inside the lower part and I_a is the intensity of the laser beam after passing transparent polycarbonate which can be defined as

$$I_a = \frac{(1-R_t)P}{A} \quad (2.5)$$

where P is the power and R_t is the reflectivity of the transparent part; here for polycarbonate, it is 0.05. Depending upon these governing equations, the finite element model of the laser transmission welding has been developed.

2.4.3. Model Creation

The model geometry has been created in COMSOL interface using model builder. The model parameters used are shown in Table 2.3. Only some portion of total physical weld profile has been considered for numerical simulation. Due to material symmetry, only half part of the total zone is considered. The geometric model selected for simulation is shown in Figure 2.9.

Table 2.3 Model parameters used in finite element simulation

Length	L	15 mm
Width	W	2.5 mm
Thickness	Th	0.5 mm

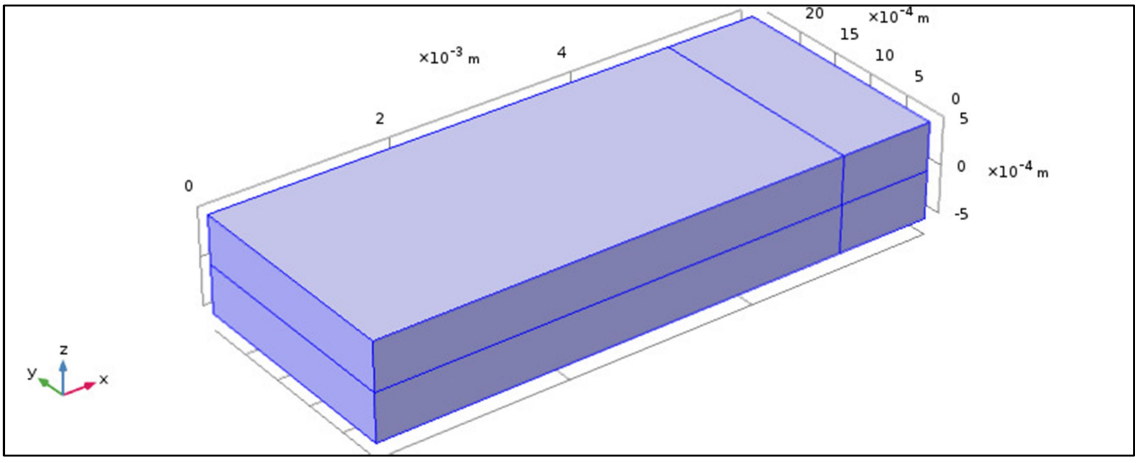

Figure 2.9 Geometric model used in simulation

2.4.4. Material Assigning

In the COMSOL interface, the material has been assigned using the temperature dependent property values from Figure 2.2 and Figure 2.3. The upper part is assigned as polycarbonate same as the physical experiment and the lower part have been assigned as acrylic.

2.4.5. Boundary Conditions

The boundary conditions have been given as par the physical experimentations. The upper plate has been transparent, so heat flux in the upper plate has been selected as zero. The lower part is governed by the heat flux equation 2.4. The initial temperature is selected as 293.15 K. Convective heat flux is applied to all boundary surfaces, which is governed by the equation 2.2. Surface to ambient radiation is mostly affecting the top most and bottom most face following equation 2.3.

2.4.6. Mesh Creation:

In order to formulate the finite element model the geometry should be discretized to small elements. In this work, free 3D tetrahedral elements have been selected as in most of the literature for heat transfer study this tetrahedral mesh structure was used. The symmetric half portion of the heat interaction zone has been made finely meshed with maximum element size 0.05 mm. The model after meshing has been shown in Figure 2.10.

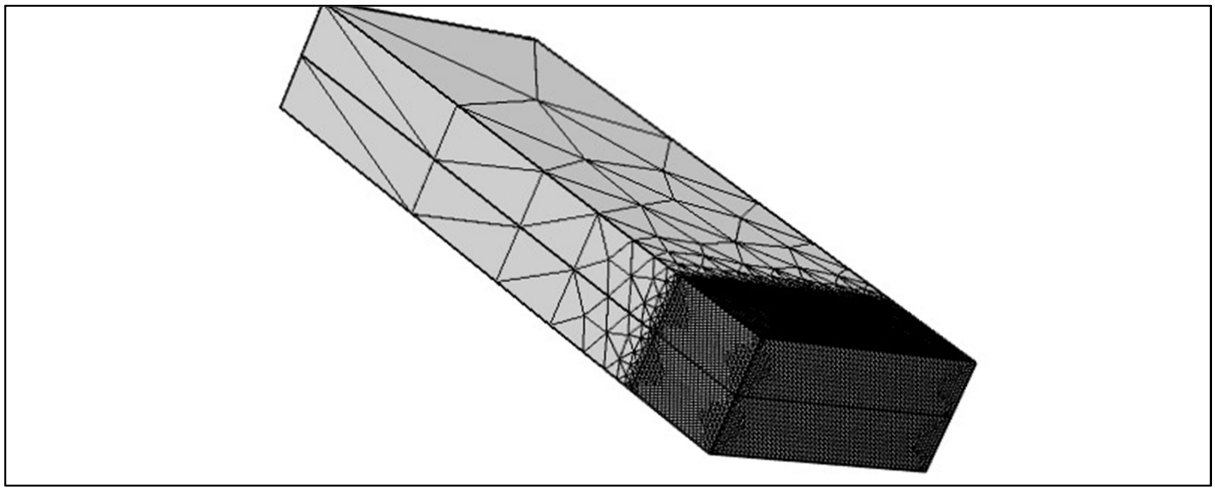

Figure 2.10 Meshing of geometric model

2.4.7. Solver Configuration

For solving the finite element formulation time-dependent solver has been chosen. The solution of the model has been temperature profile at each and every nodal point of the free tetrahedral elements. A fully coupled study consisting of nonlinear shape function with 1000 numbers of iteration have been chosen. The solutions then analyzed to get the value of weld width detail results has been discussed further.

3. Results and Discussion

The results of experiment and simulation have been shown in this chapter. Response surface analysis along with mathematical modeling including ANOVA has been done and discussed in details. The results from the simulation are also analyzed and validated with the experimental results.

3.1. Experimental Results

According to experiment planning that discussed earlier experiments has been conducted. The samples after lap joint using laser transmission welding have been shown in Figure 3.1. The measurement of weld width and HAZ (heat affected zone) has been done using transmitting microscope with an objective lens of 50X magnifications. To measure weld width and HAZ microscopic image at four different locations has been taken and analyzed by appropriate image processing technique discussed earlier. The microscopic image of minimum weld width on different location has been shown in Figure 3.2 and maximum weld width have been shown in Figure 3.3

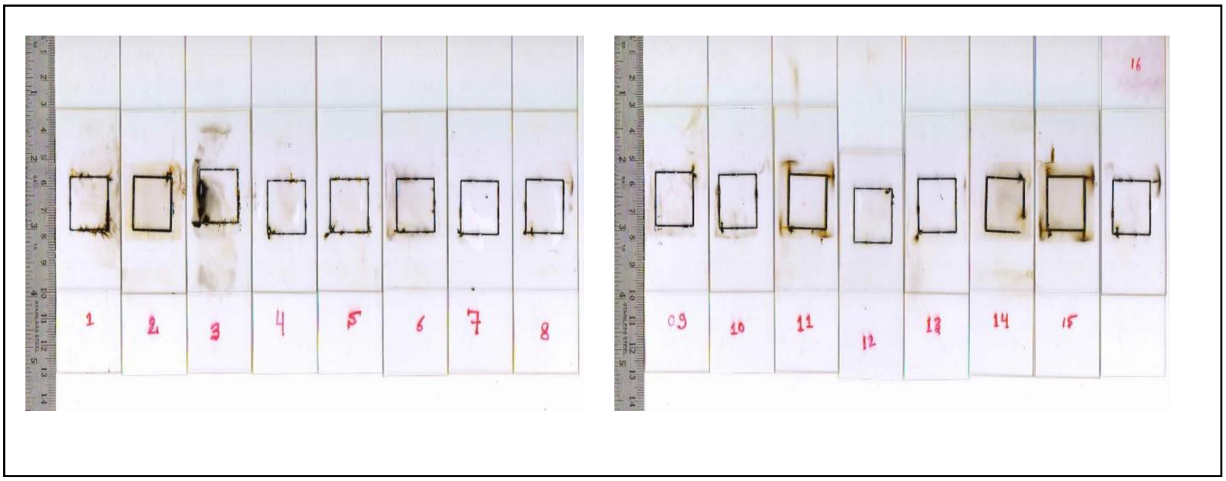

Figure 3.1 Lap welded samples

The microscopic images for HAZ minimum and maximum are shown in Figure 3.4 and Figure 3.5 respectively. The ultimate load of the weld has been considered as the strength of the joint as obtained from the load vs elongation curve. The load vs elongation curve for maximum and minimum ultimate load has been shown in Figure 3.6 and Figure 3.7, respectively

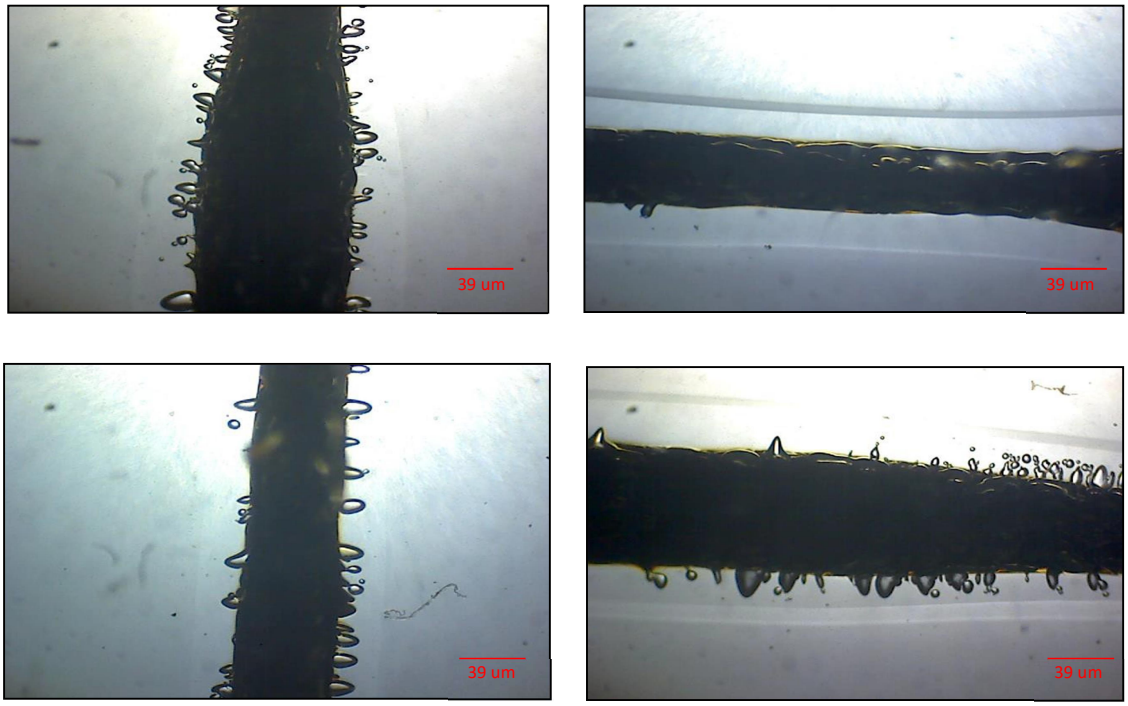

Figure 3.2 Microscopic view of sample having minimum weld width (Experiment no.4)

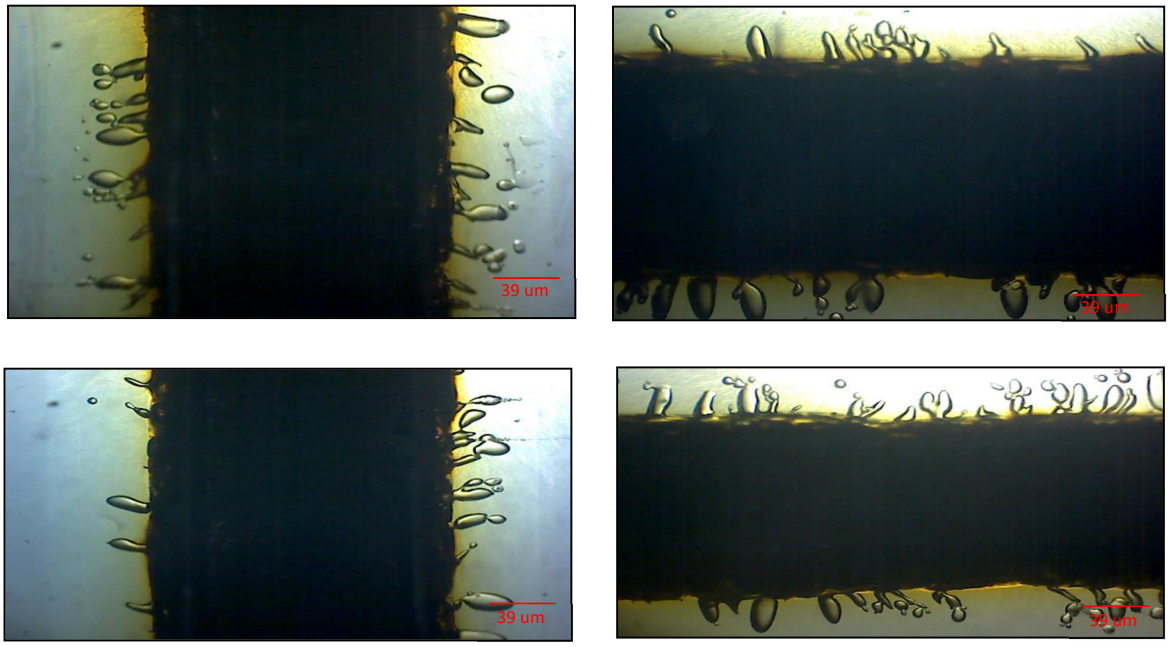

Figure 3.3 Microscopic view of sample having minimum weld width (Experiment no.18)

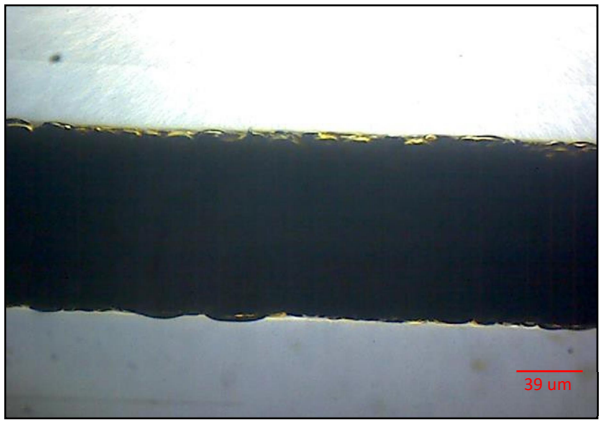

Figure 3.4 Microscopic image of sample having minimum HAZ

Figure 3.5 Microscopic image of sample having minimum HAZ

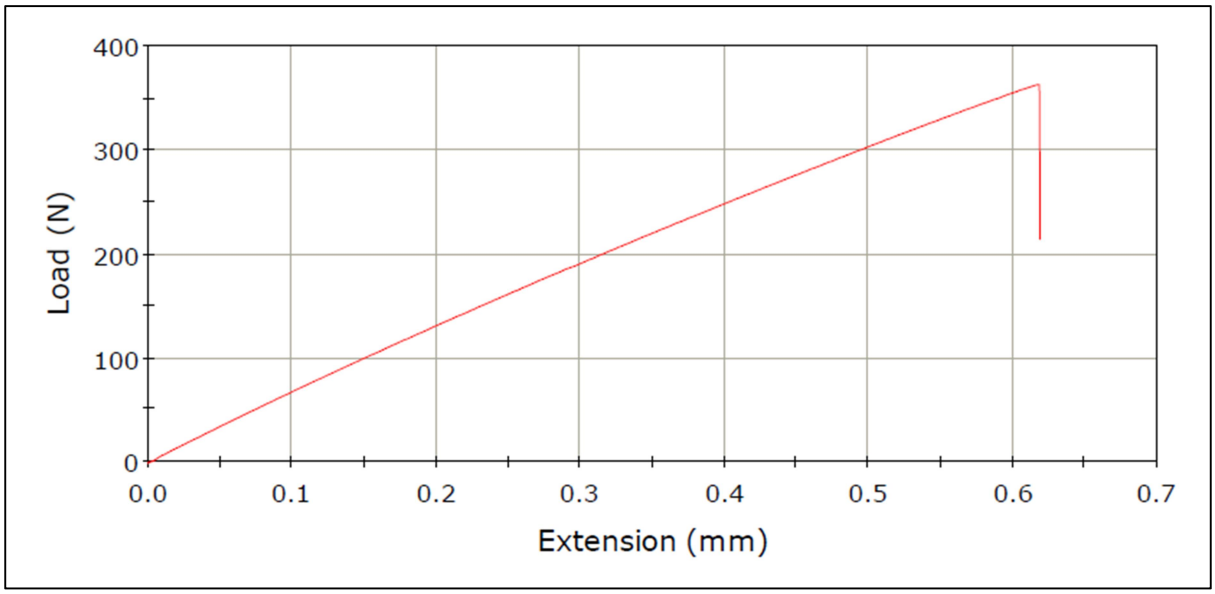

Figure 3.6 Load vs extension graph for the maximum load (Experiment 3)

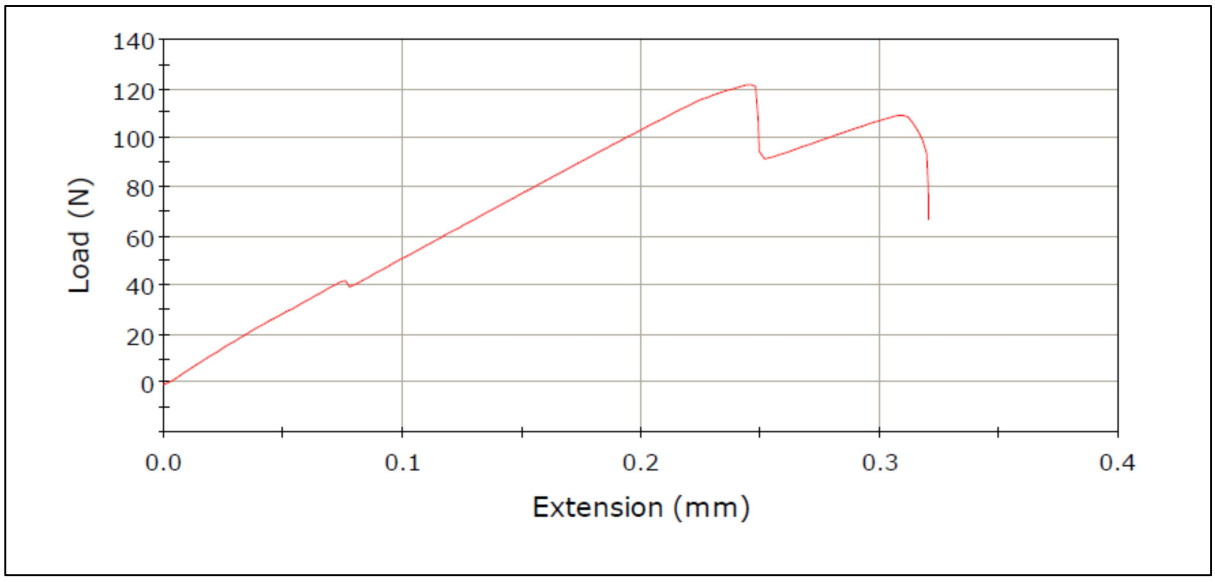

Figure 3.7 Load vs extension graph for the minimum load (Experiment 14)

From the observed result according to the experimental plan the result table has been prepared. The result of the experiments having responses as weld width HAZ and ultimate load are shown in Table 3.1.

Table 3.1 Experimental result table

Sl No	Power (W)	frequency(kHz)	Scanning speed (mm/s)	Weld width (μm)	HAZ (μm)	Ultimate load (N)
1	8.35	300.00	2.00	127.16	34.92	318.24
2	8.35	400.00	1.00	224.3	85.87	161.08
3	7.89	350.00	2.34	112.65	24.27	372.60
4	7.42	300.00	2.00	114.09	20.85	340.10
5	8.35	400.00	2.00	121.5	40.22	242.00
6	7.89	350.00	1.50	166.1	42.35	150.46
7	7.11	350.00	1.50	140.61	35.98	270.23
8	7.89	350.00	1.50	177.55	43.45	155.20
9	7.89	350.00	1.50	177.84	43.02	192.29
10	7.89	265.91	1.50	162.23	56.84	155.46
11	7.42	400.00	1.00	233.04	66.2	170.10
12	7.42	400.00	2.00	131.79	31.25	362.38
13	7.89	350.00	1.50	177.17	45.87	176.20
14	7.42	300.00	1.00	224.45	79.49	121.15
15	8.35	300.00	1.00	234.83	95.35	132.90
16	7.89	350.00	1.50	177.55	44.83	155.20
17	7.89	350.00	1.50	177.84	41.81	178.50
18	7.89	350.00	0.66	304.64	105.8	221.17
19	8.67	350.00	1.50	150.38	61.28	208.48
20	7.89	434.09	1.50	189.11	52.61	196.58

The experimental result table shows that the weld width varies from 112.65 μm to 304.64 μm, HAZ varies from 20.85 μm to 105.8 μm and ultimate load varies from 121.15 N to 372.60 N. pictorial view of lowest and highest ultimate load after pull test has been shown in Figure 3.8. During pull test it has been observed that the breaking occurred near the weld zone in most of the cases. The maximum loads that can withstand by the welded samples are less than the original strength of both of the transparent substrates. During laser scanning, decomposition occurs which may lead to degradation in material properties in fused region at the interface but the rest of the part remains intact. All the samples have failed through the fused material or across the upper sheet. But none of the materials have failed across the lower sheet i.e. acrylic sheet.

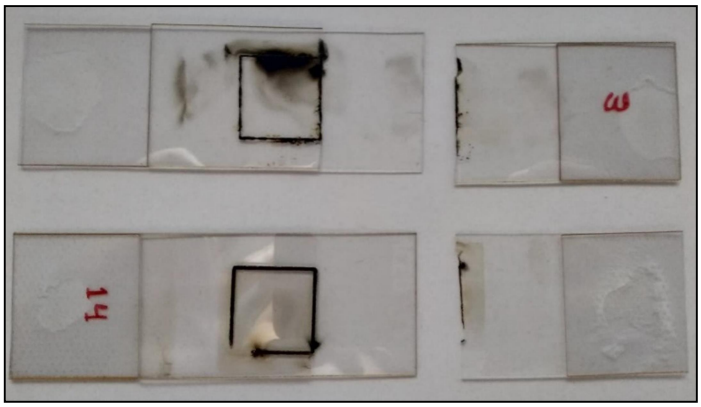

Figure 3.8 Photograph of the samples having the highest ultimate load (experiment no 3) and lowest ultimate load (experiment 14)

The mathematical models for each of the responses have been obtained and from experimental results, three dimensional response surface plots and contour plots have been obtained.

3.1.1 Main Effect Plots

The main effect plots of weld width are shown in Figure 3.9. It shows the variation of weld width with respect to power, frequency and scanning speed.

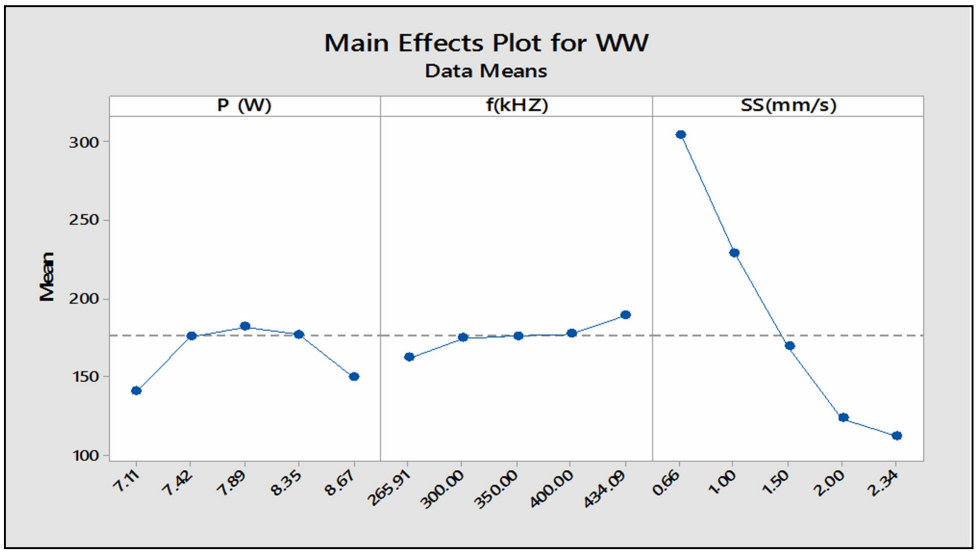

Figure 3.9 The main effect plot for weld width

The main effect plot of HAZ is shown below in Figure 3.10 which shows the variation of HAZ with respect to power, frequency and scanning speed.

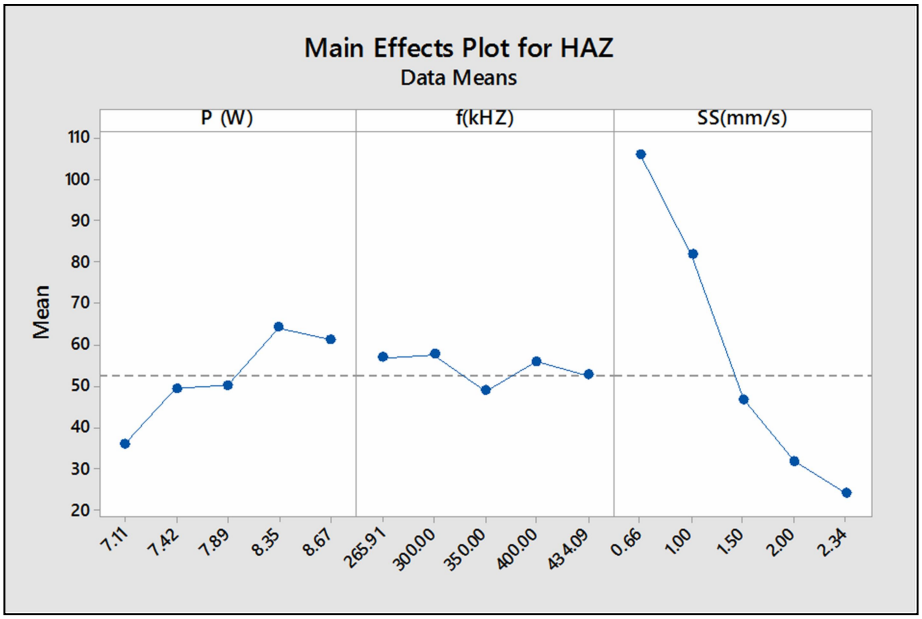

Figure 3.10 The main effect plot for HAZ

From the Figure 3.9 above it has been observed that with increase of power, weld width increases in low power range then suddenly drops for higher power. From Figure 3.10it is evident that HAZ have increasing trend. Though due to some measurement error some abnormality has been observed in case of weld width but the increasing trend has been observed as power density increases with the increasing value of laser power. In both the figure it is shown that with increasing scanning speed weld width and HAZ decreases. This is due to as the scanning speed increases energy per unit length, i.e. line energy decreases, due to less interaction time very low amount of heat is delivered to the joint. It is found that frequency does not play a vital role in controlling weld width as well as HAZ of the welded samples.

The main effect plots of breaking load are shown in Figure 3.11 shows the variation of ultimate load (UL) with respect to power, frequency and scanning speed.

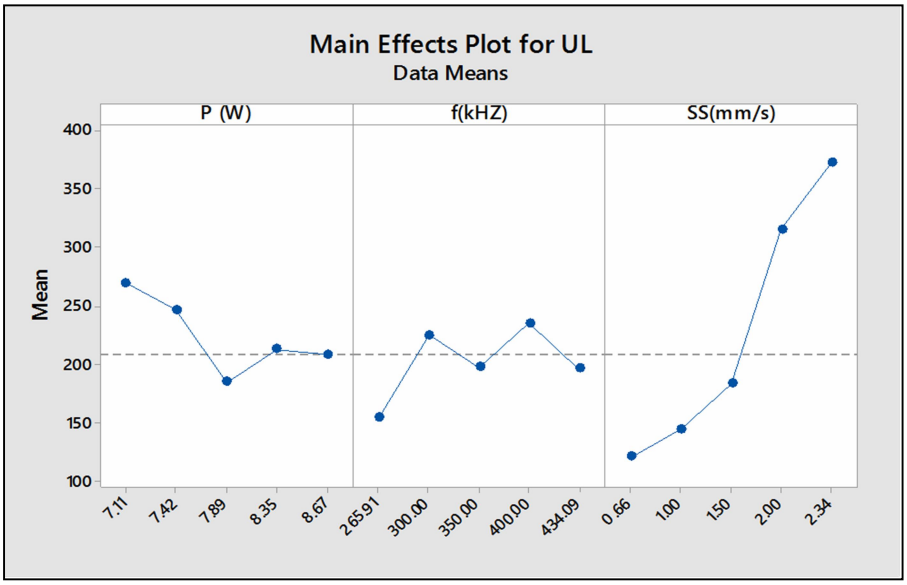

Figure 3.11 The main effect plot for ultimate load

It is evident from Figure 3.11 that with increasing power ultimate load has a decreasing trend though there is some abnormality in the result. Due to more power, there is more power density which interact in the welding zone so more heat is generated as more heat is generated more material gets evaporated which lead to larger weld zone and low strength. Ultimate load increases with increasing scanning speed as heat interaction time is low, so evaporation and weld width is low which result in more strength. The frequency has got a nominal effect on controlling the ultimate load.

3.1.2 Analysis of Variance (ANOVA)

To investigate the influence of process parameters on ultimate load, weld width and HAZ of weld, RSM based analysis has been made and mathematical model for each response has been developed. The goal is to correlate mathematical relationships between the process parameters and responses. A second order quadratic polynomial equation is applied to develop the regression equation (mathematical model). MINITAB 18 software is used for the analysis of the measured responses and the mathematical models with the best fit. The effect of each parameter is studied on the basis of the developed mathematical models.

3.1.2.1. ANOVA for Weld Width

The ANOVA table of the quadratic model for weld width (WW) is given in Table 3.2. If the associated p-value is less than 0.05 for the model indicates that the model terms are statistically significant. The main effect of the power (P), scanning speed (SS), frequency (f),

the quadratic effect of the scanning speed (S^2), power (P^2) and two way interaction of Pf and SSf are the significant model terms associated with the weld width. The adequacy measures R^2 (99.23%), adjusted R^2 (98.53%) and predicted R^2 (95.62%) are in reasonable agreement, which indicates adequate model. The lack-of-fit is not significant to the pure error, as desirable. The regression equation for weld width (WW) is shown in equation (3.1):

$$WW = -3292 + 867P + 1.780f - 277.4SS - 49.76P^2 - 0.000019f^2 + 46.55SS^2 - 0.2271Pf + 0.53PSS + 0.0699fSS. \quad (3.1)$$

Table 3.2 ANOVA table for weld width

Source	DF	Adj SS	Adj MS	F-Value	P-Value	Remarks
Model	9	45128.4	5014.3	142.85	0.000	Significant
Linear	3	40878.3	13626.1	388.18	0.000	Significant
P (W)	1	26.4	26.4	0.75	0.406	Significant
f(kHz)	1	220.3	220.3	6.28	0.031	Significant
SS(mm/s)	1	40631.6	40631.6	1157.52	0.000	Significant
Square	3	3989.5	1329.8	37.88	0.000	Significant
P (W)*P (W)	1	1655.0	1655.0	47.15	0.000	Significant
f(kHz)*f(kHz)	1	0.0	0.0	0.00	0.977	Not Significant
SS(mm/s)*SS(mm/s)	1	1945.3	1945.3	55.42	0.000	Significant
2-Way Interaction	3	247.6	82.5	2.35	0.134	Not Significant
P (W)*f(kHz)	1	223.0	223.0	6.35	0.030	Significant
P (W)*SS(mm/s)	1	0.1	0.1	0.00	0.954	Not Significant
f(kHz)*SS(mm/s)	1	24.4	24.4	0.70	0.424	Significant
Error	10	351.0	35.1			
Lack-of-Fit	5	240.7	48.1	2.18	0.206	Not Significant
Pure Error	5	110.3	22.1			
Total	19	45479.4				

3.1.2.2. ANOVA for HAZ

The ANOVA table of the quadratic model for HAZ is given in Table 3.3. If the associated p-value is less than 0.05 for the model indicates that the model terms are statistically significant. The main effect of the power (P), scanning speed (SS) and frequency(f) are the significant model terms associated with the HAZ. Most of the quadratic and tow way interaction terms are also significant except the Pf term. The adequacy measures R^2 (99.77%), adjusted R^2 (99.56%) and predicted R^2 (98.78%) are in reasonable agreement, which indicate adequate model. The lack-of-fit is not significant to the pure error, as desirable. Regression equation for HAZ is shown in equation (3.2)

$$HAZ = 777 - 102.1P - 1.356f - 155.0SS + 8.28\,P^2 + 0.001574f^2 + 30.38SS^2 - 0.0070Pf - 6.70\,PSS + 0.1923\,fSS \quad (3.2)$$

Table 3.3 ANOVA table for HAZ

Source	DF	Adj SS	Adj MS	F-Value	P-Value	Remarks
Model	9	10253.3	1139.25	475.53	0.000	Significant
Linear	3	9079.5	3026.49	1263.28	0.000	Significant
P (W)	1	753.2	753.16	314.38	0.000	Significant
f(kHz)	1	14.8	14.76	6.16	0.032	Significant
SS(mm/s)	1	8311.5	8311.54	3469.31	0.000	Significant
Square	3	985.1	328.35	137.06	0.000	Significant
P (W)*P (W)	1	45.8	45.79	19.11	0.001	Significant
f(kHz)*f(kHz)	1	223.2	223.16	93.15	0.000	Significant
SS(mm/s)*SS(mm/s)	1	828.9	828.87	345.98	0.000	Significant
2-Way Interaction	3	204.6	68.21	28.47	0.000	Significant
P (W)*f(kHz)	1	0.2	0.21	0.09	0.772	Not Significant
P (W)*SS(mm/s)	1	19.4	19.42	8.11	0.017	Significant
f(kHz)*SS(mm/s)	1	185.0	184.99	77.22	0.000	Significant
Error	10	24.0	2.40			
Lack-of-Fit	5	12.2	2.44	1.03	0.486	Not Significant
Pure Error	5	11.8	2.36			
Total	19	10277.2				

3.1.2.3. ANOVA for Ultimate Load

The ANOVA table of the quadratic model for the ultimate load (UL) is given in Table 3.4. If the associated p-value is less than 0.05 for the model indicates that the model terms are statistically significant. The main effect of the power (P), scanning speed (SS) and frequency (f) are the significant model terms associated with the ultimate load. Most of the quadratic and tow way interaction terms are also significant except the f2 term. The adequacy measures R^2 (98.01%), adjusted R^2 (96.23%) and predicted R^2 (91.25%) are in reasonable agreement, which indicates adequate model. The lack-of-fit is not significant to the pure error, as desirable. The regression equation for the ultimate load (UL) is shown in equation (3.3):

$$UL = 4889 - 1599P + 6f + 710SS + 123P^2 + 0.00164f^2 + 117.2SS^2 - 0.742\ Pf - 80.8\ PSS - 0.750fSS \quad (3.3)$$

Table 3.4 ANOVA table for ultimate load

Source	DF	Adj SS	Adj MS	F-Value	P-Value	Remarks
Model	9	122977	13664.2	54.85	0.000	Significant
Linear	3	93950	31316.7	125.70	0.000	Significant
P (W)	1	4007	4007.2	16.08	0.002	Significant
f(kHz)	1	884	883.5	3.55	0.089	Significant
SS(mm/s)	1	89059	89059.5	357.47	0.000	Significant
Square	3	20495	6831.5	27.42	0.000	Significant
P (W)*P (W)	1	10133	10132.7	40.67	0.000	Significant
f(kHz)*f(kHz)	1	242	241.7	0.97	0.348	Not Significant
SS(mm/s)*SS(mm/s)	1	12340	12340.5	49.53	0.000	Significant
2-Way Interaction	3	8024	2674.6	10.74	0.002	Significant
P (W)*f(kHz)	1	2382	2382.3	9.56	0.011	Significant
P (W)*SS(mm/s)	1	2825	2825.5	11.34	0.007	Significant
f(kHz)*SS(mm/s)	1	2816	2816.1	11.30	0.007	Significant
Error	10	2491	249.1			
Lack-of-Fit	5	1089	217.8	0.78	0.606	Not Significant
Pure Error	5	1402	280.5			
Total	19	125469				

3.1.3. Contour Surface and Plots

A set of 3D Surface plots and contour plots of weld width, HAZ and breaking load have been generated with the help of the developed model.

3.1.3.1. Weld Width

Response surface plots and contour plots for weld width are shown in Figure 3.12 to Fig. 3.14. Figure 3.12 shows the combining effect of power and scanning speed, from this figure it can be seen that higher scanning speed results from narrow weld width and higher power results wider weld width. Figure 3.13 shows the combining effect of power and frequency which indicates that the first weld width increases with increasing power and then decreases slightly. With increasing frequency, the weld width also increases, because the density of laser input power also increases per time cycle with the increase of the frequency. Figure 3.14 shows that for any range of power, weld width decreases rapidly for increasing scanning speed and slightly for higher frequency. From these figures, it is seen that weld width varies significantly depending upon power and scanning speed.

So it can be concluded that increasing the power input results in wider weld width and more base material decomposition and lesser power results in the less molten weld area and narrow weld width.

3.1.3.2. HAZ

Figure 3.15 to Figure 3.17 show the surface plots and contour plots for HAZ. Figure 3.15 shows the combining effect of power and scanning speed. Higher scanning speed results in narrow HAZ and higher power results in wider HAZ. When both the value of power and scanning speed is high, it results high value of HAZ. Figure 3.16 indicates the combining effect of power and frequency. When both the value of power and frequency is high, a higher value of HAZ is obtained. HAZ increases with increasing power and frequency. With increasing frequency, the density of laser input power also increases. Figure 3.17 shows the combining effect of frequency and scanning speed. HAZ decreases rapidly for increasing scanning speed and slightly for higher frequency. It can be seen that HAZ varies significantly depending upon power and scanning speed. Frequency shows a very little effect on it.

So it can be concluded that greater power input results in greater HAZ and higher value of scanning speed result lower value of HAZ.

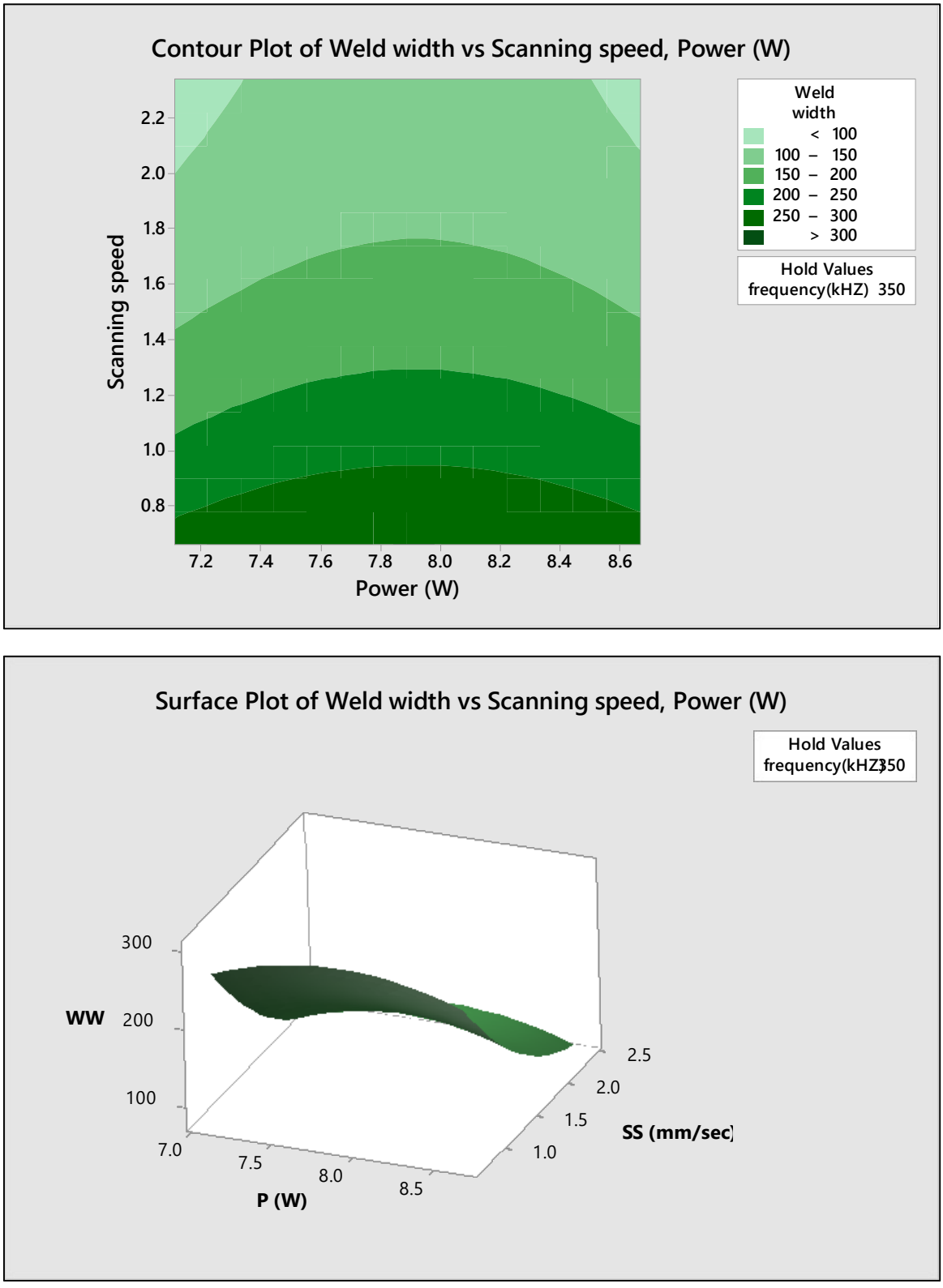

Figure 3.12 Contour and surface plots for weld width (WW) vs scanning speed (SS) and power (P) when frequency (f) is 350 kHz

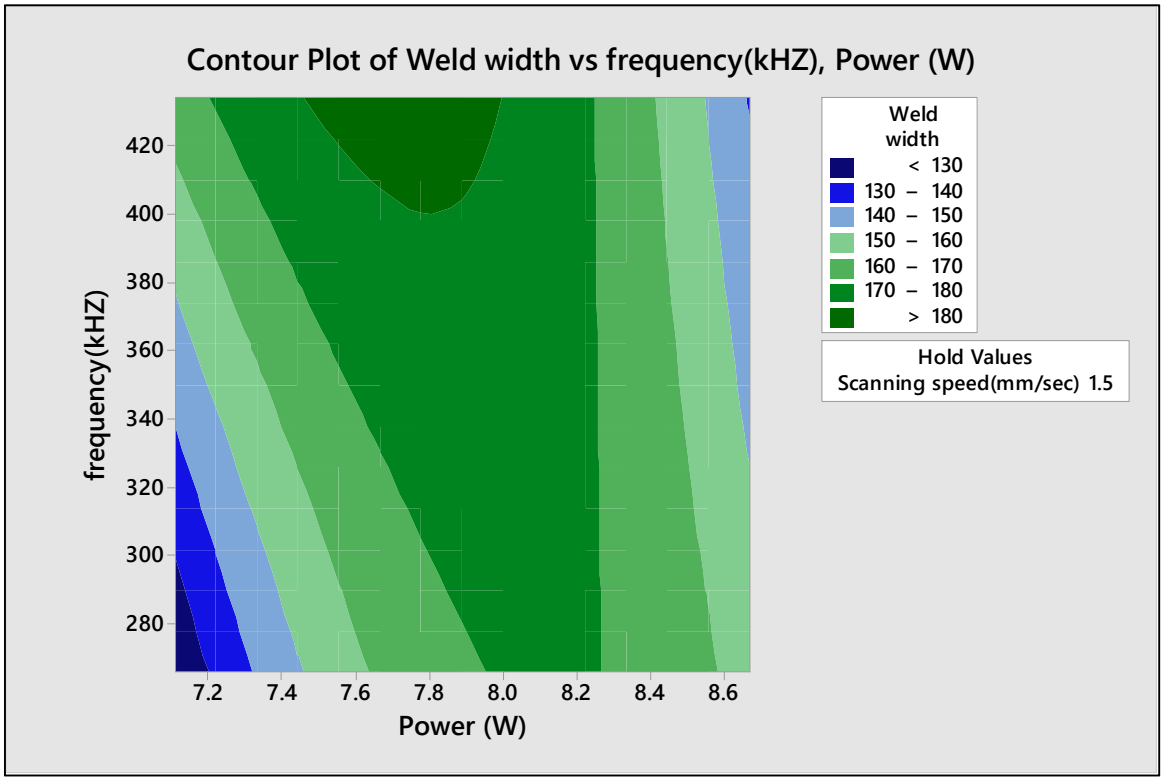

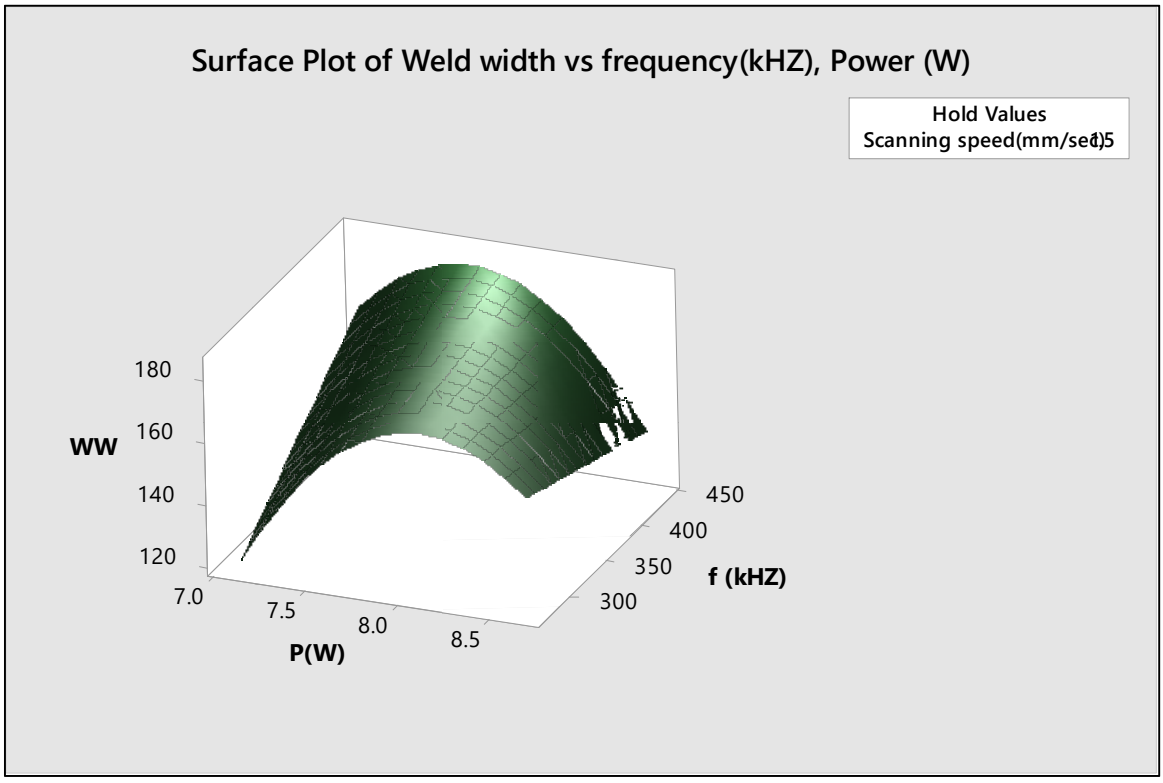

Figure 3.13 contour and surface plot for weld width vs frequency (f) and power (P) when scanning speed (SS) = 1.5 mm/s

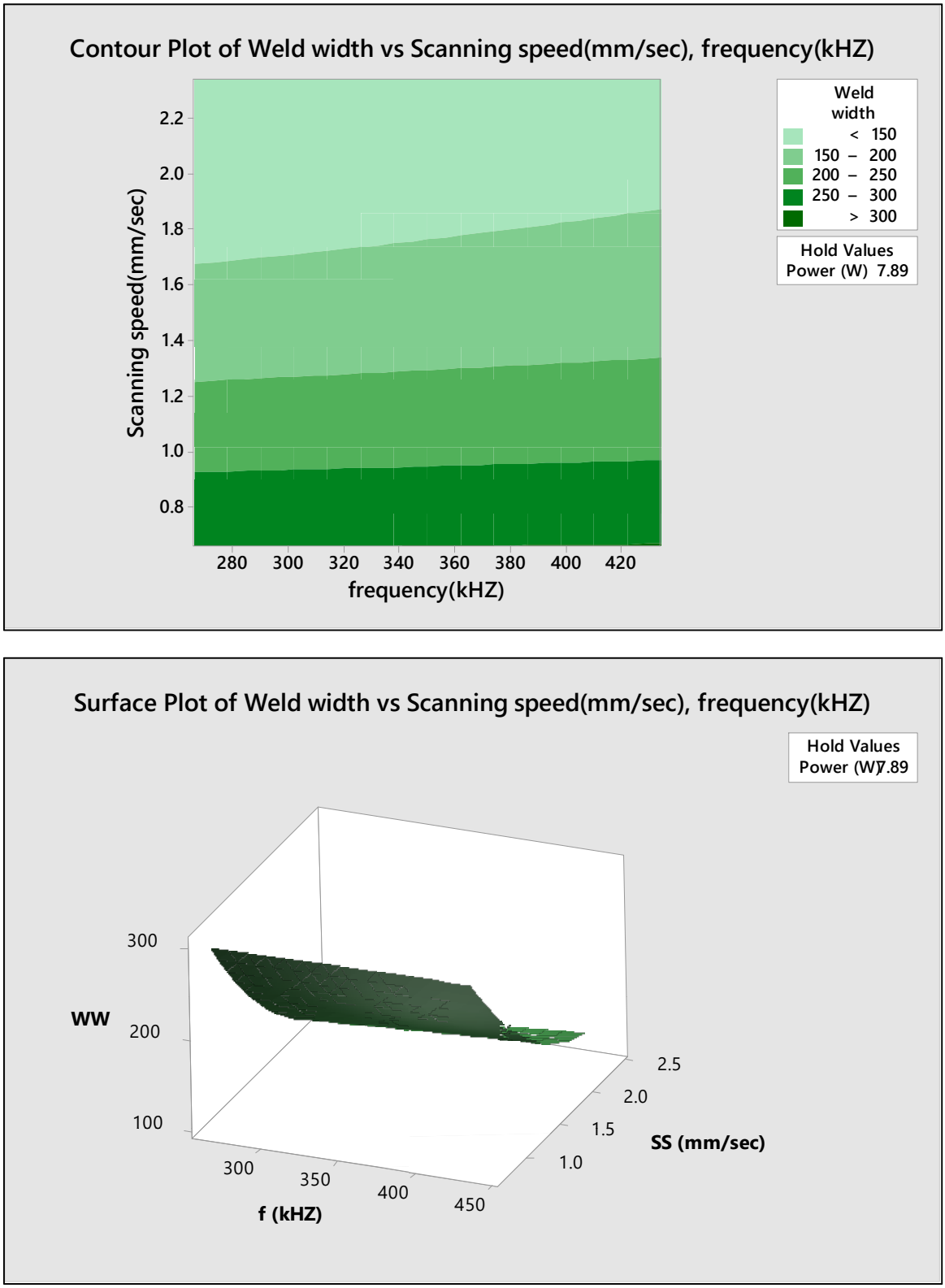

Figure 3.14 contour and surface plot for weld width vs frequency (f) and scanning speed (SS) when power (P) = 7.89 W

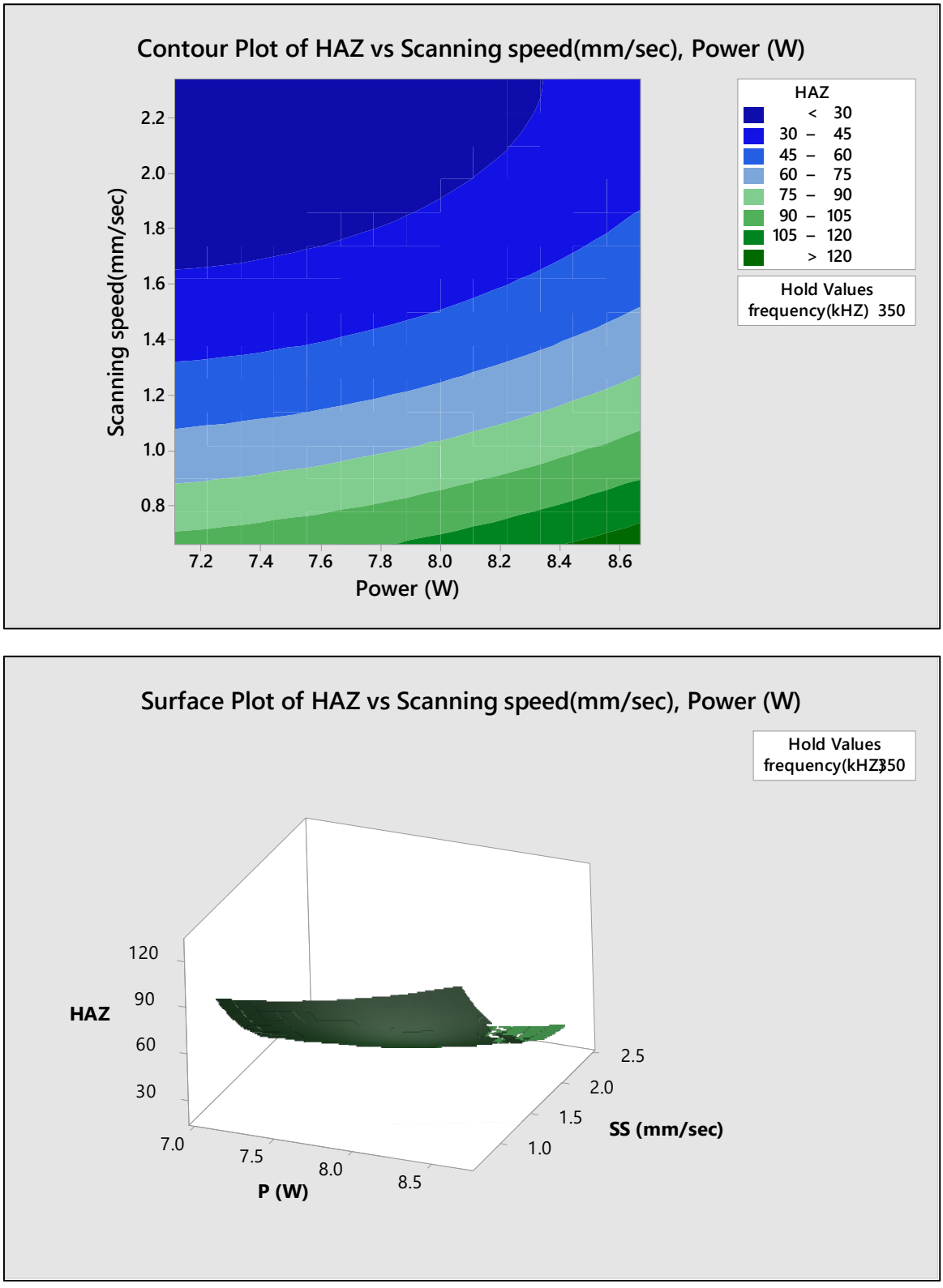

Figure 3.15 contour and surface plot for HAZ vs scanning speed (SS) and power (P) when frequency (f) =350 kHz

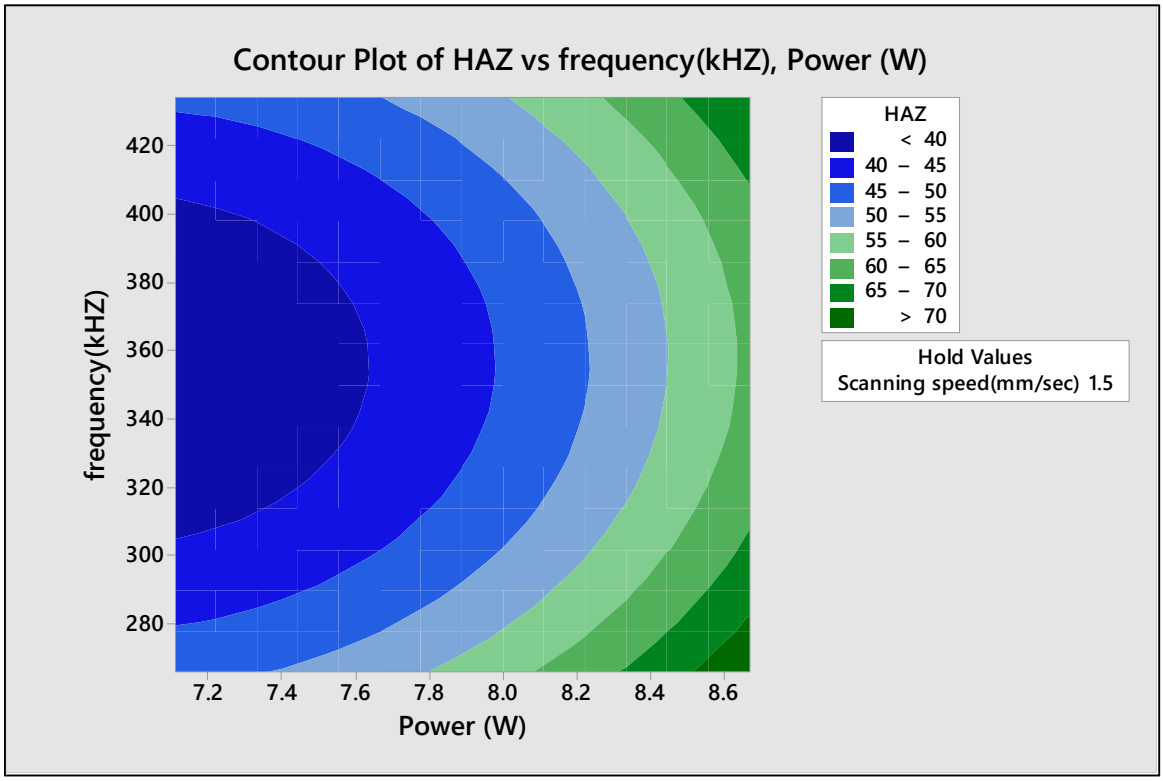

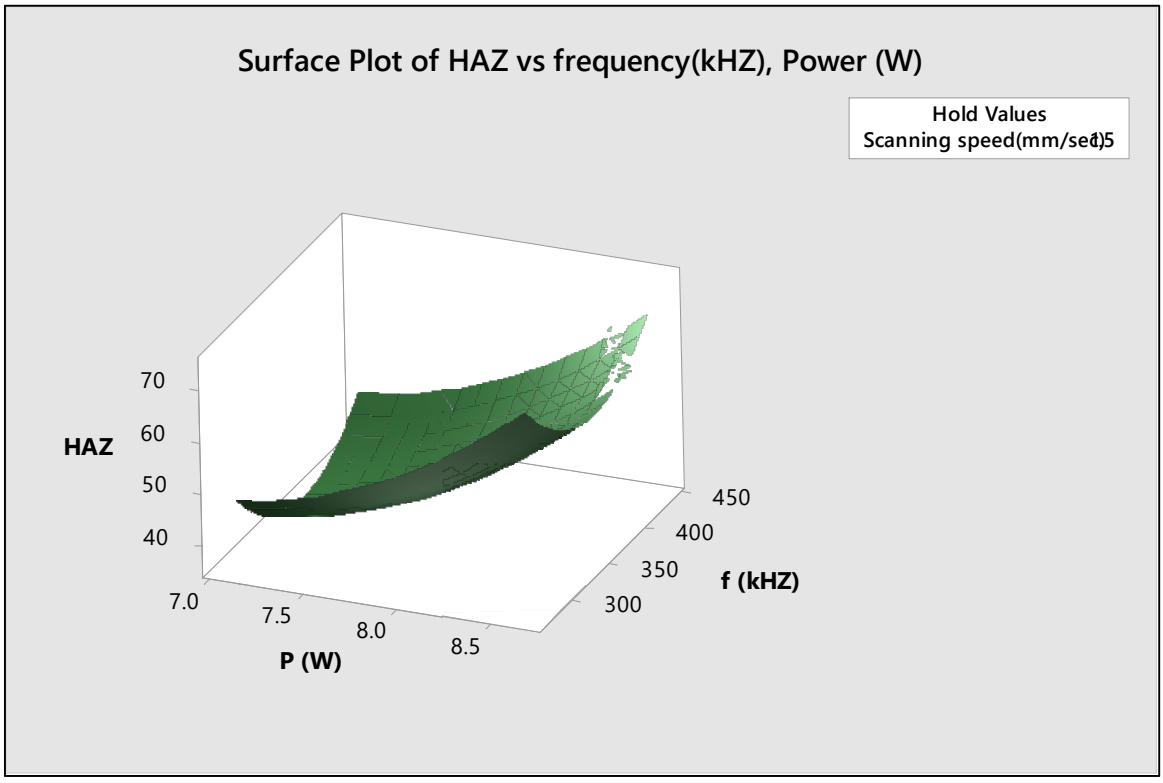

Figure 3.16 contour and surface plot for HAZ vs frequency (f) and power (P) when scanning speed (SS) = 1.5 mm/s

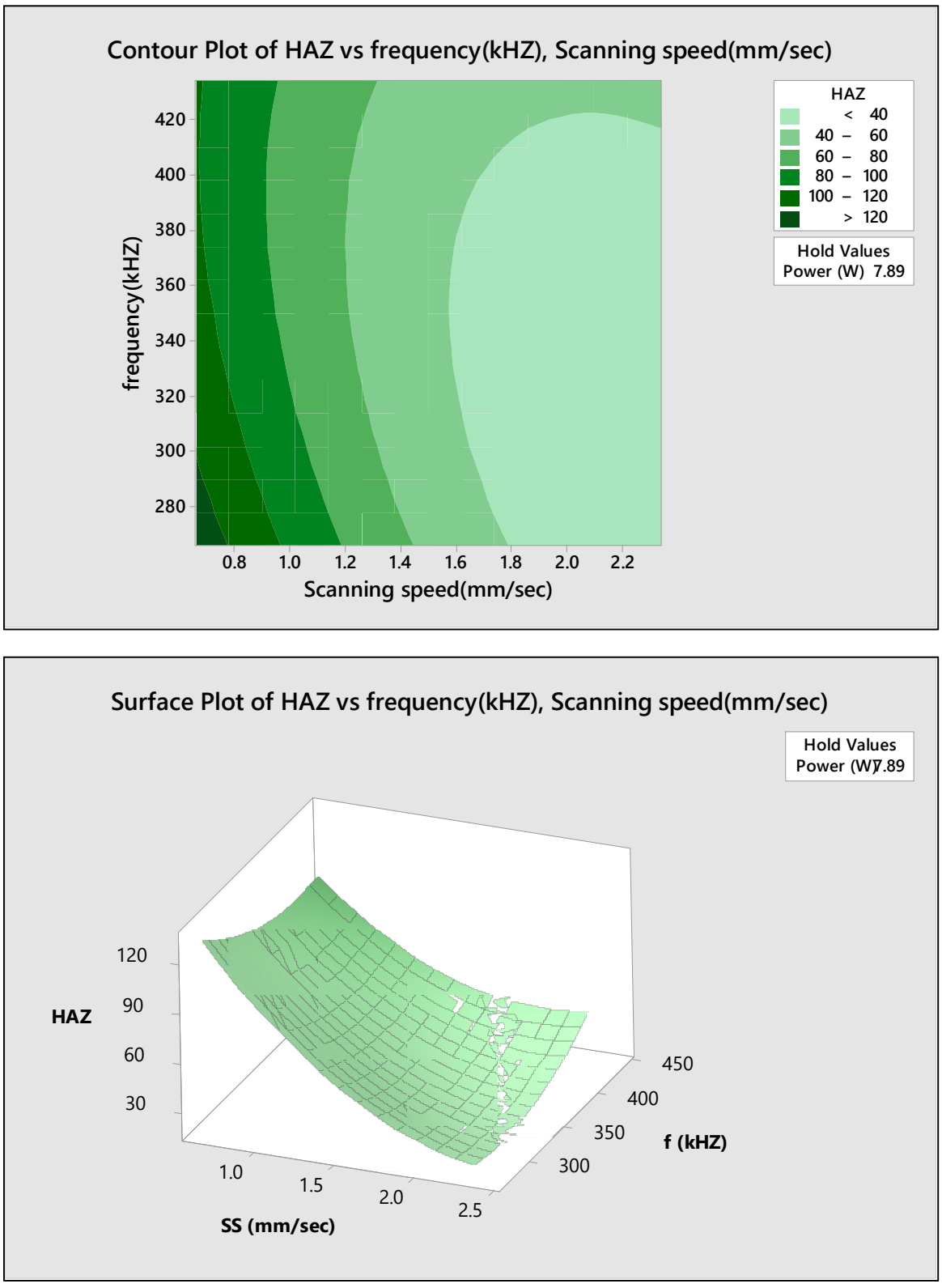

Figure 3.17 contour and surface plot for HAZ vs frequency (f) and scanning speed (SS) when power (P) = 7.89 W

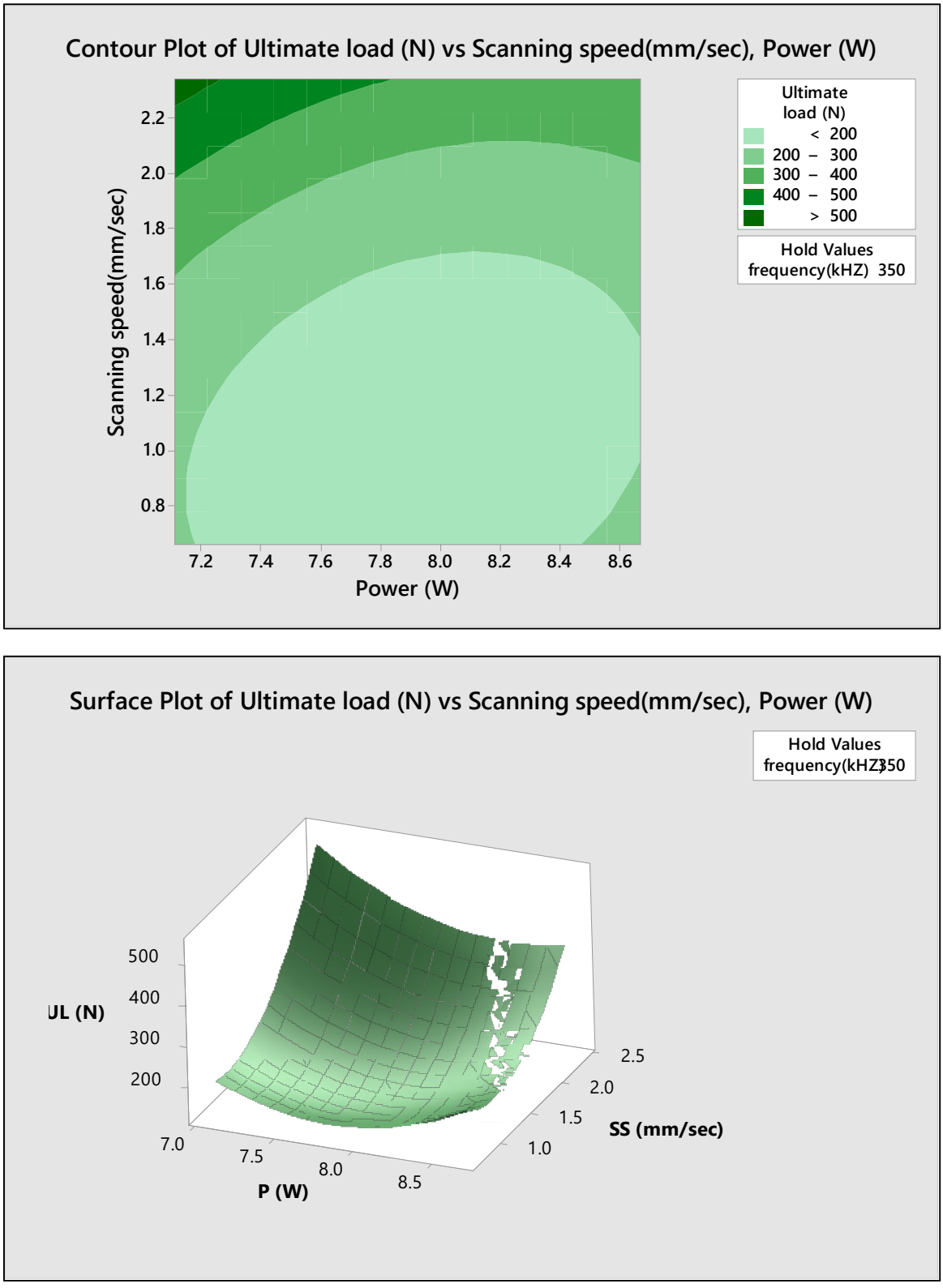

Figure 3.18 contour and surface plot for ultimate load vs scanning speed (SS) and power (P) when frequency (f) =350 kHz

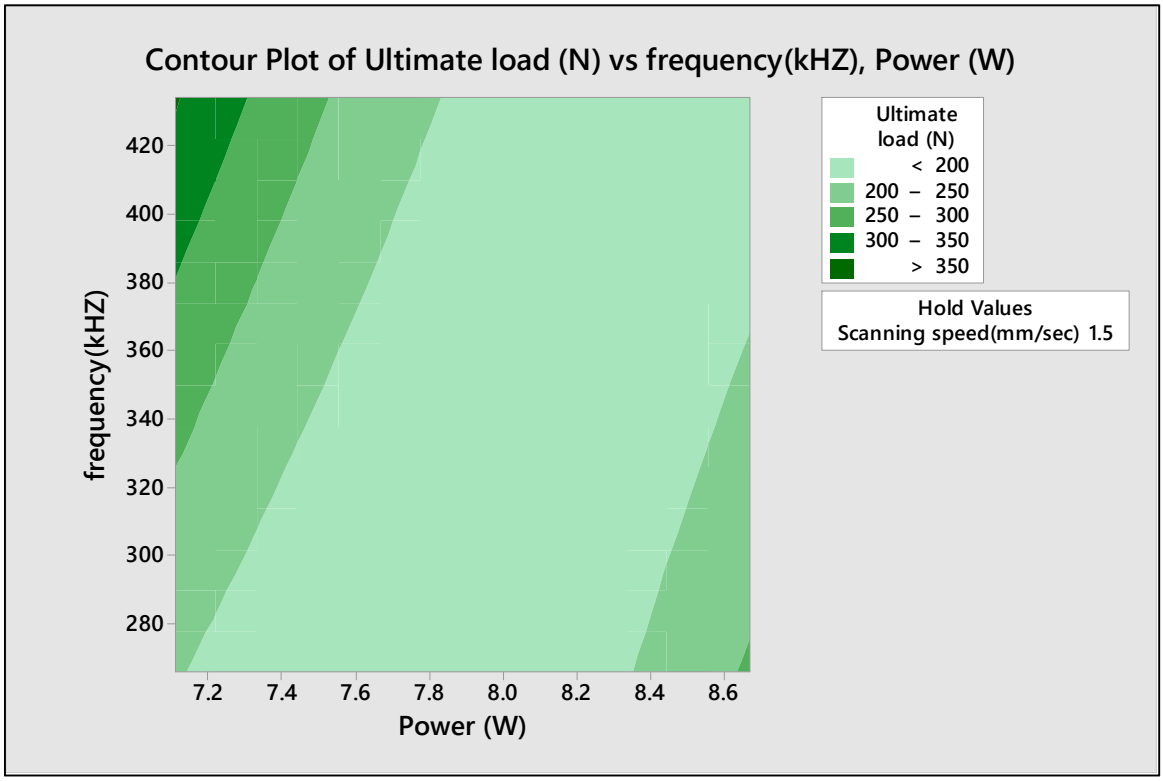

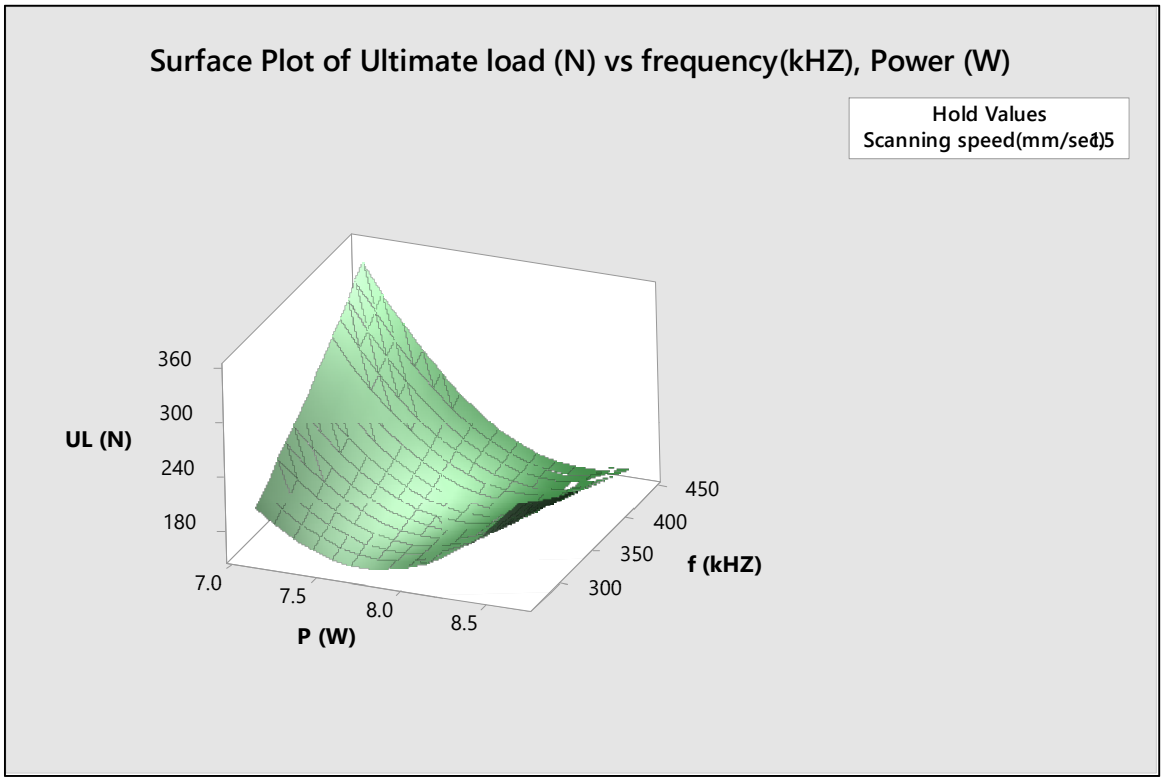

Figure 3.19 contour and surface plot for ultimate load vs frequency (f) and power (P) when scanning speed (SS) = 1.5 mm/s

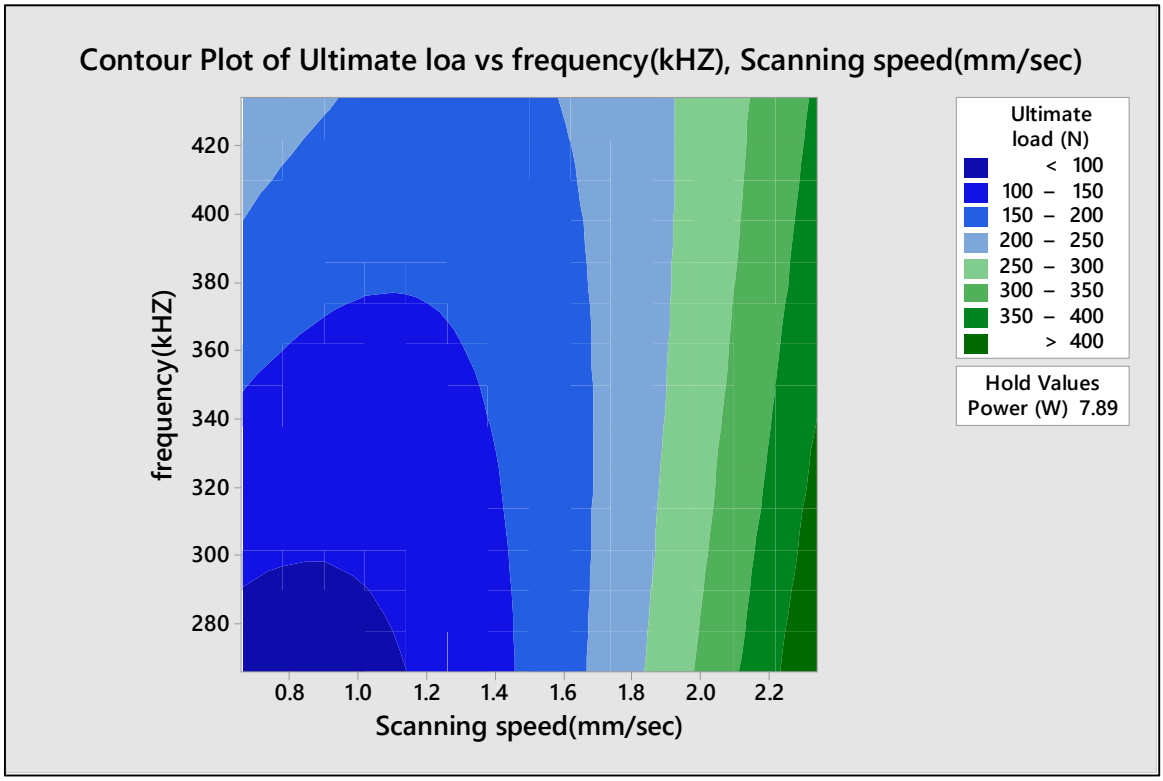

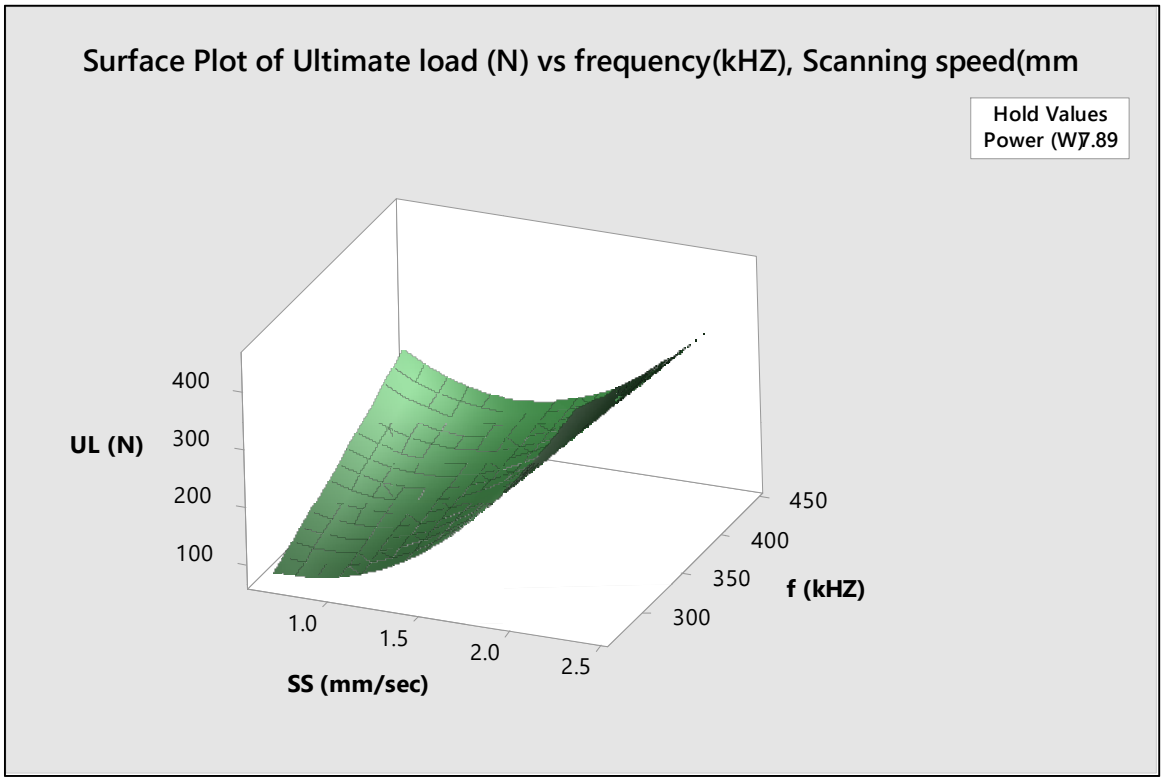

Figure 3.20 contour and surface plot for ultimate load vs frequency (f) and scanning speed (SS) when power (P) = 7.89 W

3.1.3.3. Ultimate Load

Response surface plots and contour plots for breaking load are shown in Figure 3.18 to Figure 3.20. In case of Figure 3.18, breaking load decreases for higher scanning speed. Lower scanning speed provides higher interaction time to absorb sufficient heat energy. It is essential to melt both welding interfaces and generate strong weld. Increase in scanning speed, results poor weld because the line energy (input energy per unit length) decreases as the scanning speed increases as a result, due to less interaction time very low amount of heat is delivered to the joint. With the increase of power, first the breaking load increases then it starts decreases due to large material decomposition. Figure 3.19 shows the combining effect of power and frequency. Breaking load depends on power and frequency. With the increase of power results wider weld width and more base material decomposition which leads to good weld. Therefore breaking load also increases with the increase of power. Figure 3.20 shows that, breaking load first increases and then decreases from lower to higher range of frequency. Lower scanning speed and higher power results better welds. Variations in frequency do not show any remarkable change in breaking load throughout**.**

3.1.4. Optimization

RSM based single objective optimization and multi-objective optimizations have been done, in order to find out the optimum parametric condition. The optimum condition is identified for maximization of weld width, minimization of HAZ and maximization of breaking load individually and then simultaneously. MINITAB 18 software is used for optimization.

3.1.4.1.Weld Width Optimization

Figure 3.21 shows the single objective optimization results for maximum weld width on the basis of the developed mathematical model. Figure 3.21 shows that maximum weld width can be achieved is 303.26 μm with the value of composite desirability (D) taken close to 1 at the power of 7.72 W, scanning speed of 0.66 mm/s and frequency of 434.1 kHz.

3.1.4.2.HAZ Optimization

Figure 3.22 shows the single objective optimization results for maximum HAZ on the basis of the developed mathematical model. Figure 3.22 shows that minimum HAZ that can be achieved is 16.94 μm with the value of composite desirability (D) taken as 1 at the power of 7.25 W, scanning speed of 2.34 mm/s and frequency of 303.28 kHz.

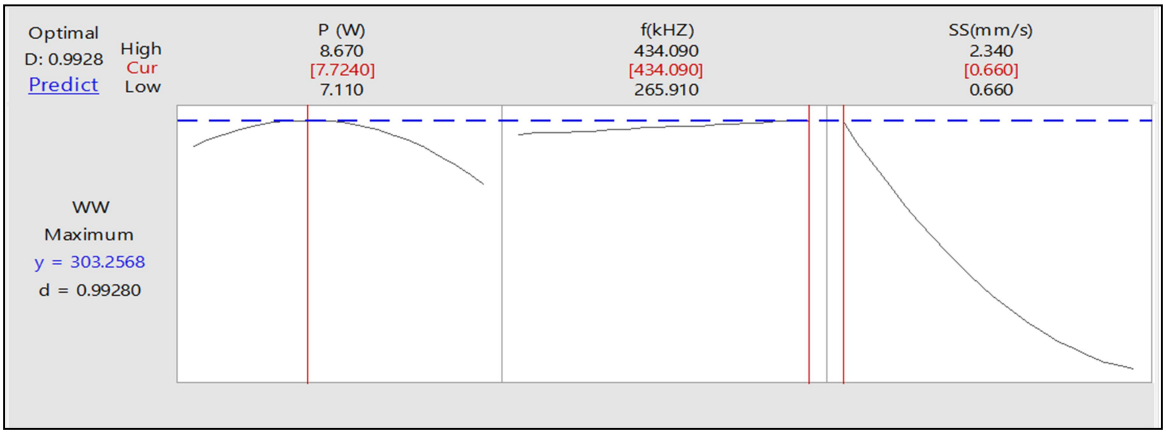

Figure 3.21 Single objective optimization of weld width

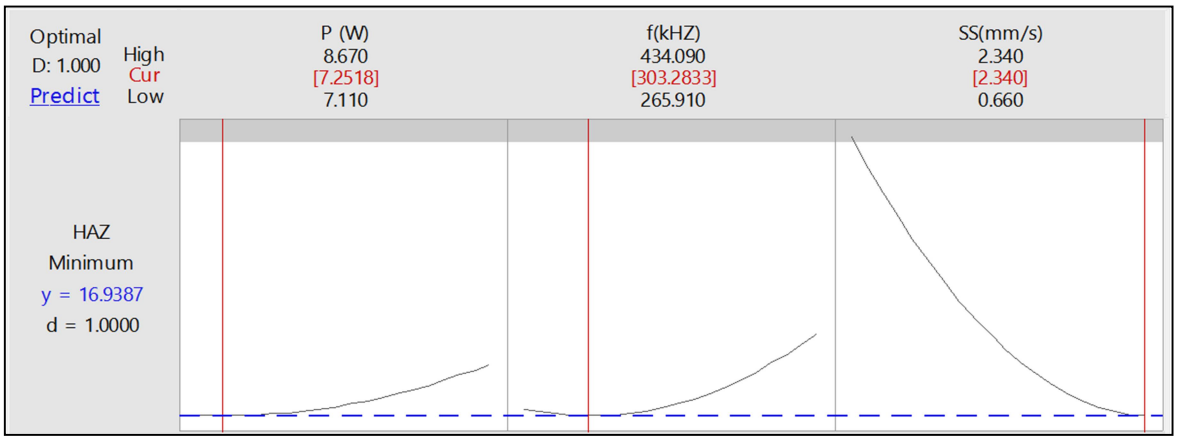

Figure 3.22 Single objective optimization of HAZ

3.1.4.3.Ultimate Load Optimization

Figure 3.23 shows the single objective optimization results for the maximum ultimate load on the basis of the developed mathematical model. Figure 3.23 shows that maximum ultimate load can be achieved is 563.65 N with the value of composite desirability (D) taken as 1 at power of 7.11 W, scanning speed of 2.34 mm/s and frequency of 434.1 kHz.

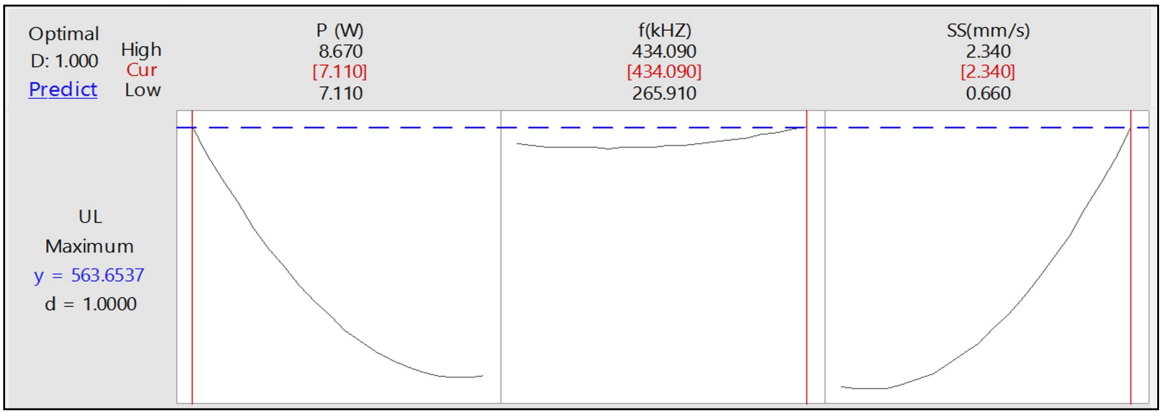

Figure 3.23 Single objective optimization of ultimate load

3.1.4.4. Multi-objective Optimization

Figure 3.23 shows the multi-objective optimization analysis where three responses have been analyzed together in one setting. In multi-objective optimization, the goal is set to maximize the weld width, maximize the breaking load and minimize the HAZ. In Figure 3.23, each row of the graph corresponds to a response variable and each column corresponds to one of the parameters considered during the experiment. Each cell shows the changes in the response as a function of one of the process parameters while others kept constant. Inside the graphs, vertical lines represent current parameter settings and a horizontal dotted line represents the current response values. The numbers displayed at the top of the column show the high, current and low level value of the parametric settings in the experimental design. Goal for the each response (maximum or minimum), predicted response at current parameter settings and individual desirability scores are shown at the left side of the each row. The current parameter settings are power of 7.11W, scanning speed of 1.15 mm/s and frequency of 434.09 kHz to achieve the optimal output conditions of maximum breaking load of 303.43 N, maximum weld width of 205.97 µm, minimum HAZ of 59.25 µm. The composite desirability factor (D), displayed at the upper left corner of the graph is 0.5813.

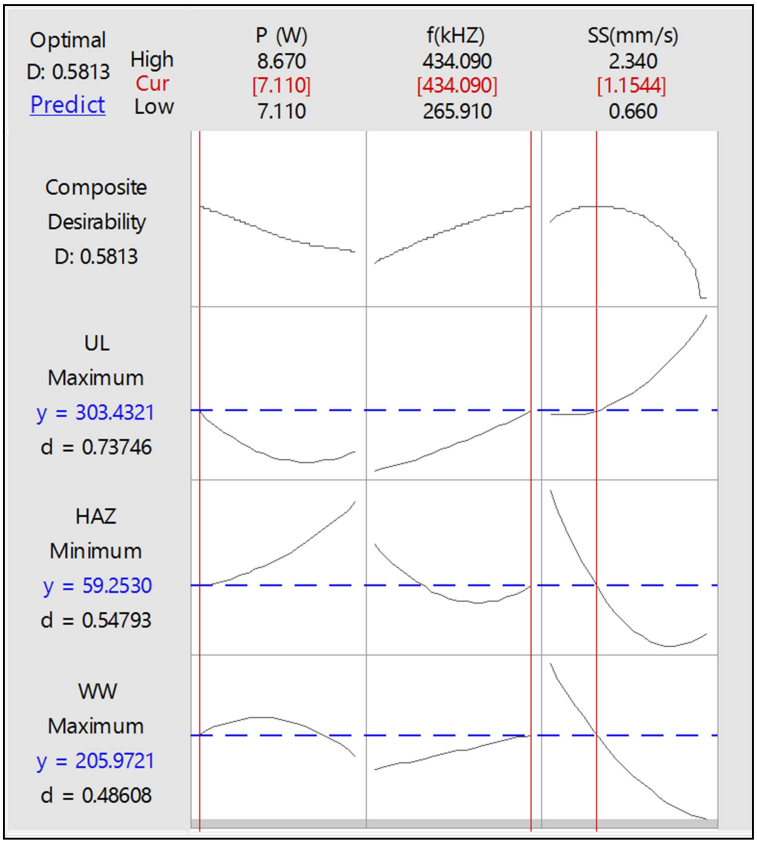

Figure 3.23 Multi-objective optimization plot

3.2. Simulation results

Validation for the capability of the developed finite element model has been checked as, the results of temperature distributions have been found and from that weld widths have been measured. The weld width has been then compared with the experimental result. The temperature distribution for different position at different time has been observed. The parameters used are same as the experimental planning i.e. power 8.35 W and scanning speed 2 mm/sec. In the following paragraphs the results of temperature and weld width analysis have been shown.

Temperature Analysis: The laser welding model solution with aforesaid parameters has been done. The temperature distributions have been shown in different location in Figure 3.24.

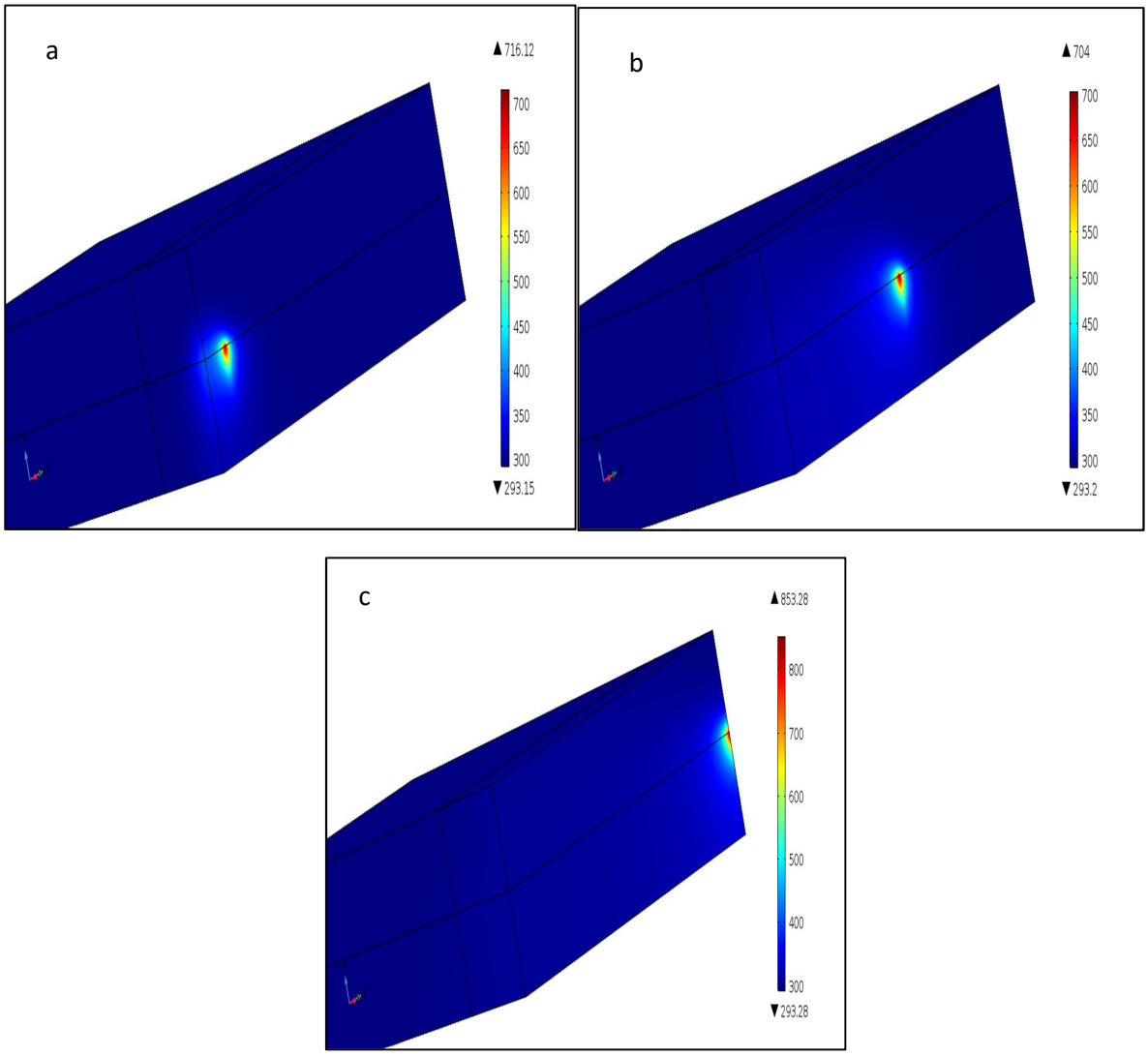

Figure 3.24 Temperature Distribution of welding at different location of welding zone (a) At the beginning of the welding (t =0.1s) (b) at the center (t = 0.625s) (c) at the end (t = 1.25s)

It is evident from the temperature distribution shown in Figure 3.24 that more heat is absorbed in the lower plate, which is acrylic. The upper polycarbonate plate gets some heat only by mode of conduction and gets fused to create the welding joints. More temperature has been observed at the beginning and at the end as compared to the center point it is due to the fact that at the beginning and ending heat could not decapitate to material bulk. This observation have given validation to performing experiment considering a square welding profile rather than straight line lap welding. From the simulation it has also been observed that the temperature is high in a precise localize location which creates a micro level weld width, but as the power density is high the fusion of materials have been occurred successfully resulting good welding strength.

The temperature distribution of center point i.e. at t = 0.625 s for total welding time has been shown in Figure 3.25. It is observed that temperature at a particular point reaches a peak for a short time then it gets reduced for which only melting of material occurs but not evaporation which in terms result in good quality welding. It is also observed from the graph the beam temperature distribution follows a Gaussian profile, which validates the assumption.

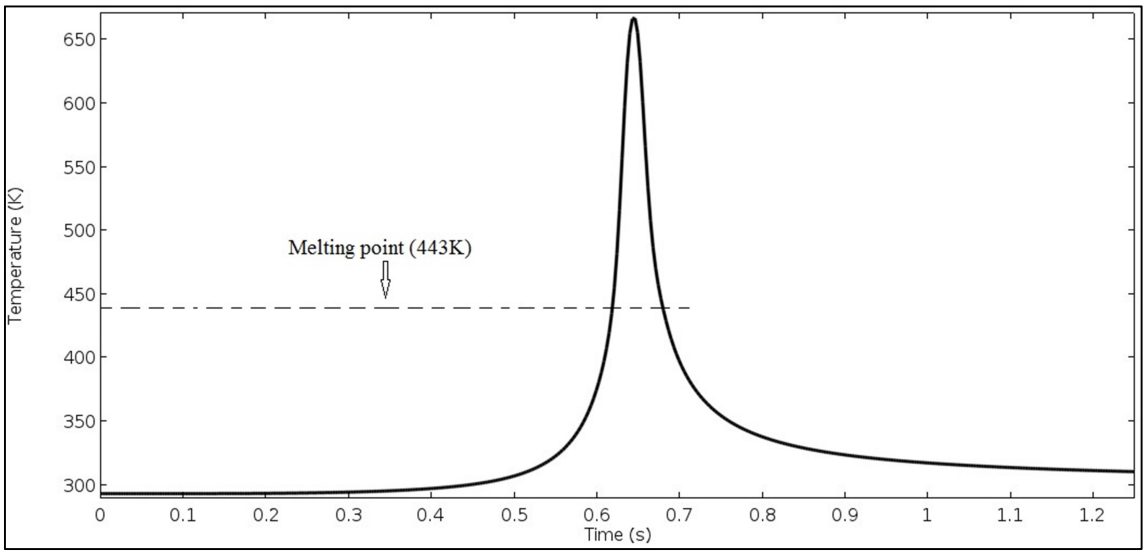

Figure 3.25 Temperature distribution of center point for all time steps

From the simulation results, it is clearly shown that the heat interaction mainly happens on the acrylic plate which is the lower part, so only the lower absorbent part has been considered now for thermal study to observe the temperature distribution in the interface. Figure 3.26 (a) shows the temperature distribution surface plot in the beginning of the welding (t =0.1s), Figure 3.26 (b) shows the temperature distribution surface plot at center of the welding profile (t = 0.625 s)and Figure 3.26 (c) shows the temperature distribution surface plot at extreme end (t =1.25 s).

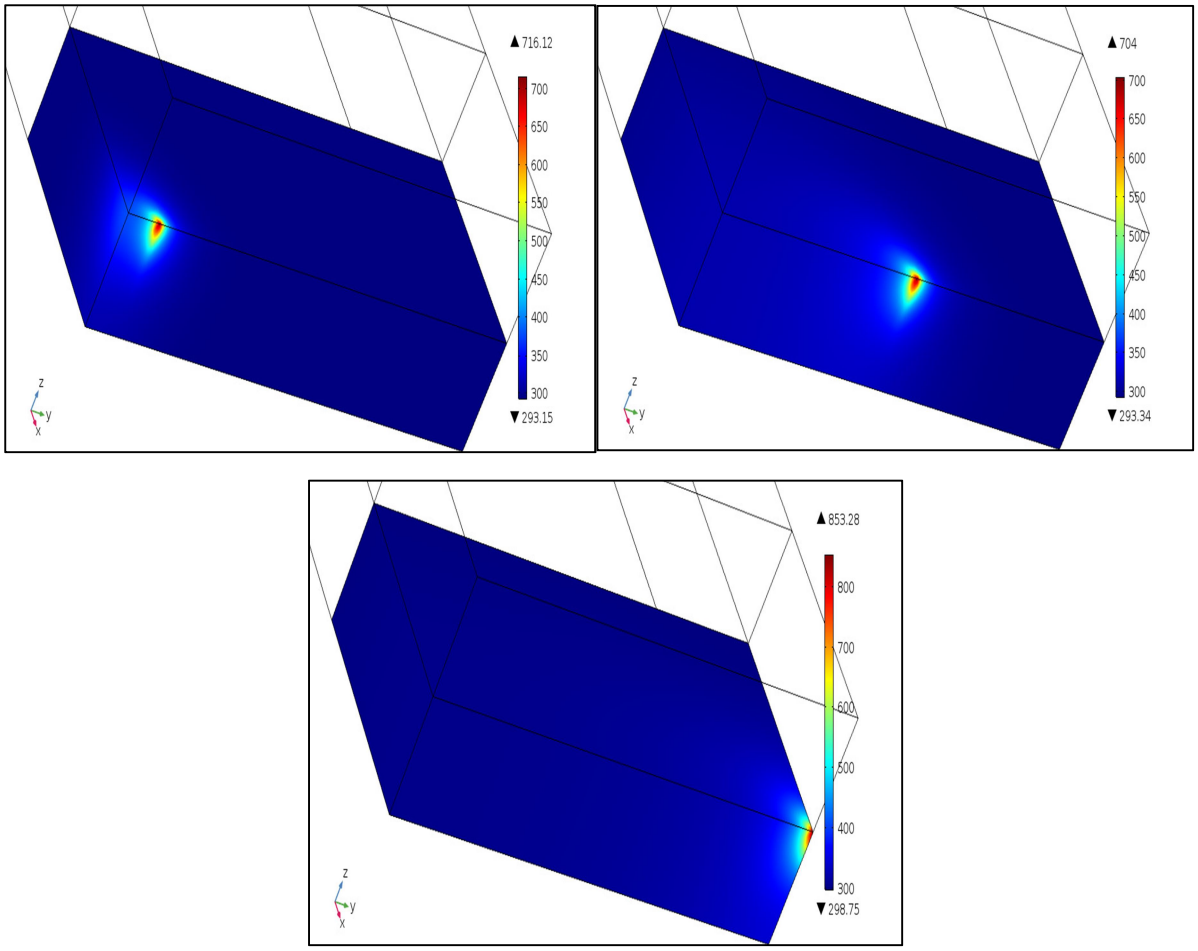

Figure 3.26 Temperature distribution surface plot (a) in the beginning of the welding (t =0.1s), (b) at center of the welding profile (t = 0.625 s) and (c) at extreme end (t =1.25 s).

The figure shows the temperature distribution along with the interface of two material where fusion has occurred. It is evident from Figure 3.26that maximum heat is in the centre of the laser beam. Preheating has been observed to be in the small domain, which in result decreases the HAZ and quality will be increased.

Weld Width Analysis: A close view of temperature distribution along the interface has been shown in Figure 3.27. The clear temperature contours are observed from the figure. From that, the regions having temperature more than the melting point temperature of the materials (443K) are considered to be weld width. Now by taking a line along with the interface at centre point the temperature distribution of every point on that line have been observed. The temperature distribution along the line has been plotted in Figure 3.28.

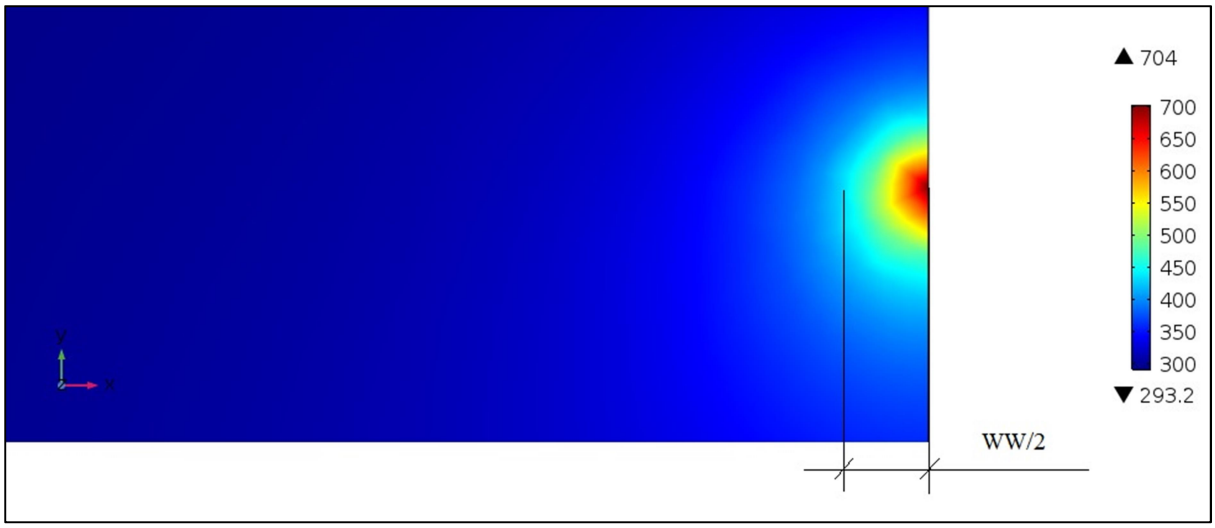

Figure 3.27 Temperature Contour of the interface for weld width measurement

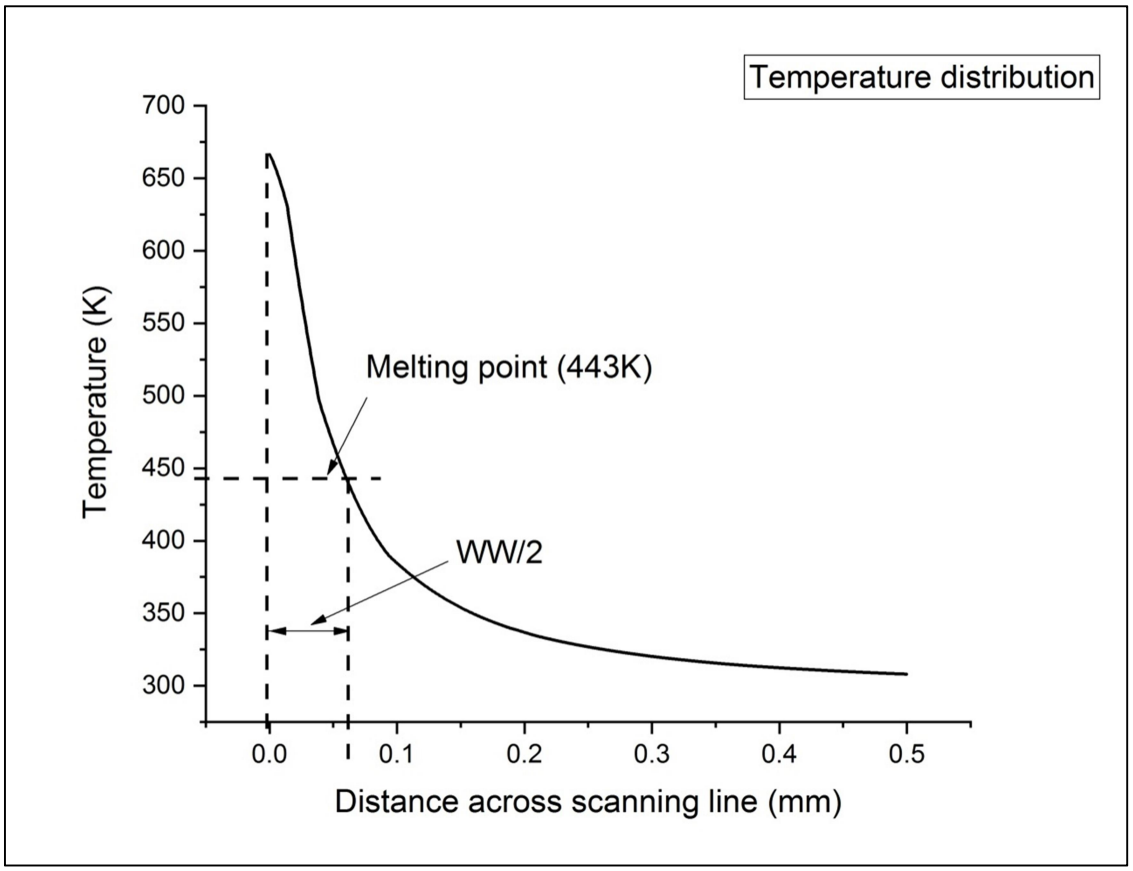

Figure 3.28 Temperature Distribution along the scanning line for weld width

In the graph, a horizontal line on the melting point of acrylic which has more melting point than acrylic have been drawn (dashed in Figure 3.28) and then from the intersection another horizontal line have been drawn. The intersection between the x-axis and the vertical line (dashed in Figure 3.28) gives the distance value which is half of the weld width, as the model have been considered only the half portion. For process parameters as 8.35 W power and 2 mm/s scanning speed the weld with from simulation have obtained as 123 μm and the experimental weld width for the same set of process parameters have been 124.55 μm. So it has been observed that violation of response is so low. The weld width for other sets of process parameters have been measured in the same manner and tabulated in Table 3.5.

Table 3.5 Weld width from simulation

Sl No.	Power (W)	Scanning Speed (mm/s)	Weld Width (μm)
1	8.35	2.00	123.00
2	8.35	1.00	199.00
3	7.89	2.34	109.20
4	7.42	2.00	107.20
5	7.89	1.50	162.80
6	7.11	1.50	129.20
7	7.42	1.00	266.00
8	7.89	0.66	318.00
9	8.67	1.50	133.00

3.3. Comparison with Experiment and Validation:

The same process parameters have been used in the experiment and simulation for comparing them. In the simulation, frequency has been assumed to be constant so the design table for simulation has only 9 sets of process parameters. Taking each of these 9 sets of process parameters simulation have been done. From the solution of the numerical simulation, temperature distribution can be observed from which the weld width for all the process parameters can be measured using the aforesaid method. The experiment has the same set of parameters so the weld widths from the experiment and simulation have been

compared and percentage error have been calculated. The comparisons along with percentage error are tabulated in Table 3.6. Error is calculated as,

$$\%Error = \frac{|Experimental\ Value - Aproximate\ \ Simulation\ Value\ |}{Experimental\ Value} \times 100\%$$

Table 3.6 Comparison between experiment and simulation

Sl No.	Power (W)	Scanning speed (mm/s)	Experimental WW (μm)	Simulation WW (μm)	Percentage Error (%)
1	8.35	2.00	124.55	123.00	1.24
2	8.35	1.00	229.56	199.00	13.31
3	7.89	2.34	112.65	109.20	3.06
4	7.42	2.00	114.09	107.20	6.03
5	7.89	1.50	177.02	162.80	8.03
6	7.11	1.50	140.61	129.20	8.11
7	7.42	1.00	227.63	266.00	16.85
8	7.89	0.66	304.64	318.00	4.38
9	8.67	1.50	150.83	133.00	11.82

From the table, it is seen that the error percentage is in low range with a maximum error of 16.85 % where the minimum error is as low as 1.24%. This indicates that model, which have been made using numerical simulation is adequate. Thus model has been validated as per experiments. Some error is there due to the considered assumptions for modeling the problem but the error is seen to be an acceptable range.

3.4. Depth of Penetration Measurement Using Simulation

The simulation model has been proved to be an adequate model of the experiment. Thus, depth of penetration measurement which is a complex process experimentally can be predicted using simulation. For process parameters power 3.5 W and scanning speed 2 mm/s the depth of penetration has been predicted. Figure 3.29 shows the temperature distribution in depth direction. From that the regions having temperature more than the melting point temperature of the acrylic (443K) are considered to be depth of penetration on acrylic (DOPA) shown in Figure 3.30 (a) and on the upper part regions having temperature more than melting point of polycarbonate (420K) are considered to be depth of penetration in

polycarbonate (DOPP) in Figure 3.30 (b). A line has been drawn at center towards down and up and temperature distributions are plotted along these lines in Figure 3.31 and Figure 3.32 respectively. In the graphs a horizontal line on melting points of the materials has been drawn (dashed) and then from the intersection another horizontal line has been drawn. The intersection between the x-axis and the vertical line (dashed) gives the distance value which is the depth of penetration. For process parameters as 8.35 W power and 2 mm/s scanning speed the DOPA is 121.37µm and 41.67 µm.

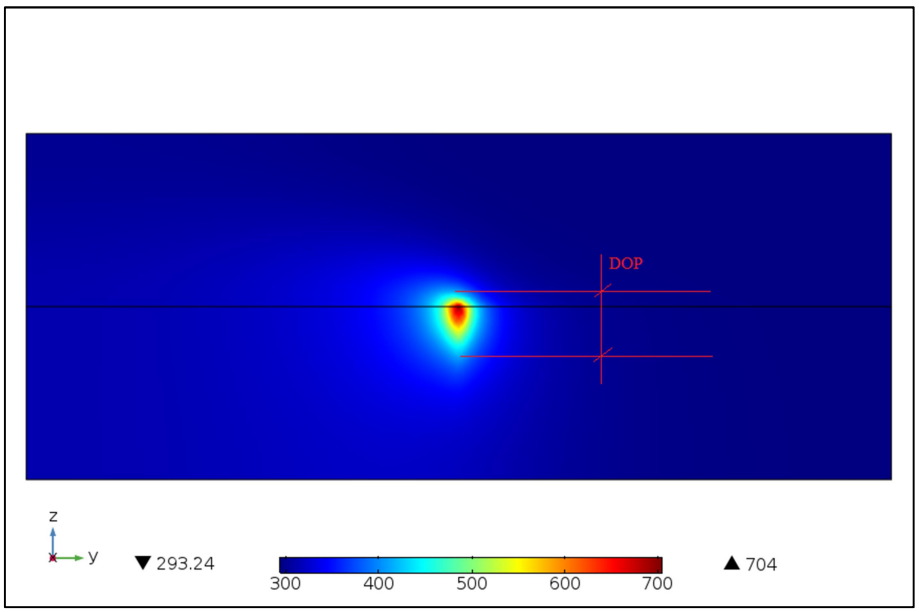

Figure 3.29 Temperature distribution in depth direction

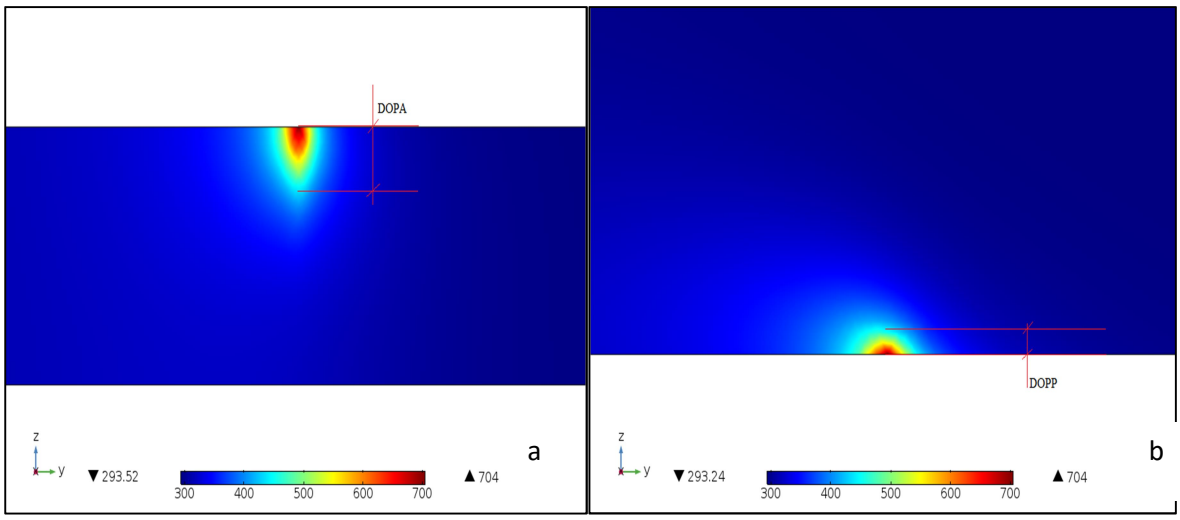

Figure 3.30 (a) DOPA , (b) DOPP

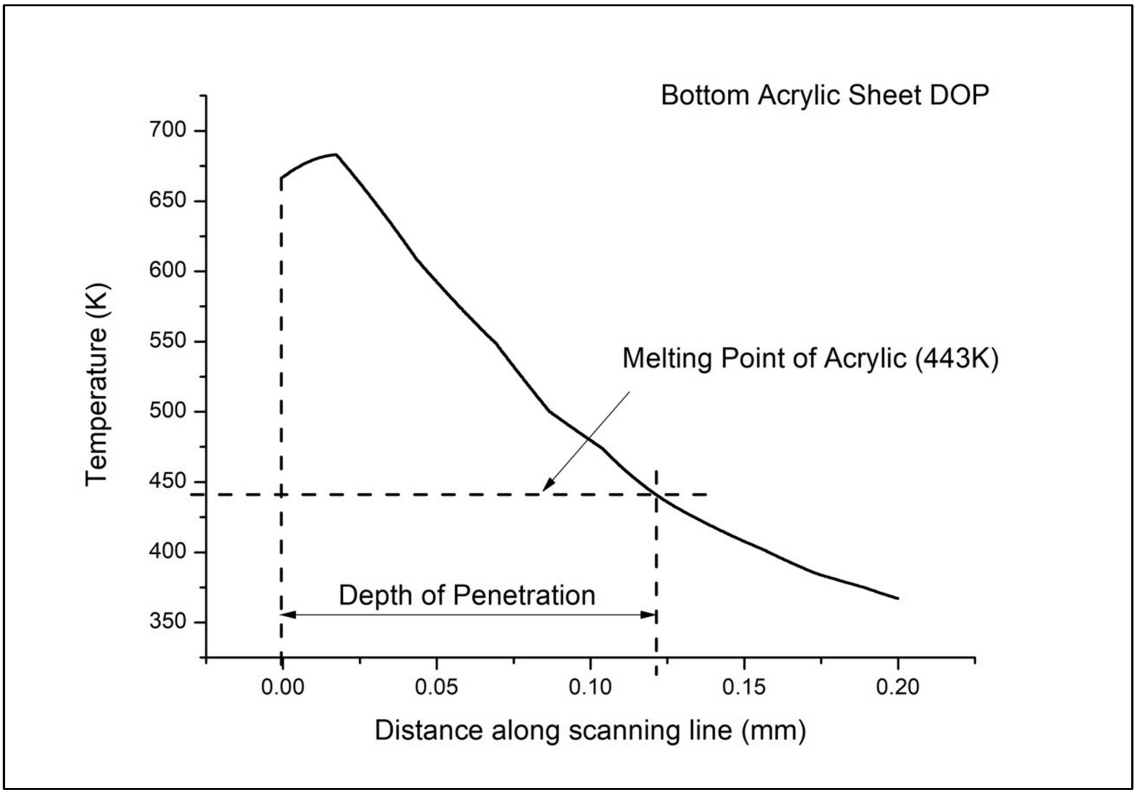

Figure 3.31 Temperature Distribution along the scanning line for DOPA

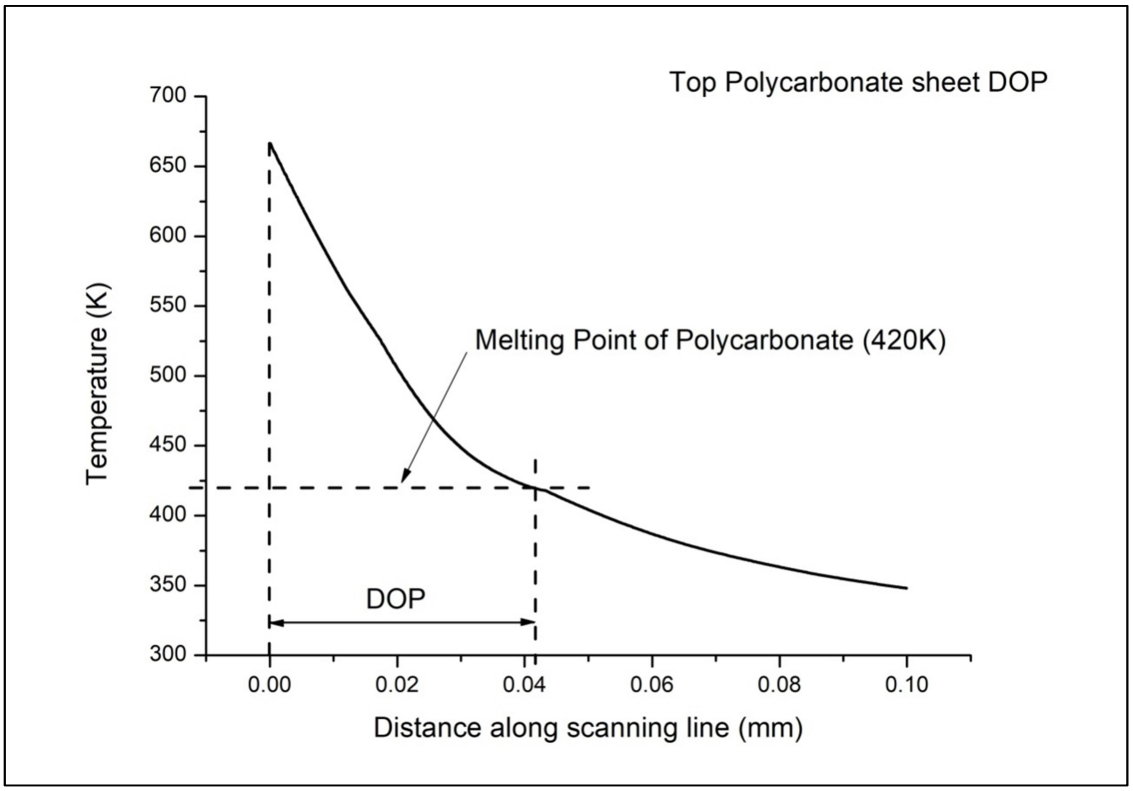

Figure 3.32 Temperature Distribution along the scanning line for DOPP

The depth of cut for other process parameters have been predicted in the same manner and tabulated in Table 3.7.

Table 3.7 Table of the depth of penetration

Sl No.	Power (W)	Scanning Speed (mm/s)	DOPA (μm)	DOPP (μm)	DOP (μm)
1	8.35	2.00	121.37	41.67	163.04
2	8.35	1.00	156.72	57.88	214.6
3	7.89	2.34	112.99	27.79	140.78
4	7.42	2.00	109.29	26.89	136.18
5	7.89	1.50	149.09	50.72	199.81
6	7.11	1.50	105.58	42.05	147.63
7	7.42	1.00	138.76	11.92	150.68
8	7.89	0.66	165.23	62.84	228.07
9	8.67	1.50	68.37	37.84	106.21

From the table it has been observed that maximum depth has been reached 228.07 μm, and 106.21 μm has been the minimum depth of penetration.

Chapter 4

4. Conclusion and Future Scope

Two transparent dissimilar plastics have been joined by through transmission laser welding process under different welding conditions to find out the optimal process parameters. Simulation has been solved for the same set of process parameters and verified with the experiments. Depth of penetration has been predicted using verified mathematical simulation.

4.1. Conclusions

Based on the above experiments and analysis, the following conclusions can be made:

I. While performing laser welding in lap joint configuration, with an increase of power weld width increases initially and get reduced at higher power maximum weld width is 304.64 µm and minimum as 112.65 µm.

II. HAZ have an increasing trend with increasing laser power, HAZ varies from 20.85 µm to 104.80 µm.

III. Weld strength is more for low power with nominal HAZ but it has low strength at higher power due to material decomposition. The ultimate strength of welding varies from minimum 121.15 N to a maximum of 372.60 N.

IV. With increasing scanning speed Weld width and HAZ both decreases while the ultimate strength shows opposite nature, i.e. the strength of the welding increasing with increasing scanning speed.

V. From the ANOVA of the weld width model is found to be adequate and chosen process parameters are found to be significant while lack of fit found to be not significant. P^2, f^2, Pf and fSS are also found to be significant model parameters.

VI. From the ANOVA of HAZ model is found to be adequate and chosen process parameters are found to be significant while lack of fit found to be not significant. Other squared and two-way interaction parameters except Pf are also found to be significant model parameters.

VII. From the ANOVA of ultimate load model is found to be adequate and chosen process parameters are found to be significant while lack of fit found to be not significant. Other squared and two-way interaction parameters except f^2 are also found to be significant model parameters.

VIII. Single objective optimization of the weld width with the objective of maximization of weld width gives maximum weld width of 303.26 μm at 7.24 W power, 0.66 mm/sec scanning speed and 434.1 kHz frequency.

IX. Minimum HAZ that can be obtained is 16.94 μm at power of 7.25 W, scanning speed of 2.34 mm/s and frequency of 303.28 kHz

X. The maximum welding strength in terms of ultimate strength that can be achieved is 563.65 N at 7.11 W power, 2.34 mm/s scanning speed and 434.1 kHz frequency.

XI. Multi-objective optimization gives the optimum set of process parameters as 7.11 W power, 1.15 mm/s scanning speed, 434.09 kHz power with an optimum response as weld width of 205.97 μm, HAZ of 59.23 μm and ultimate load as 303.43 N.

XII. Simulation has been verified with experiments and found to be adequate with an average error of 8.09 %.

XIII. Depth of penetration predicted from the simulation found a minimum of 106.21μm and a maximum of 228.07 μm.

4.2. Future Scope

The future scopes of the present work are listed below

I. From FEM model optimum set of process parameters can be found.

II. Clamping pressure can be added as process parameters.

III. Modeling can be done by varying spot diameter.

IV. CFD modeling can be incorporated to counter the porosity on the weld pool.

V. Different types of joint configuration can also be studied.

References

[1] K. Vijay, Stokes, “Joining methods for plastics and plastic composites: an overview”, Polymer Engineering and Science, 29 (1989) 1310-1325.

[2] N. Kumar, M. Mukherjee, A. Bandyopadhyay, “Study on laser welding of austenitic stainless steel by varying incident angle of pulsed laser beam”, Optics and Laser Technology, 94 (2017) 296-309.

[3] N. Kumar, M. Mukherjee, A. Bandyopadhyay, “Comparative study of pulsed Nd: YAG laser welding of AISI 304 and AISI 316 stainless steels”, Optics and Laser Technology, 88 (2017) 24-39.

[4] A. Visco, C. Scolaro, A. Quattrocchi, R. Montanini, “Response to fatigue stress of biomedical grade polyethylene joints welded by a diode laser”, Journal of the Mechanical Behavior of Biomedical Materials, 86 (2018) 390–396.

[5] T.B. Juhl, J.C. Christiansen, E.A. Jensen, “Mechanical testing of polystyrene/polystyrene laser welds”, Polymer Testing, 32 (2013) 475-481.

[6] T.B. Juhl, D. Bach, R.G. Larson, J.C. Christiansen, E.A. Jensen, “Predicting laser weldability of dissimilar polymers”, Polymer, 54 (2013) 3891-3897.

[7] N. Kumar, R. Rudrapati, P.K. Pal, “Multi-objective optimization in through laser transmission welding of thermoplastics using grey-based Taguchi method”, Procedia Materials Science, 5 (2014) 2178 – 2187.

[8] H. Nakamura, T. Masaki, “Plastics welding with diode laser”, Journal of the Japan Welding Society, 72 (2003) 189–92.

[9] B.G. Bryden, “Welding of plastics with high power diode lasers”, Industrial Robot: An International Journal, 31 (2004) 30–33.

[10] B. Acherjee, A.S. Kuar, S. Mitra, D. Misra, “Selection of process parameters for optimizing the weld strength in laser transmission welding of acrylics”, Journal of Engineering Manufacture, 224 (2000) 1529-1536.

[11] N. Kumar, N. Kumar, A. Bandyopadhyay, “Optimization of pulsed Nd:YVO_4through transmission laser welding of transparent acrylic and polycarbonate”, Materials Today: Proceedings, 5 (2018) 5235-5243.

[12] H.M. Shin, H.W. Choi, “Design of energy optimization for laser polymer joining process”, International Journal of Advanced Manufacturing Technology, 75 (2014) 1569–1576.

[13] B. Acherjee, D. Misra, D. Bose, K. Venkadeshwaran, “Prediction of weld strength and seam width for laser transmission welding of thermoplastic using response surface methodology”, Optics and Laser Technology, 41 (2009) 956-967.

[14] X. Wang, H. Chen, H. Liu, P. Li, Z. Yan, C. Huang, Z. Zhao, Y. Gu, “Simulation and optimisation of continuous laser transmission welding between PET and titanium through FEM, RSM, GA and experiments”, 51 (2013) 1245-1254.

[15] X. Wang, C. Zhang, K. Wang, P. Li, Y. Hu, K. Wang, H. Liu, “Multi-objective optimisation of laser transmission joining of thermoplastics”, Optics and Laser Technology 44 (2012) 2393–2402.

[16] J. Jiao, Z. Xu, Q. Wang, L. Sheng, W. Zhang, “CFRTP and stainless steel laser joining: Thermal defects analysis and joining parameters optimisation”, Optics and Laser Technology 103 (2018) 170–176.

[17] Ch.V. Katsiropoulos, G.A. Moraitis, G.N. Labeas, Sp.G. Pantelakis, “Optimisation of laser welding process for thermoplastic composite materials with regard to component quality and cost”, Plastics, Rubber and Composites, 38 (2009) 153-161.

[18] Y. Ai, P. Jiang, X. Shao, C. Wang, P. Li, G. Mi, Y. Liu, W. Li, “A defect-responsive optimisation method for the fiber laser butt welding of dissimilar material”, 90 (2016) 669-681.

[19] Y.S. Tarng, W.H. Yang, S.C. Juang, “The use of fuzzy logic in the Taguchi method for the optimisation of the submerged Arc welding process”, International Journal of Advanced Manufacturing Technology, 16 (2000) 688–694.

[20] R. Kumar, G.S. Brar, “Optimization of process parameters for MIG Welding by Taguchi method”, International Journal of Scientific Research Engineering and Technology, 6 (2017) 756-768.

[21] M. Chen, G. Zak, P.J. Bates, “Description of transmitted energy during laser transmission welding of polymers”, Weld World, 57 (2013) 171–178.

[22] M. Chen, G. Zak, P.J. Bates, “3D finite element modelling of contour laser transmission welding of polycarbonate”, Welding in the World, 53 (2009) R188-R197.

[23] M. Aden, “Influence of the laser-beam distribution on the seam dimensions for laser-transmission welding: A simulative approach”, Lasers in Manufacturing and Materials Processing, 3 (2016) 100-110.

[24] M. Geiger, T. Frick, M. Schmidt, “Optical properties of plastics and their role for the modelling of the laser transmission welding process”, Production Engineering Research and Development, 3 (2009) 49–55.

[25] I. Hadriche, E. Ghorbel, N. Masmoudi, G. Casalino, “Investigation on the effects of laser power and scanning speed on polypropylene diode transmission welds”, International Journal of Advanced Manufacturing Technology, 50 (2010) 217–226.

[26] F. Lambiase, S. Genna, R. Kant, “Optimization of laser-assisted joining through an integrated experimental-simulation approach”, International Journal of Advanced Manufacturing Technology, 97 (2018) 2655–2666.

[27] G. Casalino, E. Ghorbel, “Numerical model of CO_2 laser welding of thermoplastic polymers”, Journal of Materials Processing Technology, 207 (2008) 63-71.

[28] T. Zoubeir, G. Elhem, “Numerical study of laser diode trans mission welding of a polypropylene mini-tank: Temperature field and residual stresses distribution”, Polymer Testing 30 (2011) 23–34.

[29] X. Wang, H. Chen, H. Liu, “Investigation of the relationships of process parameters, molten pool geometry and shear strength in laser transmission welding of polyethylene terephthalate and polypropylene”, Materials and Design 55 (2014) 343–352.

[30] P. Mollicone, D. Camilleri, T.G.F. Gray, T. Comlekci, “Simple Thermo- Elastic–Plastic models for welding distortion simulation”, Journal of Materials Processing Technology, 176 (2006) 77–86.

[31] H. Murakawa, D. Deng, W. Liang, “Determination of welding deformation in fillet-welded joint by means of numerical simulation and comparison with experimental measurements”, Journal of Materials Processing Technology, 183 (2007) 219–225.

[32] F. Beckar, H. Potente, “A step towards understanding the heating phase of laser transmission welding of polymers”, Polymer Engineering and Science, 42 (2002) 365-374.

[33] H. Liu, W. Liu, X. Zhong, B. Liu, D. Guo, X. Wang, “Modeling of laser heat source considering light scattering during laser transmission welding”, Materials and Design, 99 (2016) 83–92.

[34] M. Ilie, J.C. Kneip, S. Matteï, A. Nichici, C. Roze, T. Girasole, “Through-transmission laser welding of polymers– temperature field modeling and infrared investigation”, Infrared Physics & Technology, 51 (2007) 73-79.

[35] Z. Chen, Y. Huang, F. Han, D. Tang, “Numerical and experimental investigation on laser transmission welding of fiberglass-doped PP and ABS”, Journal of Manufacturing Processes, 31 (2018) 1-8.

[36] J.M.P. Coelho, M.A. Abreu, F.C. Rodrigues, “Modeling the spot shape influence on high-speed transmission lap welding of thermoplastic films”, Optics and Lasers in Engineering, 46 (2008) 55–61.

[37] D. Flock, M. Sickert, E. Haberstroh, “Temperature measurement in laser transmission welding of plastics”, Gummi FasernKunststoffe, 11 (2012) 704–708.

[38] M. Ilie, E. Cicala, D. Grevey, S. Mattei, V. Stoica, “Diode laser welding of ABS: Experiments and process modeling”, Optics and Laser Technology 41 (2009) 608–614.

[39] T. Purtonen, A. Kalliosaari, A. Salminen, “Monitoring and adaptive control of laser processes”, Physics Procedia, 56 (2014) 1218-1231.

[40] J. Shao, Y. Yan, “Review of techniques for on-line monitoring and inspection of laser welding”, Journal of Physics: Conference Series 15 (2005) 101–107.

[41] M. Speka, S. Mattei, M. Pilloz, M. Ilie, “The infrared thermography control of the laser welding of amorphous polymers”, NDT&E International 41 (2008) 178 – 183.

[42] R. Truckenmiiller, R. Ahrens, Y. Cheng, G. Fischer, V. Saile, “An ultrasonic welding based process for building up a new class of inert fluidic micro-sensors and actuators from polymers”, Sensors and Actuators, 132 (2006) 385– 392.

[43] E. Ghorbel, G. Casalino, S. Abed, “Laser diode transmission welding of polypropylene: Geometrical and microstructure characterisation of weld”, Materials and Design 30 (2009) 2745–2751.

[44] C.Y. Wang, P.J. Bates, M. Aghamirian, G. Zak, R. Nicholls, M. Chen, “Quantitative morphological analysis of carbon black in polymers used in laser transmission welding”, Welding in the World, 51 (2007) 85-90.

[45] S. Abed, P. Laurens, C. Carretro, J.R. Deschamps, C. Duval, “Diode laser welding of polymers: microstructures of the welded zone for polypropylene”, Proceedings of ICALEO (2001) 112-117.

[46] L. Ma, L. Song, H. Wang, L. Fan, B. Liu, “Synthesis and characterisation of poly(propylene carbonate) glycol-based waterborne polyurethane with a high solid content”, Progress in Organic Coatings, 122 (2018) 38-44.

[47] D. Hansch, D. Haaf, H. Putz, H.G. Treusch, A. Gillner, R. Poprawe, “Welding of Plastics with Diode Laser”, Proceedings of ICALEO (1998) 81-86.

[48] X.F. Xu, P.J. Bates, G. Zak, “Effect of glass fibre and crystallinity on light transmission during laser transmission welding of thermoplastics”, Optics & Laser Technology 69 (2015) 133-139.

[49] D. Grewell, P. Rooney, “Relationship between optical properties and optimised processing parameters for through transmission laser welding of thermoplastics”, Journal of Reinforced Plastics and Composites, 23 (2004) 13-18.

[50] M. Wehner, P. Jacobs, R. Poprawe, “Rapid prototyping of micro-fluidic components by laser beam processing”, Proceedings of SPIE, 6459 (2007) 1-12.

[51] E. Haberstorh, W.M. Hoffman, R. Poprawe, F. Sari, “Laser transmission joining in microtechnology”, Microsystem Technology, 12 (2006) 632-639.

[52] R.G. Bray, V. Kagan, A. Chambers, “Forward to better understanding of optical characterisation and development of coloured polyamides for the infra-red/laser welding: part 1- efficiency of polyamides for infra-red welding”, Journal of Reinforced Plastics and Composites, 22 (2003) 533-547.

[53] “An experimental study of laser welding of dissimilar transparent plastics”, M.Tech. Thesis by Raktim Bhattacharya, Jadavpur University, 2017

[54] “Intoduction to Finite Element method” Book by Dr. C.S. Jog, Department of Mechanical Engineering, IISC, Bangalore.

[55] https:// en. Wikipedia.org/FEM

[56] https:// hi-fem.org